ROADWAY SAFETY INSTITUTE

Human-centered solutions to advanced roadway safety

Developing and Validating a Model of Left-Turn Crashes to Support Safer Design and Operations

Gary Davis

Jingru Gao

Department of Civil. Environmental, and Geo- Engineering
University of Minnesota

Abhisek Mudgal

Texas Transportation Institute

Final Report

CTS 18-18

University of Minnesota Driven to Discover℠
The University of Akron
Illinois University of Illinois at Urbana-Champaign
Southern Illinois University Edwardsville
Western Michigan University

Technical Report Documentation Page

1. Report No. CTS 18-18	2.	3. Recipients Accession No.	
4. Title and Subtitle Developing and Validating a Model of Left-Turn Crashes to Support Safer Design and Operations		5. Report Date September 2018 6.	
7. Author(s) Gary Davis, Jingru Gao, Abhisek Mudgal		8. Performing Organization Report No.	
9. Performing Organization Name and Address Department of Civil, Environmental, and Geo- Engineering University of Minnesota 500 Pillsbury Drive SE Minneapolis, MN 55455		10. Project/Task/Work Unit No. CTS#2015021 11. Contract (C) or Grant (G) No. DTRT13-G-UTC35	
12. Sponsoring Organization Name and Address Roadway Safety Institute Center for Transportation Studies University of Minnesota 200 Transportation and Safety Building 511 Washington Ave. SE Minneapolis, MN 55455		13. Type of Report and Period Covered Final Report 14. Sponsoring Agency Code	
15. Supplementary Notes http://www.roadwaysafety.umn.edu/publications/			
16. Abstract (Limit: 250 words) This report documents work done to advance the state of art in crash simulation. This includes: (1) A field study to collect data on drivers' left-turn gap acceptance and turning times, and development of statistical models that can be incorporated into a crash simulation model; (2) The use of Markov Chain Monte Carlo computational tools to quantify uncertainty in planar impact reconstruction of two-vehicle crashes; (3) A method for combing the results from planar impact reconstruction with event data recorder pre-crash data to estimate descriptive features of actual left-turn crashes. This is applied to several left-turn crashes from the National Highway Traffic Safety Administration's NASS/CDS database; (4) A left-turn crash simulation model incorporating the above results. Initial model checking is performed using estimates from the reconstructed NASS/CDS cases as well as results from a previous study on left-turn crash risk. Also described is a method for simulating crash modification effects without having to first simulate crashes as rare outcomes in very large numbers of gap acceptances.			
17. Document Analysis/Descriptors Simulation, Crash reconstruction, Traffic safety, Event data recorders		18. Availability Statement No restrictions. Document available from: National Technical Information Services, Alexandria, Virginia 22312	
19. Security Class (this report) Unclassified	20. Security Class (this page) Unclassified	21. No. of Pages 122	22. Price

Developing and Validating a Model of Left-Turn Crashes to Support Safer Design and Operations

FINAL REPORT

Prepared by:

Gary A. Davis
Jingru Gao
Department of Civil, Environmental, and Geo- Engineering
University of Minnesota

Abhisek Mudgal
Texas Transportation Institute

September 2018

Published by:

Roadway Safety Institute
Center for Transportation Studies
University of Minnesota
200 Transportation and Safety Building
511 Washington Ave. SE
Minneapolis, MN 55455

ACKNOWLEDGMENTS

The funding for this project was provided by the United States Department of Transportation's Office of the Assistant Secretary for Research and Technology for the Roadway Safety Institute, the University Transportation Center for USDOT Region 5 under the Moving Ahead for Progress in the 21st Century Act (MAP-21).

The authors wish to acknowledge those who made this research possible, including the funding agencies and Stephen Zitzow, of the Minnesota Traffic Observatory, for collecting the video data.

TABLE OF CONTENTS

LIST OF FIGURES

LIST OF TABLES

CHAPTER 1: INTRODUCTION

In Minnesota, during 2012, there were almost 3300 crashes involving a vehicle turning left into oncoming traffic, including over 1100 fatal and personal injury crashes (Crash Facts, 2012). The Minnesota Strategic Highway Safety Plan (MnDOT, 2007) identified "Improving the Design and Operation of Highway Intersections" as a Critical Emphasis Area, with turning-lane construction and signal-timing improvements being identified as desired safety strategies. These include provision of left-turn (LT) lanes and decisions regarding protective or permissive LT phasing.

In permissive LT treatments, the turning driver is required to yield to opposing vehicles and make the turn when presented with a gap, of sufficient duration, between opposing vehicles. Permissive LT treatments are used at unsignalized intersections and at signalized intersections where the frequency of adequate gaps accommodates the LT demand. Protective LT treatments, used at signalized intersections, involve giving exclusive right of way to LT drivers for some portion of a signal's cycle. Protective LT treatments are recommended when the combination of opposing and LT traffic volumes is so high that the LT drivers would experience unacceptable delays under permissive treatments. A hybrid option is a protective-permissive phase, where a short protective interval is followed by an interval where LTs are permitted.

Protective LT treatments may also be used when special conditions at an intersection make it difficult for drivers to judge gaps, increasing the risk of crashes between turning and opposing (or through) vehicles. These can include situations where the speeds of the opposing vehicles are high, or where sight distance restrictions make it difficult for the LT drivers to identify safe gaps. This latter situation, where the layout of opposing LT lanes creates sight distance obstructions when opposing LTs are present, was identified by McCoy et al. (2001). One particularly interesting example was an intersection described in Davis and Aul (2007), where a conversion from two-way stop control to signalized control, with permissive LT phasing on the major approaches, was followed by a clear increase in LT crashes. The LT crashes then essentially disappeared when protective LT treatments were implemented. A review of police crash reports found that the crash-involved LT drivers tended to identify situations where opposite direction LT vehicles waiting for gaps tended to obstruct the view of opposing traffic. However, using protective LT treatments when opposing traffic volumes are low can lead LT drivers to believe they are being needlessly delayed, while using protective LT treatment when LT volumes are low reduces the capacity available for accommodating other movements. As with many traffic engineering decisions, the use of protective LT treatments can involve finding the right balance between the safety provided by protective LT treatments and the delay those treatments can cause.

The *Highway Capacity Manual* can be used to estimate the delays resulting from different LT treatments, but estimating their safety effects is still something of an open question. Hauer (2004) reviewed 36 reports and papers, and found that protective-only LT treatments tended to have the lowest LT crash experience, but that the difference between permissive-only and permissive-protective treatments was less clear. Hauer also noted that methodological weaknesses in many of these studies

limited their usefulness. In a cross-sectional study involving 197 four-legged signalized intersections Wang and Abdel-Aty (2008) found that protected-only LTs were associated with a decrease in the frequency of LT crashes, while intersections with permissive-protective treatments tended to have higher frequencies of LT crashes than did those with permissive-only treatments. On the other hand, in an empirical Bayes before-after study, Srinivasan et al. (2012) found that changing from permissive to protective-permissive phasing was followed by a 14% reduction in LT crashes.

This issue has become even more important with the recent use of a flashing yellow arrow (FYA) to indicate permitted LTs, instead of the traditional green circle. Srinivasan et al. (2012) found that the frequency of LT crashes increased when protective LT treatments were replaced with permissive LTs with a FYA, but that when a FYA replaced green-circle permissive or permissive-protective LT treatments, LT crash frequencies decreased. The authors also reported substantial variability in the apparent effect of FYAs across the intersections in their sample. There is currently strong interest in using FYAs to implement within-day changes in LT treatment. That is, protective LT phasing would be used during those times when warranted to reduce delay to LT drivers, or when the risk of LT crashes is unacceptably high, and permissive LT treatments indicated by FYAs would be used during those times when permissive treatments reduce delay and crash risk is acceptably low. This requires being able to predict how the risk for LT crashes changes as intersection and traffic characteristics change within the course of a day.

When predicting operational impacts, micro-simulation programs allow the analyst to specify a richer set of situations than are captured by the *Highway Capacity Manual*, and it has been suggested that simulation programs could play a similar role in predicting safety impacts. In a review of road safety simulation efforts, Archer (2005) identified an ability to "tailor a model to meet the specific criteria of an existing real-world traffic situation" (p. 122) as the major potential advantage to using safety simulation models, but concluded that "… there are few micro-simulation modeling environments that are capable of representing the high level of detail and flexibility for this type of work" (p. 135). More recently Young et al. (2014) noted "there are signs that simulation will become a useful tool in analyzing the safety of the traffic system", but that there are "a number of areas where further work is required." (p. 24). These include using "the crash as the measure of performance" as opposed to simulated surrogate measures, and better knowledge of "driver behavior in crashes." Davis and Aul (2007) described a Monte Carlo simulation model that combined an empirically determined gap selection model with a simple kinematic model for braking by the opposing vehicle. Although this model gave, after some calibration adjustments, results that were reasonable, further development was needed. In particular, the gap selection model in Davis and Aul (2007) was developed using data reported in Davis and Swenson (2004), where the sample size was not large and the approach speeds of opposing traffic were relatively low. Another weakness was that, since crashes tend to be rare events, many millions of simulated gap acceptances were needed to produce a reasonable sample of simulated crashes. This feature is in part responsible for recent focus on simulated surrogate measures either as safety indicators or as additional independent variables in traditional safety performance functions (Shahdah et al., 2015).

This report documents work done to advance the state of art in crash simulation. Chapter 2 describes a field study to collect data on drivers' left-turn gap acceptance and turning times, and development of statistical models that can be incorporated into a crash simulation model. Chapter 3 describes how Markov Chain Monte Carlo computational tools can be used to quantify uncertainty in reconstruction of two-vehicle crashes. Chapter 4 then presents a method for combining the results from Chapter 3 with event data recorder pre-crash data to estimate descriptive features of actual left-turn crashes. This is applied to several left-turn crashes from the National Highway Traffic Safety Administration's NASS/CDS database. Finally, Chapter 5 describes a left-turn crash simulation model incorporating the findings from Chapter 2. Results from Chapter 4, and from a previous case-control study of left-turn crash risk are used to perform initial model checking. Chapter 5 also describes a method for simulating crash modification effects without having to first simulate crashes as rare outcomes in very large numbers of gap acceptances.

CHAPTER 2: MODELING GAP ACCEPTANCE AND CLEARANCE TIME FOR LEFT-TURNING DRIVERS

2.1 LEFT-TURN GAP-ACCEPTANCE

The behavior of drivers when accepting or rejecting gaps affects both the tendency for crashes to occur at a location and the operational efficiency of that location and so continues to be a subject of interest. The *Highway Capacity Manual* (2010) uses a step-function model of gap-acceptance, in which all gaps below a cutoff gap are rejected while all gaps greater than the cutoff are accepted. However, field observation of gap-acceptance quickly reveals, for any cutoff, either instances where gaps below the cutoff are accepted or gaps above the cutoff are rejected. This leads to the idea of allowing the probability of accepting a gap to vary with the gap's features, and several researchers have shown how gap-acceptance can be treated as a discrete choice problem (Daganzo, 1981; Mahmassani and Sheffi, 1981; Madanat et al., 1994; Kita, 1993; Gattis and Low, 1999). This allows modeling of how variables other than gap duration might affect a driver's decision to attempt using a gap, and also allows the statistical methods developed for fitting and testing discrete choice models to be used in gap-acceptance research. As an example, Kita (1993) found that drivers merging onto an expressway were more likely to accept shorter gaps as they approached the end of the merging lane.

It is commonly assumed in gap-acceptance modeling that the time-to-arrival (or gap) of the opposing vehicle is the most reliable feature associated with a gap-acceptance decision. However, human factors research has suggested that the situation may be more complicated. For example, Caird and Hancock (1994) found, in a laboratory study, that their subjects' perceived time-to-arrival was affected by the perceived size of the oncoming vehicle, with a tendency to perceive larger vehicles as arriving sooner than smaller vehicles. Staplin (1995), in a controlled field study, found drivers aged 65 and older tended to identify the same distance to the opposing vehicle as acceptable, irrespective of whether the oncoming vehicle was traveling at 30 mph or 60 mph. This suggests that older drivers tend to select shorter gaps when the speed of the opposing vehicle is high. Davis and Swenson (2004) conducted a field study of LT gap-acceptance, in which permitted LTs at a signalized intersection were recorded on video, with the camera's field of view being large enough to also capture the approaches of opposing vehicles. From the video it was possible to measure the distance and speed of the opposing vehicles when the associated gap became available, as well as the predicted time-to-arrival given by the ratio of distance to speed. Davis and Swenson (2004) found the distance of the opposing vehicle was the most reliable single predictor of whether or not a gap was accepted. They also found that adding speed marginally improved the prediction. Ragland et al. (2006) performed a study of driver's gap-acceptance behavior on permitted left-turns at five intersections in the San Francisco Bay Area. The researchers filtered out gaps of more than 12 sec since these were universally accepted. They took this approach since they only used gap as the predictor for modeling driver's gap-acceptance. This approach, however, precludes one from fully understanding the impact of other factors such as speed and distance. More recently, Hutton et al. (2014) studied LT gap acceptance behavior using data from the Strategic Highway Research Program's Naturalistic Driving Study (NDS). The intent here was to use gap acceptance as a

surrogate for left-turn crash risk, and logistic regression was used to relate the probability of accepting a gap to the gap's duration. They reported that the critical gap, i.e. the gap duration where acceptance and rejection are equally likely, tended to be shorter in situations where sight distance was compromised.

Overall, these findings suggest that a gap-acceptance model which uses simple gap duration as its sole predictor may give misleading results.

2.2 FIELD STUDY OF LEFT-TURN GAP ACCEPTANCE

2.2.1 Data Collection and Reduction

One advantage to assuming that gap duration is the main determinant of gap-acceptance is the relative ease in gathering field data. One simply needs to measure the times between vehicle arrivals using a stopwatch, and record the decisions made by waiting drivers. But with advances in computer and video technology it is now possible to extract vehicle motion data that were previously difficult to obtain. As part of an earlier study (Davis and Mudgal, 2013) video recordings were made of vehicles making left-turns at the intersection of Robert Street (N-S) and Mendota Road (E-W), in Inver Grove Heights, Minnesota and a limited reduction of the video encompassing 39 left-turns, was conducted. In this study the data reduction was extended in include 153 left-turns and a total of 749 gap selection decisions. An overhead view of this intersection is shown in Figure 2.1, where arrows indicate the paths of the conflicting (left-turning and through) vehicles.

Figure 2.1 Data collection site (satellite imagery – Google Maps 2012).

At the time of the study Robert Street had two through lanes and one exclusive left-turn lane in both directions. In addition, south-bound LTs had a brief protective phase followed by a longer permissive phase, indicated by a green circle. Opposing traffic was separated by a double yellow line. The left-turning behavior of south-bound vehicles waiting for adequate gaps in north-bound through traffic was considered in the study. In the Davis and Swenson (2004) study, it was possible to locate the video camera on the roof of a tall building overlooking the study intersection. At Robert and Mendota, however, no convenient rooftop existed, and so portable data collection equipment developed at the Minnesota Traffic Observatory (MTO) was used. This consisted of cabinet, mounted on wheels, which contained equipment for digitally recording video, and a battery to power the camera and recording system. The digital video camera was mounted on a pole which can be raised to a height of about 30 feet. Figure 2.2 shows the equipment while Figure 2.3 depicts the camera's view (looking southward along Robert Street) of the intersection.

Video data had been collected on 11th, 12th and 13th of September 2012. The recording started at about 3 pm on 11th and ended at about 9 am on 13th. The weather on September 11 was sunny and dry but rainy on September 12. The rainy conditions tended to make reduction of video difficult so this study focused on reducing and analyzing data from the peak period (3 PM – 6 PM) on September 11.

Figure 2.2 MTO equipment used in the study.

Figure 2.3 Camera view of the intersection (looking southward along Robert Street).

Left-turn events (arriving, waiting for a gap and accepting a gap) were saved into small video clips using VirtualDub (version 1.9.11). Time sequences of x and y coordinates of the vehicle at successive (5 frames per second) video frames were obtained using VideoPoint (version 2.5). As one clicks on the video frame in VideoPoint, the screen coordinates are recorded and the video frame advances. Because of perspective and scale differences between the video image and the real world, the two-dimensional rectification method described by Bleyl (1976) was used to develop equations which transformed the screen coordinates extracted by VideoPoint to the corresponding real-world coordinates. The transformations take the form

$$x_m = \frac{c_1 + c_2 x_p + c_3 y_p}{c_4 x_p + c_5 y_p + 1} \qquad y_m = \frac{c_6 + c_7 x_p + c_8 y_p}{c_4 x_p + c_5 y_p + 1} \tag{2.1}$$

where the eight c_i's are calibration coefficients, the x_m and y_m are the real-world coordinates of a point, and the x_p and y_p are the coordinates of that point in the image on the computer screen. The calibration coefficients were found by using eight sets of known coordinate pairs to create a set of sixteen simultaneous equations with the coefficients as eight unknowns. After solving for the calibration coefficients using least-squares, equation (2.1) gives the corresponding real-world location for anywhere on the screen as long as the entire scene is on a single plane. Due to the flat nature of the area under observation, this assumption was deemed acceptable, but to check the accuracy of the method other known points in the screen image were translated, with results that were accurate to within three feet for measurements in a 500-foot field of view.

The output (spreadsheets in .xls format) obtained from VideoPoint was processed using the R statistical language (R Core Team, 2015) to segregate the individual south-bound through vehicles corresponding

to each left-turning vehicle waiting for an adequate gap. As indicated above, each file contained the screen trajectories (x and y co-ordinates) for the opposing vehicles associated with a left-turning vehicle, while inspection of the video gave the left-turning driver's binary choice to accept or reject a gap. If the driver rejected a gap, the next gap began when the front of the opposing vehicle crosses the pedestrian crosswalk on Robert Street. The instant when the opposing vehicle's front bumper crossed the pedestrian crosswalk was taken as the instant when this vehicle was no longer generating a gap. This process continued until a gap was accepted. The process of extracting parameters was automated with R statistical language (R Core Team, 2015) and R2WinBUGS package (Sturtz et al., 2015). Figure 2.4 summarizes the data reduction and analysis tasks along with the software used to accomplish those tasks.

Gap selections which involved opposing vehicles emerging from a driveway (located at about 500 feet upstream of the intersection on Robert Street), or opposing vehicles stopping because the signal turned red, turning right, or turning left, were not considered in the analysis. In addition, situations where the LT vehicle did not encounter any oncoming vehicles (gap of unlimited size) at the time of turning left were also eliminated. In other words, only those opposing vehicles which were in free flow conditions, as either single vehicles or vehicles as part of a moving platoon, were considered in the analysis of gap acceptance behavior.

In addition to data on gaps, the trajectories of the LT vehicles as they made the turning maneuvers were also extracted from the video using Videopoint and rectified to give real-world trajectories. The LT clearance time was defined as the time between when an accepted gap became available and when the turning vehicle passed the point of conflict with the opposing vehicle, and this was obtained for each turning movement.

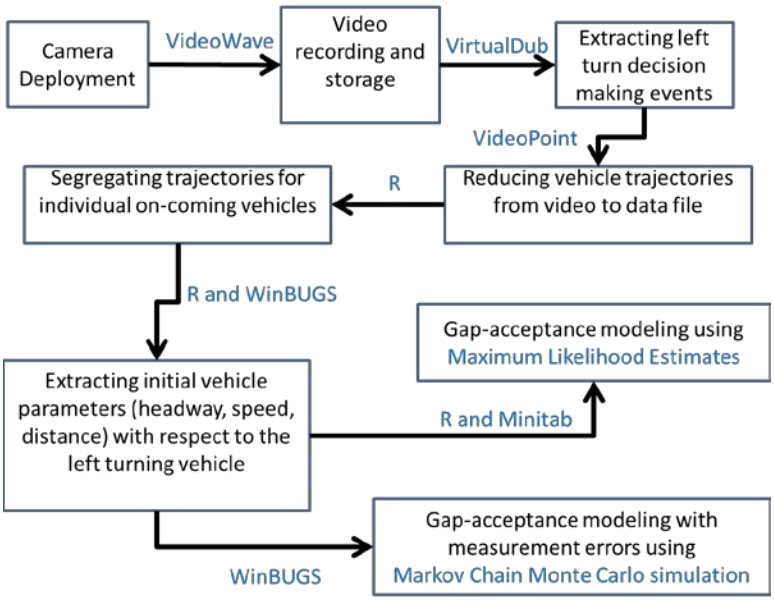

Figure 2.4 Flow chart for data reduction and analysis.

Table 2.1 Descriptive statistics for opposing vehicle characteristics, all vehicles

	Mean	Std. Deviation	25%	50%	75%	Mean from (Davis & Swenson 2004)
Gap (sec)	3.7	2.6	1.9	2.9	4.7	3.50
Speed (mph)	35.6	9.0	28.4	35.4	42.3	21.6
Distance (feet)	188.2	136.8	99.0	148.6	234.7	135.7
Clearance Time (sec)	3.0	1.0	2.4	2.8	3.5	---

The final data set of this study comprised of 749 gap choices made by 153 left-turning drivers. Table 2.1 shows summary statistics for the opposing vehicles. Note that the average speed (36 mph) of the opposing vehicles was higher than that observed in the Davis and Swenson (2004) study where the average speed was 22 mph. Moreover, note the higher average distance in the present study. Both of these parameters depict that the characteristics of gap decision for the left-turning drivers were different from the earlier study. Table 2.2 and Table 2.3 shows summary statistics for the opposing vehicles for accepted and rejected gaps, respectively. Figure 2.5-Figure 2.7 show distributions of gap duration, speed, and distance for accepted and rejected gaps.

Table 2.2 Descriptive statistics for opposing vehicle characteristics, accepted gaps

	Mean	Std. Deviation	25%-ile	50%-ile	75%-ile
Gap (sec)	7.2	2.7	5.2	6.7	8.7
Speed (mph)	34.3	7.9	27.8	33.9	40.2
Distance (feet)	360.0	161.4	250.3	316.2	430.9

Table 2.3 Descriptive Statistics for Opposing Vehicle Characteristics, Rejected Gaps

	Mean	Std. Deviation	25%-ile	50%-ile	75%-ile
Gap (sec)	2.8	1.6	1.8	2.5	3.4
Speed (mph)	36.0	9.3	28.4	36.0	42.6
Distance (feet)	142.6	82.9	91.2	127.3.3	172.9

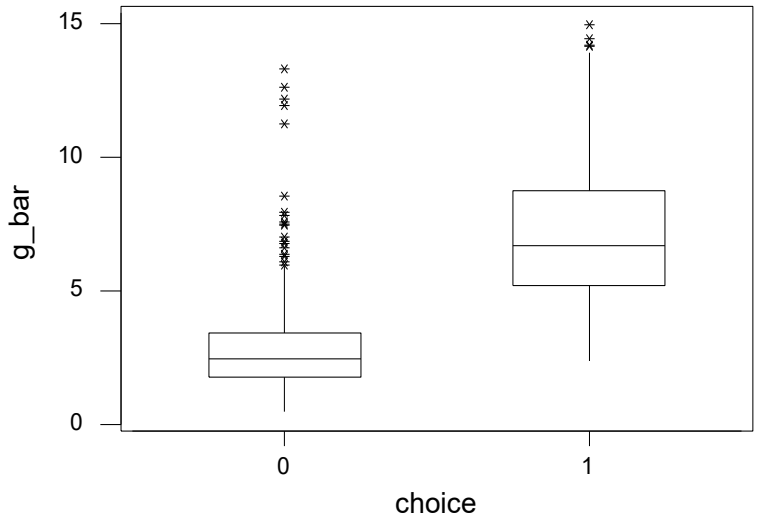

Figure 2.5 Boxplot for rejected (choice=0) and accepted (choice=1) gap durations, in seconds.

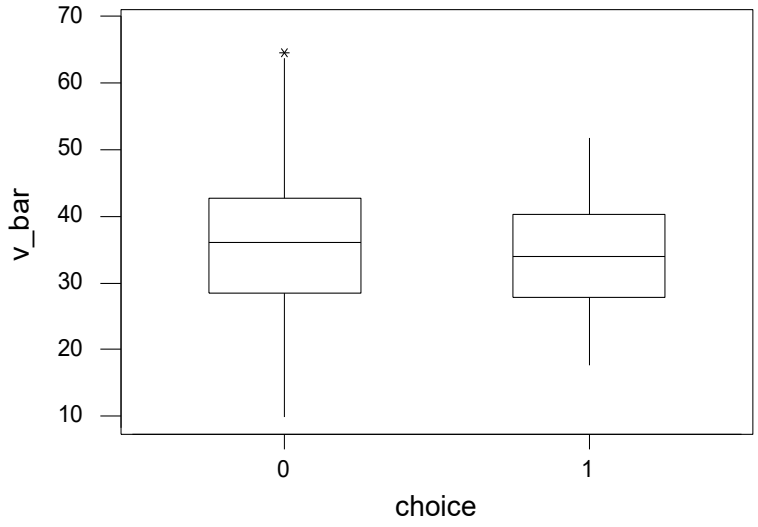

Figure 2.6 Boxplot for rejected (choice=0) and accepted (choice=1) opposing vehicle speeds, in mph.

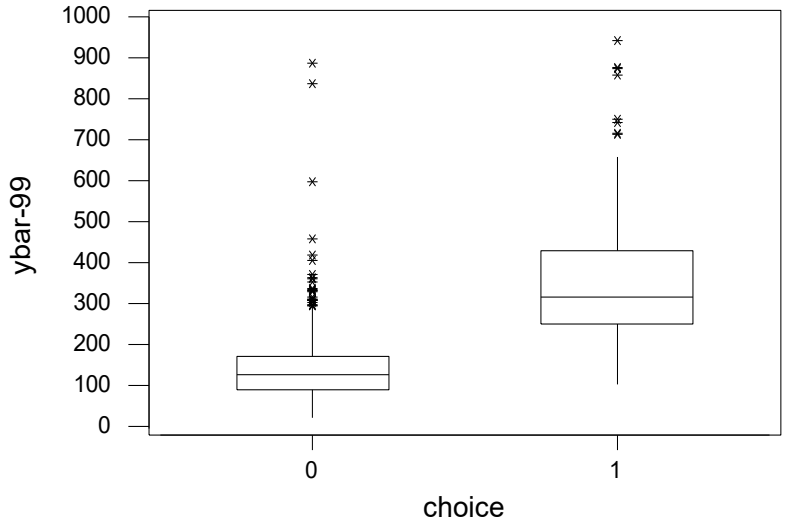

Figure 2.7 Boxplot for rejected (choice=0) and accepted (choice=1) opposing vehicle initial distances, in feet.

2.3 FITTING GAP ACCEPTANCE MODELS

As indicated above, the primary objective of this study was to identify physical variables that were most reliably associated with gap-acceptance decisions. Logit models of the form:

$$\pi_i = \frac{\exp(\beta_0 + \sum_{k=1}^{p} \beta_k (x_{i,k}))}{1 + \exp(\beta_0 + \sum_{k=1}^{p} \beta_k (x_{i,k}))} \qquad (2.2)$$

were used to related gap features to the acceptance/rejection decision. Here π_i denotes the probability that gap i is accepted, $x_{i,k}$ denotes the value of variable k for gap i, and the β_k denote coefficients to be estimated. Nine models, with different combinations of gap, speed, and distance as predictors, were fit using maximum likelihood, taking the Bayes posterior means of each opposing vehicle's features as error-free measurements. To assess model fit, the negative log likelihood (or equivalently, the deviance) can be used, with smaller values being indicative of better fit. However, since adding parameters to a model never decreases the likelihood, this criterion will be biased in favor of less parsimonious models. To account for this, penalized likelihood methods add a penalty to the likelihood, with the penalty term increasing as the number of parameters increases, but at present there appears to be no consensus on which penalty term is most appropriate. Carlin and Louis (2000) have suggested using the Bayesian Information Criterion (BIC), given by

BIC = -2*LL + p*log(N) (2.3)

where LL denotes log likelihood, p is the number of parameters used by the model, and N is the number of data points. In addition, the Hosmer-Lemeshow chi-squared test (Hosmer and Lemeshow, 2000), which compares an observed distribution of gap choices to that predicted by the fitted model, was computed.

Table 2.4 Estimation results for 5 gap acceptance models using untransformed predictors

Model	Predictors	Estimate	Standard Error	Z-statistic	BIC	Hosmer-Lemeshow
1	Constant	-3.4	1.5	-2.3	421.7	25.0 (0.002)
	gap	0.33	0.30	1.1		
	speed	-0.06	0.04	-1.5		
	distance	0.013	0.006	2.0		
2	**Constant**	**-5.48**	**0.37**	**-14.7**	**413.3**	**27.3 (0.001)**
	gap	**0.94**	**0.075**	**12.5**		
3	Constant	-0.61	0.36	-1.7	778.3	13.1 (0.109)
	speed	-0.02	0.01	-2.0		
4	Constant	-5.1	0.34	-14.7	452.9	18.7 (0.017)
	distance	0.017	0.0014	12.2		
5	**Constant**	**-1.9**	**0.56**	**-3.4**	**415.5**	**21.3 (0.006)**
	speed	**-0.11**	**0.02**	**-6.0**		
	distance	**0.019**	**0.0016**	**12.2**		

Table 2.4 shows estimated coefficients and goodness-of-fit results for five models which used untransformed speed, distance, and/or gap as predictors of gap acceptance. Each of these was fitted using maximum likelihood, and smaller values of the BIC criterion indicate better fit. Of these the model which used gap only as its predictor had the lowest BIC (413.3), while the model which used speed and distance as predictors was only slightly worse (BIC=415.5). Note though that for both of these the Hosmer-Lemeshow goodness of fit test was statistically significant at that 0.01 level, suggesting weak fit between the models and the data.

Table 2.5 Estimation results for four models using log-transformed gap, speed, or distance as decision predictors

Model	Predictors	Estimate	Standard Error	Z-statistic	BIC	Hosmer-Lemeshow
6	**Constant**	**-8.3**	**0.6**	**-13.0**	**375.5**	**8.8 (0.363)**
	Log(gap)	**4.8**	**0.4**	**12.2**		
7	Constant	0.5	1.2	0.5	779.9	14.3 (0.074)
	Log(speed)	-0.5	0.3	-1.6		
8	Constant	-24.6	2.0	-12.5	416.1	7.8 (0.455)
	Log(distance)	4.4	0.4	12.2		
9	**Constant**	**-14.3**	**2.3**	**-6.2**	**377.9**	**7.8 (0.456)**
	Log(speed)	**-3.8**	**0.6**	**-6.2**		
	Log(distance)	**5.0**	**0.4**	**12.1**		

Table 2.5 summarizes results from fitting four additional models with similar structure to those appearing in Table 2.4, but now with the natural logarithms of the speed, distance and gap as predictors. Using BIC, the best fitting model of these is the one with log-gap as the sole predictor (BIC=375.5) followed by the model with the logarithms of speed and distance as predictors (BIC=377.9). For both of these the Hosmer-Lemeshow tests indicate that hypotheses of adequate fit would not be rejected. Note also that in all cases, the BIC values for the models in Table 2.5 are substantially lower than those of their counterparts in Table 2.4

The above analyses used only the BIC and the Hosmer-Lemeshow goodness-of-fit test to check model adequacy. Since the Hosmer-Lemeshow goodness-of-fit statistic is asymptotically distributed as chi-squared only when the expected frequencies are "large," it is recommended that all expected frequencies be greater than five to guarantee that the p-value using the chi-squared distribution be accurate enough to support hypothesis testing (Hosmer and Lemeshow, 2000). For example, Table 2.6 shows the observed (O) and estimated expected (E) frequencies for each decile of the Hosmer-Lemeshow test from the "best" model so far, Model 6.

Table 2.6 Observed (O) and estimated expected (E) frequencies for each decile of gap acceptance probability, defined by fitted values (Prob.) from Model 6

Decile	Prob.	Choice = 1 (Accept)		Choice = 0 (Reject)		Total
		O	E	O	E	
1	0.00141	0	0.4198964	75	74.95801	75
2	0.00401	0	0.18843282	75	74.81157	75
3	0.00879	0	0.47078035	75	74.52922	75
4	0.0203	1	1.05712815	74	73.94087	75
5	0.041	1	2.29528348	74	72.70472	75
6	0.0932	2	4.81668829	72	69.18331	74
7	0.192	11	10.198009	64	64.80199	75
8	0.457	28	22.83854503	47	52.16145	75
9	0.777	50	46.71567303	25	28.28433	75
10	0.992	64	68.38547021	11	6.62453	75

Examining Table 2.6, six estimated expected frequencies are less than the recommended minimum of five. We could combine those adjacent six rows to increase the estimated expected frequencies, but

doing so would reduce the number of degrees-of-freedom, causing the Hosmer and Lemeshow test to lose power. The developers of the test point out that when Hosmer-Lemeshow goodness-of-fit statistic is calculated from fewer than six groups the null hypothesis that the model fits will almost never be rejected (Hosmer and Lemeshow, 2000).

Considering the limitation of using Hosmer-Lemeshow goodness-of-fit test in this case, the overall assessment of model fit was examined using a combination of tests including the Hosmer-Lemeshow test, the Osius and Rojek (Osius and Rojek, 1992) normal approximation to the distribution of the Pearson chi-square statistic, and Stukel's (Stukel, 1988) test, as suggested by Hosmer et al. (1997). In addition, the area under the receiver operating characteristic curve (AUC), indicating how well the model predicts (Hanley and McNeil, 1982), was calculated.

Table 2.7 Goodness-of-fit measures for 5 gap acceptance models using untransformed predictors

Model	BIC	Hosmer-Lemeshow	Osius&Rojek	Stukel	AUC
1	420.9942	24.968 (0.001574)	0.2203661 (0.8255861)	50.779 (9.409e-12)	0.9428
2	413.2593	27.305 (0.0006262)	0.2867775 (0.7742827)	52.759 (3.496e-12)	0.9437
3	778.2583	12.925 (0.1144)	-0.03751255 (0.9700763)	7.1018 (0.007701)	0.5477
4	452.9343	18.849 (0.01569)	0.4575692 (0.647262)	47.344 (5.241e-11)	0.9279
5	415.6524	21.303 (0.006385)	0.2476949 (0.8043705)	50.627 (1.015e-11)	0.9403

Windmeijer (1998) points out that one should use Osius and Rojek test with caution. According to Windmeijer, large or small estimated probabilities, near 1 or 0, should be excluded when computing the test statistic. In our analysis, thresholds for large and small predicted probabilities were adopted from the default value in Weesie's (1998) STATA (StataCorp, 1999) program, namely 1.0×10^{-5} and $1-1.0\times10^{-5}$. Stukel's test is not actually a goodness-of-fit test since "it does not compare observed and fitted values"

(Hosmer and Lemeshow, 2000). This test can be used to check the adequacy of the proposed model by comparing it to one with two additional predictors that allow for either heavier or lighter tails than the standard logit regression model does. Table 2.7 and Table 2.8 summarize the goodness-of-fit measures applied to the nine models described above.

Table 2.8 Goodness-of-fit measures for 4 gap acceptance models using log-transformed predictors

Model	BIC	Hosmer-Lemeshow	Osius&Rojek	Stukel	AUC
6	375.5102	8.7563 (0.3633)	-0.0006457371 (0.9994848)	16.365 (0.0002796)	0.9437
7	779.8727	14.14 (0.07818)	0.5192112 (0.6036135)	8.7716 (0.00306)	0.5477
8	416.7163	7.9446 (0.4389)	0.0004981756 (0.9996025)	10.051 (0.006568)	0.9279
9	377.8541	7.819 (0.4513)	-0.0005885429 (0.9995304)	15.324 (0.0004704)	0.9461

Using a 0.05 significance level, the Osius and Rojek tests indicate that the null hypothesis that model fits would not be rejected for all 9 models, while the null hypothesis of adequate fit in Stukel's tests would be rejected for all 9 models. Judging by the AUC, Model 3 and Model 7 show poor predictive ability, while other 7 models have good and similar predictive ability. Model 6 still seemed to be the "best" model, and further analysis on it was done. In order to improve model fit, two types of modifications were made to Model 6: (1) centering the predictor "log(gap)"; and (2) adding a quadratic term of predictor "log(gap)", $(\log(gap))^2$. Table 2.9 summarizes results from fitting Model 6 and its variants resulting from two modifications mentioned above.

As Table 2.9 indicates, centering the predictor generated little difference in coefficient estimates as the range of gaps was not very wide. Additional discussion will thus focus on models with the non-centered predictors.

Table 2.9 Estimation results for 4 gap acceptance models on the basis of Model 6

Model	Predictors	Estimate	Standard Error	Z-statistic
6	(Intercept)	-8.2736	0.6376	-12.98
	log(gap)	4.8475	0.3963	12.23
6-1	(Intercept)	-16.664	2.5458	-6.546
	log(gap)	15.3885	2.9224	5.266
	$(\log(gap))^2$	-3.1762	0.8187	-3.88
6-2	(Intercept)	-2.906	0.2283	-12.73
	centered log(gap)	4.8475	0.3963	12.23
6-3	(Intercept)	-3.5189	0.3625	-9.707
	centered log(gap)	8.3545	1.1517	7.254
	$(\text{centered } \log(gap))^2$	-3.1762	0.8187	-3.88

The quadratic term of "log(gap)", $(\log(gap))^2$, showed a statistically significant effect on LT gap acceptance probability at 0.05 significance level. A likelihood ratio test comparing Model 6 and Model 6-1 was conducted and the results are displayed in **Error! Not a valid bookmark self-reference.**.

According to the L-R test results, the null hypothesis that the reduced model (Model 6, without quadratic term) is equivalent to Model 6-1 was rejected at 0.05 significance level and it could be concluded that adding quadratic term statistically significantly improved model fit at 0.05 significance level.

Table 2.10 Likelihood ratio test results for Model 6 and Model 6-1

Model	#Df	Loglik	Df	Chisq	Pr(>Chisq)	Signif. codes
6	2	-181.15	1	15.185	9.745e-05	***
6-1	3	-173.12				

Table 2.11 Goodness-of-fit measures of Model 6 and Model 6-1

Model	BIC	Hosmer-Lemeshow	Osius&Rojek	Stukel	AUC
6	375.5102	3.6893 (0.595)	-0.001224183 (0.9990232)	16.365 (0.0002796)	0.9437
6-1	**366.9435**	**2.2296** **(0.8165)**	**2.592826e-05** **(0.9999793)**	**1.7532** **(0.4162)**	**0.9439**

Table 2.11 shows the goodness-of-fit measures of Model 6 and Model 6-1. Model 6-1, with the quadratic term of "log(gap)", has a lower BIC than Model 6, indicating better fit. The null hypothesis of Hosmer-Lemeshow goodness-of-fit test and Osius and Rojek test that model fits the data, would not be rejected at 0.05 significance level for both models. Stukel's test results indicate inadequate fit of Model 6 but adequate fit of Model 6-1 at 0.05 significance level. AUC values suggest that those two models have similar predictive power. To sum up, Model 6-1 seems to be "best" model among all models established and has adequate fit.

Figure 2.8 shows the fitted curves of Model 6 and Model 6-1.

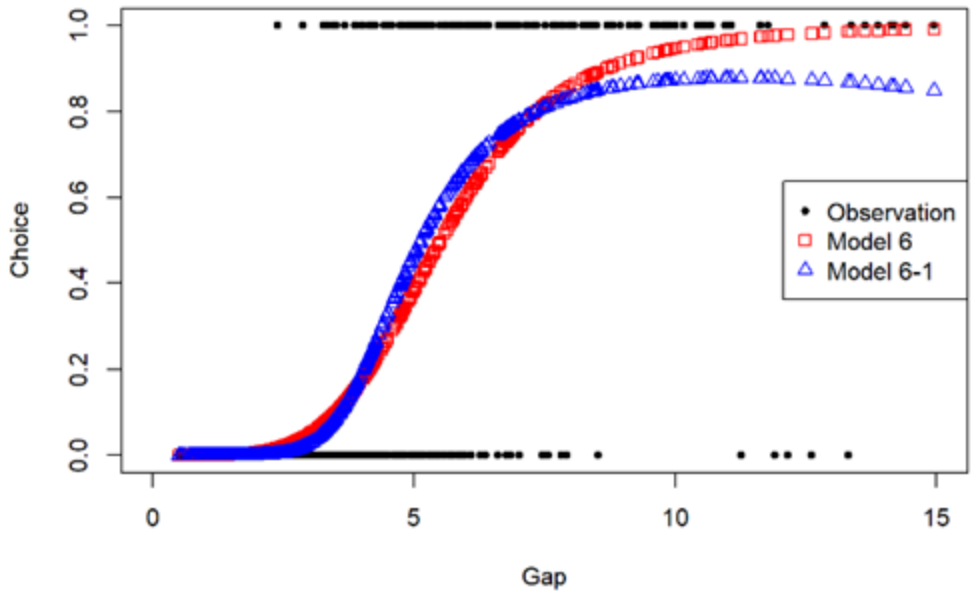

Figure 2.8 Fitted curves of Model 6 and Model 6-1.

Judging from Figure 2.8, Model 6 tends to overestimate gap acceptance probabilities at the tails of the gap distribution, short (<4.0 secs) or long (>8.0 secs) gaps. Note also that gap acceptance probability in Model 6-1 reaches a maximum that is lower than 1.0. The maximum gap acceptance probability estimated from Model 6-1 was approximately 0.88 and the gap corresponding to this probability was approximately equal to exp(-15.3885 /(2× -3.1762)) ≈ 11.27341 seconds, which is within the range of gaps where there were very few rejections (Figure 2.8).

As LT crashes tend to occur only when the available gap is less than LT turning time, interest here focused on the shorter gaps where a LT crash is more likely to occur. For this reason, logit regression analysis on the best models previously selected, namely Model 6 and Model 6-1, was done with cases where gaps greater than the maximum LT turning time (8.0 secs) were excluded.

Table 2.12 shows estimated coefficients for Model 6 and Model 6-1 based on cases with gaps not exceeding the maximum LT turning time only. As can be seen, the quadratic term (log(gap)) 2, now shows an insignificant effect on LT gap acceptance. A likelihood ratio test comparing Model 6 and Model 6-1 was conducted and the results are displayed in Table 2.13.

Table 2.12 Estimation results for model 6 and model 6-1 based on cases with gap not exceeding the maximum LT turning time

Model	Predictors	Estimate	Standard Error	Z-statistic
6	(Intercept)	-9.3363	0.8104	-11.52
	log(gap)	5.5719	0.5155	10.81
6-1	(Intercept)	-15.212	4.121	-3.691
	log(gap)	13.613	5.391	2.525
	(log(gap)) 2	-2.662	1.736	-1.534

Table 2.13 Likelihood ratio test results for model 6 and model 6-1 based on cases with gap not exceeding the maximum LT turning time

Model	#Df	Loglik	Df	Chisq	Pr(>Chisq)	Signif. codes
6	2	-155.07	1	2.7771	0.09562	.
6-1	3	-153.68				

(Signif. codes: 0 '***' 0.001 '**' 0.01 '*' 0.05 '.' 0.1 ' ' 1)

According to the L-R test results, the null hypothesis that the reduced model (Model 6, without quadratic term) holds would not be rejected at 0.05 significance level and it could be concluded that adding quadratic term did not statistically significantly improve model fit.

Finally, Table 2.14 shows the goodness-of-fit measures of Model 6 and Model 6-1. Model 6, without the quadratic term of "log(gap)", has slightly lower BIC than Model 6-1, indicating better fit. The null hypothesis of Hosmer-Lemeshow goodness-of-fit test and Osius and Rojek test that model fits, would not be rejected at 0.05 significance level for both models. Stukel's test results indicate that both models are adequate at 0.05 significance level. AUC values suggest that the predictive probability of those two models are almost the same. Since adding the quadratic term would not statistically significantly improve model fit at 0.05 significance level, Model 6 was regarded as the best model when only cases with gaps not exceeding the maximum LT turning time were considered. Figure 2.9 shows the fitted curves of Model 6 and Model 6-1.

Table 2.14 Goodness-of-fit measures for model 6 and model 6-1 based on cases with gap not exceeding the maximum LT turning time

Model	BIC	Hosmer-Lemeshow	Osius&Rojek	Stukel	AUC
6	**323.2141**	**3.4678** **(0.6283)**	**-0.001354209** **(0.9989195)**	**3.2437** **(0.1975)**	**0.9325**
6-1	326.9766	3.1006 (0.6845)	-0.0002782522 (0.999778)	0.2408 (0.8866)	0.9325

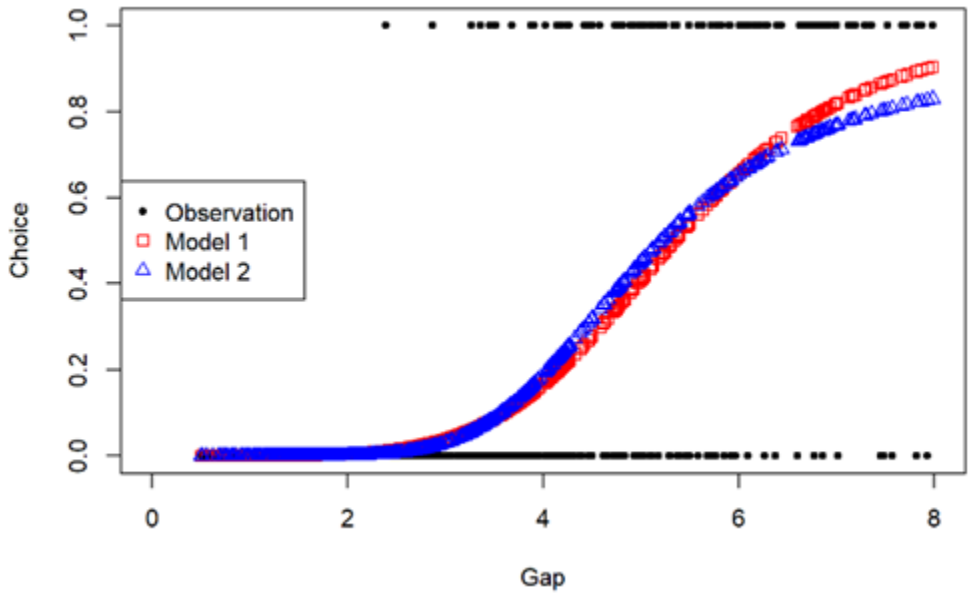

Figure 2.9 Fitted curves of model 6 and model 6-1 based on cases with gaps not exceeding the maximum LT turning time.

As shown in Figure 2.9, after cases with gap exceeding the maximum LT turning time being excluded from logit regression analysis, the prediction difference between Model 6 and Model 6-1 is not as outstanding as shown in Figure 2.8. It seems that, in previous analyses where all cases were considered, the function of the quadratic term was to account for observed rejections of long gaps where LT crashes are not likely to occur.

2.4 ANALYSIS OF LEFT-TURNING TIMES

As noted in Section 2.2 , the trajectories of the LT turning vehicles were also extracted from the video and rectified to give real-world positions. The time elapsing between when a gap became available and when the turning vehicle passed the point of conflict was recorded and these became data on clearance

times. Table 2.15 presents descriptive statistics for the clearance times while Figure 2.10 is a histogram summarizing the distribution of the clearance times.

Table 2.15 Descriptive statistics for LT clearance times

	Mean	Std. Deviation	25%	50%	75%
Clearance time (sec)	3.0	1.0	2.4	2.8	3.5

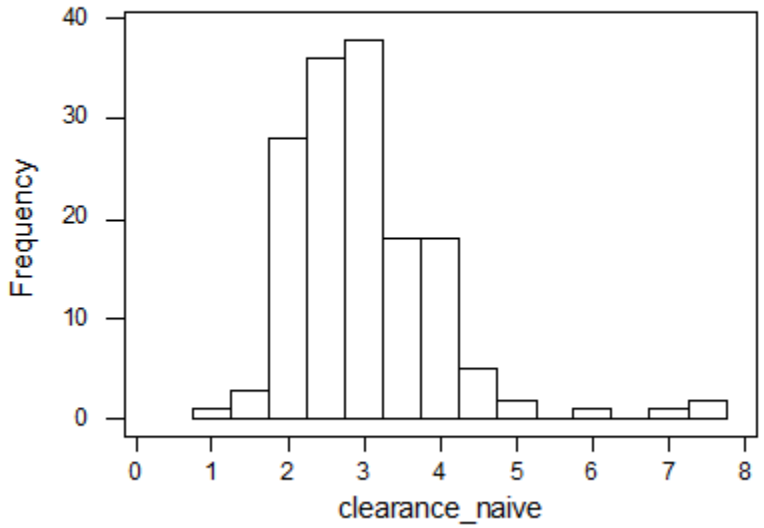

Figure 2.10 Histogram for left-turn clearance times.

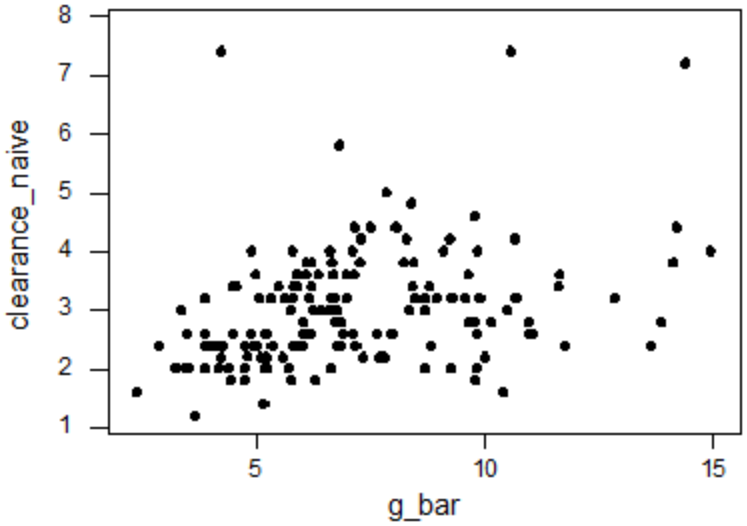

Figure 2.11 Scatter plot of Clearance Time vs Gap.

Figure 2.11 shows a scatterplot of clearance time versus accepted gap duration and there appears to be a positive relation between the two. That is, there appears to be a tendency for drivers who accepted longer gaps to also take longer to complete their turning movements. Figure 2.10 shows that the distribution of clearance times is skewed, and since the natural logarithm of gap duration was the best predictor of gap acceptance, a linear regression model relating log-clearance to time to log-gap was estimated and the results of this exercise are shown Table 2.16. Figure 2.12 shows a normal probability plot of the residuals from the model described in Table 2.16, and indicates that these are approximately normally distributed.

Table 2.16 Results from regressing the logarithm of clearance time against the logarithm of accepted gap duration

Predictors	Estimate	Standard Error	Z-statistic
Constant	0.46	0.12	3.7
Log(gap)	0.32	0.063	5.0

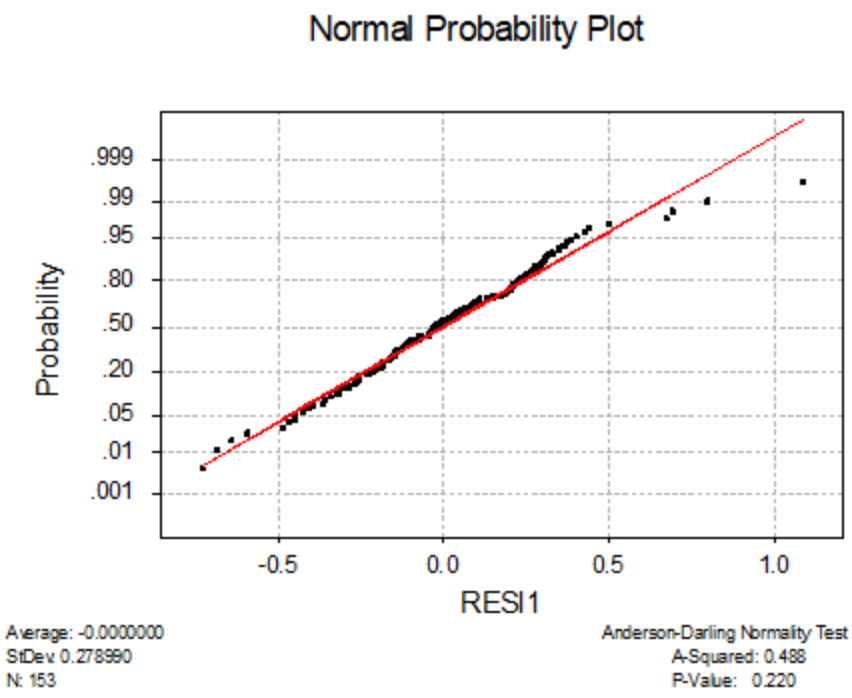

Figure 2.12 Normal probability plot of log-clearance time residuals.

CHAPTER 3: BAYESIAN UNCERTAINTY QUANTIFICATION FOR PLANAR IMPACT CRASHES

3.1 INTRODUCTION

As noted in Chapter 1, this project aims to develop a simulation model for left-turn crashes at signalized intersections. Timing a traffic signal often involves deciding on whether to offer protected or permitted left-turn treatments and the project's goal is to model how crash risk might vary as traffic conditions vary. Chapter 2 described a statistical model of left-turn gap selection, developed from video data collected at a typical signalized intersection, while Chapter 5 describes the prototype simulation model that combines this gap selection model with a simple kinematic model describing braking by opposing drivers. As part of testing and validation it was decided to compare features of crashes as simulated by the model to features of actual left-turn crashes estimated from crash reconstruction, including the speeds of the involved vehicles at impact. The National Highway Traffic Safety Administration's NASS/CDS database was mined to identify left-turn crashes and Figure 3.1 shows the scene diagram from one of these cases. Information about the crash included make, model, and year of each involved vehicle, crush measurements and the resulting delta-V estimates, and data downloaded from the vehicles' event data recorders (EDR).

For this case, the lack of tire mark information, the post impact rotation by the turning vehicle, and the possibility that the opposing driver continued steering and braking after the crash suggested that reconstruction relying on post-impact skids and conservation of linear momentum would be problematic. A spreadsheet-based reconstruction tool for two-vehicle crashes, using planar impact mechanics (PIM), has been developed by Brach and Brach (2011) where measurements of a set of parameters describing the vehicles and the collision configuration, and values for the vehicles' pre-impact speeds, can be used to predict post-impact speeds along with a variety of additional features such as total energy loss, crush energy, departure angles, and delta-V values. The tool also supports a very flexible method, using nonlinear least-squares (NLS), which can invert the reconstruction model and produce estimates of selected input features, such as pre-impact speeds, that best reproduce a set of measured outputs. The flexibility of this approach has recently been illustrated by Brach et al. (2015) but an open question is how to quantify the uncertainty that results when the model's inputs are more or less uncertain. The complexity of the equations underlying PIM precludes using simple interval arithmetic or statistical differentials, but Brach and Brach (2011) illustrate how sensitivity to uncertainty in a single input can be assessed by computing NLS estimates from lower and upper bounds on the uncertain quantity. For assessing the effect of multiple uncertain inputs Monte Carlo (MC) simulation is suggested. MC simulation has been appearing in the crash reconstruction literature for at least 20 years, with both Wood and O'Riordain (1994) and Rose et al. (2001) applying MC simulation to two-vehicle crashes. Researchers have linked Monte Carlo simulation with the simulation model PC-Crash (Moser et al., 2003), and have offered suggestions for using MC simulation (Ball et al., 2007). All these applications have a common structure: a computer simulates a random sample from probability distributions characterizing prior uncertainty about input variables and a model is then used to predict

outputs. Those sample inputs which generate outputs satisfying a set of constraints are accepted, while input values that fail to satisfy the constraints are rejected. The result is a sample from the conditional distribution for the inputs, given the constraints on the outputs. In Bayesian statistics this conditional distribution is called a posterior distribution.

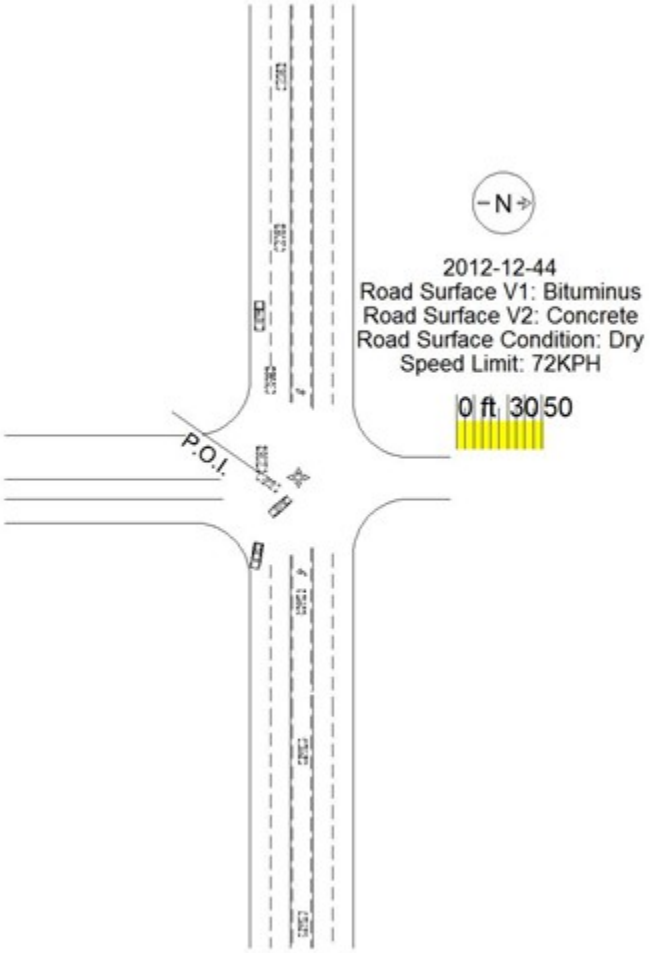

Figure 3.1 Scene diagram from NHTSA case 2012-12-044.

At about the same time that MC methods began appearing in the crash reconstruction literature, statisticians were extending computational techniques originally developed in physics (Metropolis et al., 1953) to solve an increasingly broad range of inference problems. The basic idea was to use a computer to simulate the outcomes of a Markov chain which had been constructed so that its stationary (i.e. long run) distribution was the desired posterior distribution, thus the name Markov Chain Monte Carlo (MCMC). MCMC methods have been used to reconstruct vehicle-pedestrian crashes, road-departure crashes, and two-vehicle crashes where post-crash rotation was not present (Davis, 2003; 2011; 2015).

The next section describes the Bayes crash reconstruction methodology. This is followed by example applications that include (1) crashes that were previously reconstructed by NLS, (2) staged crashes from the Research Input for Computer Simulation of Automobile Crashes (RICSAC) project, and (3) an additional staged crash from the 2016 ARC-CSI conference.

3.1.1 Bayes Crash Reconstruction and Markov Chain Monte Carlo

To begin, consider estimation of a vehicle's initial speed, denoted by v, from a known braking distance, d. The two quantities are related by the structural equation

$$d = \frac{v^2}{2\mu g} \qquad (3.1)$$

with μ denoting the braking drag factor and g the gravitational acceleration. Given values for μ and d equation (3.1) can be inverted to give an estimate of the speed v. For example, if d = 75 feet and μ = 0.725 then the speed at the start of braking would be

$$v = \sqrt{2(.725)(32.2)(75)} \approx 59 \ ft/\sec$$

It may happen though that the drag factor is not known precisely or the braking distance is subject to measurement error. For instance, bounds such as (0.55 ≤ μ ≤ 0.9) and (65 feet ≤ d ≤ 85 feet) might arise when little is known about pavement condition or the vehicle's braking effectiveness, and where the tires have left multiple, poorly-defined skidmarks of different lengths. If we are willing to follow Lindley (1991) and Draper (2013), and agree that probability theory is an appropriate logic for reasoning about uncertainty, then the problem becomes one of Bayesian inference, where a probability distribution describing our prior uncertainty about v and μ is updated, via Bayes theorem, to reflect how this prior uncertainty changes when given a measurement of the stopping distance. For example, if prior to obtaining measurements the uncertainty about v was described by a uniform distribution bounded by 20 feet/second and 100 feet/second, while the prior uncertainty about μ was described by a uniform distribution bounded by 0.55 and 0.9, then the posterior probability distribution for v given 65 ≤ d ≤ 85 can be computed and is displayed in Figure 3.2, along with v's uniform prior distribution. The posterior mean for v would be 59.2 feet/second with posterior standard deviation of 4.7 feet/second.

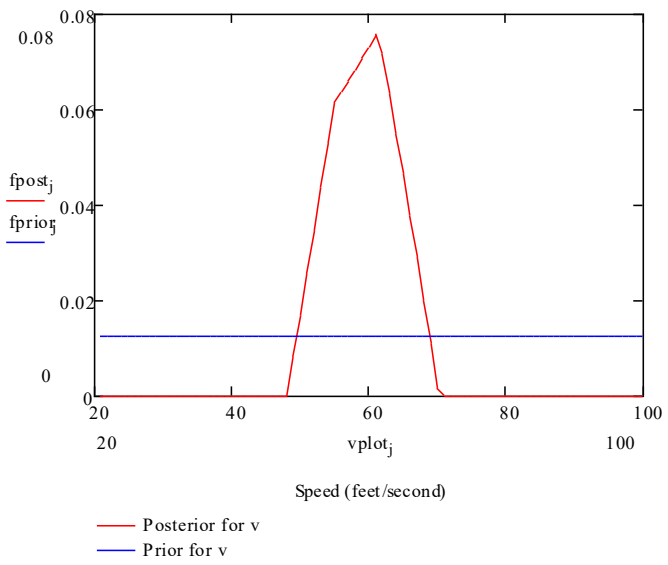

Figure 3.2 Example prior (blue line) and posterior (red line) probability distributions for vehicle's speed at the start of skid.

For this simple example it was possible to compute the posterior distribution for the speed v by employing algebra and numerical integration. For more complex models, such as the PIM model, this approach will not usually be feasible and here it remains an open question how best to account for uncertainty. MC simulation can be implemented by using a computer to simulate random samples from the prior distributions for μ and v, computing d using equation (3.1) and then rejecting those (v, μ) pairs that lead to d-values not satisfying the constraint $65 \le d \le 85$. This gives a simulated sample of the posterior probability distribution $f(v, \mu | 65 \le d \le 85)$. The posterior means, variances, and probabilities for v can then be computed by simple averaging. Applying this, an initial MC sample of 50,000 produced 4867 acceptable (v, μ) pairs, with an average initial speed of 59.1 feet/second and a standard deviation of 4.7 feet/second. This rejection rate is similar to others reported in the literature (Rose et al., 2001).

One of the simpler variants of MCMC is the Gibbs sampler (Geman and Geman, 1984). Applying Gibbs sampling to the stopping distance example leads to the following iteration:

1) Set an initial value for the drag factor μ_0, let i = 1
2) Sample v_i from a uniform distribution bounded by
$$\left(\sqrt{2\mu_{i-1}g(65)}, \sqrt{2\mu_{i-1}g(85)}\right)$$
3) Sample μ_i from a uniform distribution bounded by
$$\left(\max\left(0.55, \frac{v_i^2}{2g(85)}\right), \min\left(0.9, \frac{v_i^2}{2g(65)}\right)\right)$$
4) Let i=i+1

50,000 iterations of this algorithm gave an average initial speed of 59.25 feet/second and a standard deviation of 4.7 feet/second. Figure3. 3 shows the posterior distribution for the initial speed as simulated by the both MC rejection sampling and Gibbs sampling.

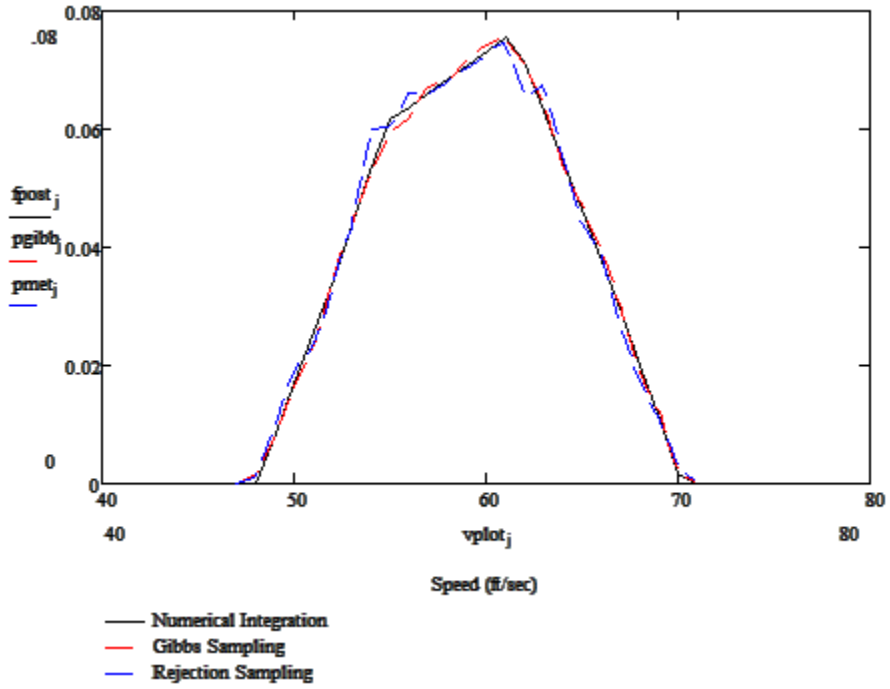

Figure 3.3 Posterior distributions for braking distance example.

3.2 EXAMPLES OF PIM-BASED CRASH RECONSTUCTION USING MCMC

3.2.1 Examples Comparing Bayes Reconstruction to NLS-Based Reconstructions

3.2.1.1 Example 1 – Reconstruction of an Intersection Collision, without EDR Data

Table 3.1 Bayes estimates of Vehicle 2 impact speed for Example 1

Variable	Posterior Summary				NLS Value
	Mean	Standard Deviation	2.5 %-ile	97.5 %-ile	
Estimate, Impact speed Vehicle 2 (feet/second)	55.8	5.6	44.8	66.4	55.5

Our first example is taken from Example 1 of Brach et al. (2015), and involved an angle crash at the intersection of a main road and a driveway. Here it was assumed that the post impact directions for

both vehicles were known from the crash scene diagram, that normal crush energy loss had been measured, and that the initial speed of vehicle 1 was known. Nonlinear least squares (NLS) was used to find the estimates for the initial speed of vehicle 1 and the coefficient of restitution that best reproduced the exit directions. The coefficient of restitution was constrained to be between 0 and 0.2 and the predicted crush energy was constrained to be within 50% of the measured value. One useful feature of Brach and Brach's PIM model is that it is very well-documented. The PIM model was coded in the MCMC tool WinBUGS (Lunn et al., 2013); simple Monte Carlo simulation was then used to test the code and identify coding errors. Once this debugging was complete Bayesian inference was carried out assuming that the measured exit angles were subject to normally-distributed measurement error having a standard deviation of 5 degrees while the measured crush energy was assumed to have a measurement error standard deviation of 13,000 foot-lbs. This latter value was chosen to roughly correspond to the ±50% constraint used in Brach et al. (2015). The coefficient of restitution was given an informative prior distribution that was uniform over (0, 0.2) while the prior for the impact speed of Vehicle 2, uniform over the interval (-100 feet/second, 100 feet/second), was essentially non-informative. Table 3.1 summarizes the results for this case.

3.2.1.2 Example 2 – Reconstruction of an Intersection Collision, with EDR Data

Table 3.2 Bayes estimates of Vehicle 2 impact speed and restitution coefficient for Example 2

Variable	Posterior Summary				
	Mean	Standard Deviation	2.5%-ile	97.5%-ile	NLS Value
Estimate, Impact speed Vehicle 2 (feet/second)	69.5	5.0	60.9	77.6	70.4
Restitution coefficient	0.13	0.08	0.007	0.28	0.109

Our second example is taken from Example 2 of Brach et al. (2015), an angle crash between a westbound vehicle equipped with an EDR and a southbound vehicle that did not have an EDR. The EDR in vehicle 1 provided measurements of the longitudinal and lateral delta-Vs associated with the crash and pre-impact speed measurements, at one-second intervals, for approximately five seconds before the crash. As with Example 1 the post-crash exit angles for the two vehicles were measured from the scene diagram, but now EDR data from vehicle 1 replaced the crush energy measurement. Using pre-impact data the pre-crash speed of vehicle 1 was set to 27.9 feet/second (19 mph) while the lateral delta-V for vehicle 1 was constrained to be 21.01 feet/second. (We recognize that treating EDR pre-impact data as representing conditions at impact is problematic (Wilkinson et al., 2006; Kusano and Gabler, 2011). The goal here was to try and produce results similar to those in Brach et al., 2015.) The

targets of the estimation exercise were the pre-impact speed of Vehicle 2 and the coefficient of restitution. Table 3.2 summarizes the results of this exercise.

Example 3 – Reconstruction of a Left-Turn Crash

Table 3.3 Posterior summaries for Example 3

Variable	Original Posterior Summary				NLS Value
	Mean	Standard Deviation	2.5%-ile	97.5%-ile	
Estimate, Impact speed Vehicle 2 (feet/second)	14.2	1.8	10.8	17.9	15.6
Restitution coefficient	0.1	0.06	0.004	0.19	0.002
Mu-percent	72.9	7.9	60.9	90.2	69.9
	Posterior with Wider Bounds on Mu-Percent				
Estimate, Impact speed Vehicle 2 (feet/second)	14.3	1.8	10.8	17.9	15.6
Restitution coefficient	0.1	0.06	0.004	0.195	0.002
Mu-percent	69.8	10.1	50.0	89.7	69.9

Our third example follows Example 3 of Brach et al. (2015). Here, left-turning vehicle 1 collided with opposing Vehicle 2. Vehicle 1 was equipped with an EDR that yielded delta-V, in both the longitudinal and lateral directions, along with measurements of pre-impact speed, at one-second intervals, for about five seconds prior to the crash. From the pre-impact data the authors determined that the driver of vehicle 1 was accelerating when the crash occurred and estimated the pre-impact speed of vehicle 1 as 25 mph. As in examples 1 and 2 the goal was to estimate the impact speed of the other vehicle and the restitution coefficient. In this case, these were estimated using the EDR data and delta-V values from vehicle 1. In addition, the authors concluded that tangential motion occurred throughout the period of engagement, and to account for this the impulse ratio was allowed to take on values below its maximum. As in the preceding examples Bayes estimates for Vehicle 2's impact speed and the restitution coefficient was computed using WinBUGS, as well as for the impulse ratio. The impact speed

for vehicle 1 was treated as known to be 25 mph and the longitudinal and lateral delta-Vs for vehicle 1 were -6.95 feet/second and -8.95 feet/second, respectively. In order to correspond to the constraints used in Figure 3.2 of the original paper, the prior distribution for the restitution coefficient was taken to be uniform between 0 and 0.2, the prior for the ratio between the impulse ratio and its maximum value (mu-percent) was taken to be uniform between 60% and 100%, and the prior for Vehicle 2's impact speed was uniform between 5 feet/second and 50 feet/second. The delta-Vs were assumed subject to normal measurement error with a standard deviation of 1.0 feet/second.

The upper half of Table 3.3 summarizes the posterior distributions for Example 3's three target quantities and compares these to the estimates presented in Figure 3.3 of the original paper, while Figure 3.4 displays graphs of the posterior densities as computed by WinBUGS. Two interesting features deserve comment. First, the posterior for the restitution coefficient is (almost) uniform between 0 and 0.2, which was its assumed prior. This means that the measured delta-Vs were essentially non-informative for the restitution coefficient. Second, the posterior for mu-percent is obviously truncated at the lower bound of 60%. This implies that the observed delta-Vs are consistent with lower values of mu-percent and unless there is strong prior reason for the 60% lower bound the estimation should be redone with a different lower bound. This was done with a lower bound of 20%. The resulting posterior distributions are shown in Figure 3.5 while the resulting posterior summaries are shown in the lower half of Table 3.3.

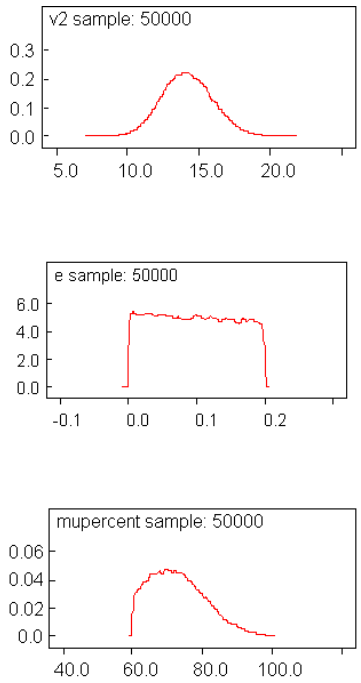

Figure 3.4 Posterior densities for Example 3's target quantities with 60% lower bound for mu-percent.

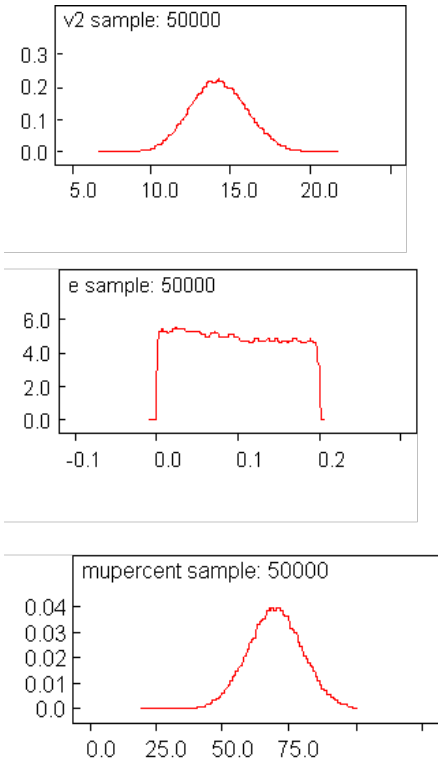

Figure 3.5 Posterior densities for Example 3's target quantities with 20% lower bound for mu-percent.

3.2.2 Reconstruction of Staged Collisions

This section describes Bayesian reconstruction of six staged collisions conducted as part of the project Research Input for Computer Simulation of Automobile Crashes (RICSAC) (Jones and Baum 1978). The goal was to compare the estimates of impact speeds to known values. RICSAC cases 1, 6, and 7, involving 60° front-side-impacts and cases 8, 9, and 10, involving 90° front-to-side impacts, were selected as approximating the conditions arising in left-turn crashes. NLS reconstructions of these collisions have been described in (Brach 1991), and measurements of vehicle and collision parameters were taken from that reference's Table 10.1. Lateral and longitudinal delta-V measurements for both vehicles were developed from the accelerometer reductions presented in Table 2-a of Brach and Smith (2002), and these were used to approximate EDR data.

In addition to EDR data, NASS/CDS cases can also contain estimates of delta-V based on crush measurements, estimates of principal directions of force (PDOF), and scale diagrams which can support estimating post-impact directions, and we were interested in seeing if incorporating these additional data might improve on estimates based solely on EDR data. In the preceding section measurement error uncertainties were chosen so as to approximate the reported NLS reconstructions; for the RICSAC cases existing literature was reviewed in order to identify reasonable values for the measurement uncertainties. Niehoff et al. (2005) reported results from several staged collisions where delta-V estimates from EDRs were compared to estimates from research-grade instrumentation. An analysis of

data listed in their Table 4 suggested that EDR measurement errors could, at least to a first approximation, be taken to be normally distributed with a standard deviation of about 3.2 feet/second. Hampton and Gabler (2010) reported a comparison of delta-V estimates from EDRs to those made from crush measurements, finding that the crush-based estimates tended to underestimate delta-Vs, with considerable scatter. We used the regression equation in their Figure 1 to relate crush-based delta-V estimates to those predicted by PIM. Kusano and Gabler's (2013) Figure 12 compared estimates of PDOF from the NASS/CDS database to directions computed using EDR data. No statistical analysis was reported but the figure suggests that the NASS/CDS estimates of PDOF were approximately unbiased and scattered roughly ± 20° around the EDR estimates. For our experiment we then chose to treat the PDOF estimation errors as normally distributed with standard deviations of 10°. Finally, measurement error for the post impact directions was also taken to be normally distributed with a standard deviation of 10°. The values used in these tests are summarized in Appendix B.

Table 3.4 Posterior summaries of estimated impact speeds (feet/second) for RICSAC tests: EDR data only

RICSAC Crash	Vehicle	Posterior Summary of Impact Speeds (feet/second)				Observed Value
		Mean	Standard Deviation	2.5%-ile	97.5%-ile	
1	1	21.7	6.4	9.4	34.5	29.0
	2	29.5	3.6	22.5	36.6	29.0
6	1	23.1	5.4	12.5	33.6	31.5
	2	36.0	3.9	19.3	34.5	31.5
7	1	36.5	5.5	25.9	47.3	42.7
	2	39.6	11.6	17.6	61.4	42.7
8	1	29.6	4.3	21.0	38.0	30.5
	2	47.5	10.6	26.9	68.0	30.5
9	1	32.0	4.5	24.0	40.1	31.1
	2	29.1	9.3	11.2	47.6	31.1
10	1	46.4	4.2	38.3	54.7	48.8
	2	41.1	7.2	26.8	55.1	48.8

Table 3.5 summarizes the estimates from the second computational experiment, where measurements of post-impact direction, PDOF, and crush-based speed were included. Since reliable measurements of these quantities were not available idealized values for the measurement were taken to be the values developed from the accelerometer measurements presented in Brach and Smith (2002) but subject to measurement errors as described above. These results should thus be interpreted as reflecting ideal, potential reductions in uncertainty. The range of posterior standard deviations for this enhanced data scenario was 3.5 feet/second to 7.7 feet/second and the 95% confidence intervals widths ranged from about 13 feet/second to 31 feet/second. Overall, including the idealized supplemental data improved the accuracy of the speed estimates.

Table 3.5 Posterior summaries of estimated impact speeds (feet/second) for RICSAC tests: EDR data supplemented by post impact angle, PDOF, and crush-based speed estimates

RICSAC Test	Vehicle	Posterior Summary of Impact Speeds (feet/second)				Observed Value
		Mean	Standard Deviation	2.5%-ile	97.5%-ile	
1	1	25.7	3.5	19.2	32.9	29.0
	2	36.6	5.5	26.2	47.8	29.0
6	1	25.0	3.4	18.5	31.8	31.5
	2	33.1	5.5	22.8	44.4	31.5
7	1	36.5	3.9	29.1	44.3	42.7
	2	40.3	6.4	28.4	53.3	42.7
8	1	29.5	3.6	22.5	36.6	30.5
	2	49.2	7.7	34.6	64.9	30.5
9	1	31.3	3.4	24.7	38.1	31.1
	2	32.3	5.8	21.9	44.5	31.1
10	1	45.7	3.6	38.7	52.9	48.8
	2	43.6	5.6	33.1	54.9	48.8

3.2.3 Application to Additional Staged Collision

One of the staged collisions at the 2016 ARC-CSI conference was a head-on collision between a 2011 Ford Crown Victoria and a 2016 Volkswagen Passat. The target impact speed for both vehicles was 30 mph (for a 60 mph closing speed) and both vehicles were driven remotely by Phantom Drivers. Both vehicles were instrumented with IST accelerometers and V-Box video/GPS systems to record crash pulses and impact speeds, and both vehicles were weighed prior to the test. Table 3.6 summarizes the test vehicle specifications and results from the test instrumentation.

Table 3.6 Vehicle specifications and results from test instrumentation

Vehicle #	Model Year	Make/Model	Scale Weight	Impact Speed		Delta-V
				V-Box	Video	IST
1	2011	Ford Crown Victoria	4180 lbs	--	28.5 mph	27.2 mph
2	2016	Volkswagen Passat	3340 lbs	34.5 mph	35.4 mph	36.3 mph

Figure 3.6 shows the longitudinal delta-Vs for the test vehicles computed by integrating the acceleration data from the IST accelerometers.

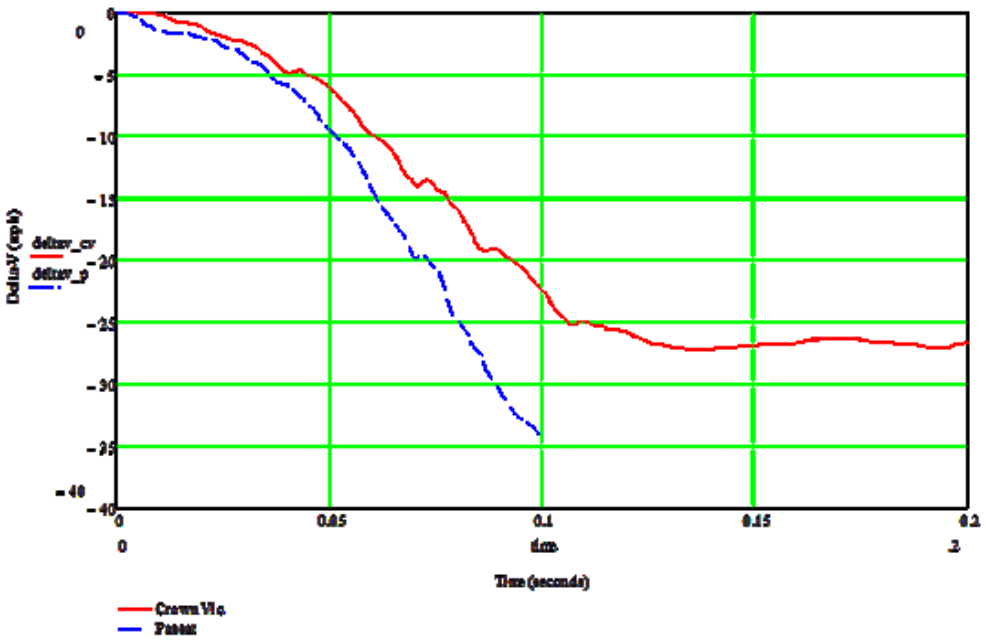

Figure 3.6 Longitudinal delta-Vs for the Crown Victoria and the Passat, computed by integrating IST accelerometer data.

A main objective for this test was to estimate the vehicle impact speeds in a head-on crash, using crash reconstruction methods and data from the vehicles' event data recorders (EDR), and then compare these to measurements made by the test instrumentation. As Figure 3.7 shows though, the achieved configuration was a partial overlap, leading to significant post-impact rotation and compromising analyses that assumed co-linearity of the centers of mass. Also, the V-Box system on the Crown Victoria suffered a data loss, while no EDR data, either pre-crash or crash pulse, were obtained from the Passat. The Crown Vic's EDR did a little better; the Airbag Control Module yielded a longitudinal crash pulse with a delta-V of -29.7 mph but pre-crash data were not available. So the objective was modified to address the following question: Given the limited EDR data, to what extent can these be leveraged with additional data, either from the scene or from the vehicles, to produce defensible estimates of impact speeds?

Figure 3.7 Overhead view showing the orientation of the test vehicles at impact.

The first source of supplemental data was estimates of overall delta-V computed from the vehicles' crush. Scale drawings of both vehicles, provided as part of the data given to conference attendees, were used to measure their crush profiles, as illustrated in Figure 3.8. Table 3.7 shows the crush measurements for both vehicles along with their estimated delta-Vs. The stiffness coefficients were provided by 4NXPRT Systems, also as part of the data given to conference attendees. Note that for both vehicles the delta-Vs estimated from crush were lower than those reported by the test instrumentation, consistent with findings reported by Hampton and Gabler (2010).

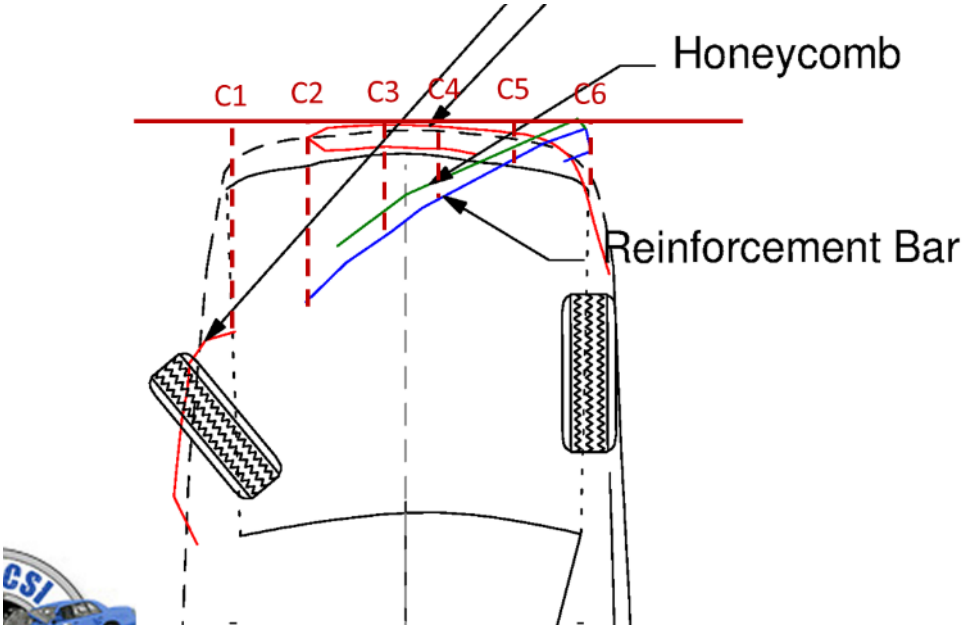

Figure 3.8 Damage diagram and points of crush measurement for the Crown Victoria.

Table 3.7 Crush analysis for ARC-CSI 2016 Crash Test 2

Vehicle	Crush Profiles (feet)							Stiffness Coefficients		Delta-V (mph)
	C1	C2	C3	C4	C5	C6	L	d0	d1	
1 (Crown Vic)	2.4	2.3	1.7	1.0	0.5	0	5.2	33.95	103.65	25.1
2 (Passat)	1.6	1.7	1.5	1.0	0.4	0	5.0	32.68	151.55	30.5

The second source of supplemental data was the changes in direction experienced by the test vehicles during the crash. In the field these would be estimated from the scene map and vehicle rest positions, but a scarcity of landmarks in the scene diagram made it difficult to identify the vehicles' pre-impact directions. To serve as a proxy for scene-based direction measurements an overhead video of the crash was loaded into the program Videopoint, coordinates for pre- and post-impact trajectories for the vehicles were determined using Videopoint's point and click feature, and pre-and post-impact directions were then estimated using linear regression. Taking the Passat's pre-crash orientation as defining the positive x-direction, this gave post-impact directions of 73° for the Crown Victoria and -126° for the Passat.

Figure 3.9 Pre- and post-impact trajectories measured using Videopoint.

As described above, our Bayesian version of planar impact mechanics was used to estimate the vehicles' impact speeds. Table 3.8 summarizes the input data for the PIM model, and also compares the measured crash data to values predicted from impact speeds of 28.5 mph for the Crown Vic and 34.5 mph for the Passat. The results displayed in Table 3.8 suggest that the crash measurements (Crown Vic delta-V, crush delta-V's, and post-impact directions) should be informative regarding the vehicles' impact speeds.

Table 3.9 summarizes the results on uncertainty reduction as provided by different data scenarios. The "No Measurements" scenario was essentially a simulation of the prior uncertainties regarding the impacts speeds as uniform between 5 feet/sec and 100 feet/sec (3.4 mph to 68.2 mph). The uncertainty reduction provided by a data configuration was assessed by comparing its posterior standard deviations to those from the "No Data" scenario. As expected, the greatest reduction in uncertainty occurred when all three data items were taken into account; the posterior standard deviations were reduced to 2.0 mph and 2.3 mph for the Crown Vic and the Passat, respectively. Almost as good was the uncertainty reduction provided by the single EDR delta-V from the Crown Vic's Airbag Control Module (ACM) plus the exit angles. By itself the EDR delta-V from the Crown Vic provided only a marginal reduction in uncertainty, as did combining the delta-V from the EDR and with those from the crush analysis. Note that the 95% confidence bounds tend to catch the "Ground Truth" impact speeds from test instrumentation, although in some cases the bounds are so wide as to be uninformative. Figure 3.10 illustrates the prior distribution for both vehicles and posterior distributions generated when all available data was taken into account. Compared to the flat prior probability distribution the posterior distributions for both impact speeds are highly, but not perfectly, informative.

Table 3.8 Summary of measurements used to estimate impact speeds, together with data items predicted by impact speeds of 28.5 mph and 34.5 mph. measured values of data items are shown in parentheses

Feature	Crown Vic (Vehicle 1)	Passat (Vehicle 2)
Weight (lbs)	4180	3440
Yaw Inertial Moment (lb-ft-sec2)	2973	2155
d (feet)	5.8	5.2
ϕ (degrees)	18	6
θ (degrees)	0	0
e	0.1	
Γ (degrees)	20	
μ%	100	
Predicted and Measured Data Items		
Longitudinal Δv (feet/second)	-43.6 (-44.4)	--
Crush Δv (feet/second)	36.8 (38.4)	44.7 (46.6)
Exit angle (degrees)	73 (70.5)	-126 (-110.9)

Table 3.9 Summary of Posterior Distributions for Impact Speeds. All Speeds are in miles/hour

Data Scenario	Vehicle	Posterior Summary				"Ground Truth"
		Mean	St. Dev.	2.5%-ile	97.5%-ile	
EDR delta-V, crush delta-Vs, exit angles	Crown Vic	29.1	2.0	25.2	33.0	28.5
	Passat	33.9	2.3	29.4	38.4	35.4 (34.5)
EDR delta -v, exit angles	Crown Vic	29.4	2.2	25.1	33.7	28.5
	Passat	34.2	2.5	29.3	39.2	35.4 (34.5)
crush delta-Vs, exit angles	Crown Vic	28.5	4.4	20.1	37.1	28.5
	Passat	33.2	5.1	23.4	43.2	35.4 (34.5)
EDR delta-V only	Crown Vic	32.1	16.3	4.9	60.4	28.5
	Passat	31.5	16.3	4.9	60.4	35.4 (34.5)
EDR delta-V, crush delta-Vs	Crown Vic	31.9	16.3	4.9	60.1	28.5
	Passat	31.2	16.3	4.7	59.7	35.4 (34.5)
No Measurements	Crown Vic	35.8	18.7	5.0	66.6	28.5
	Passat	35.9	18.6	5.0	66.6	35.4 (34.5)

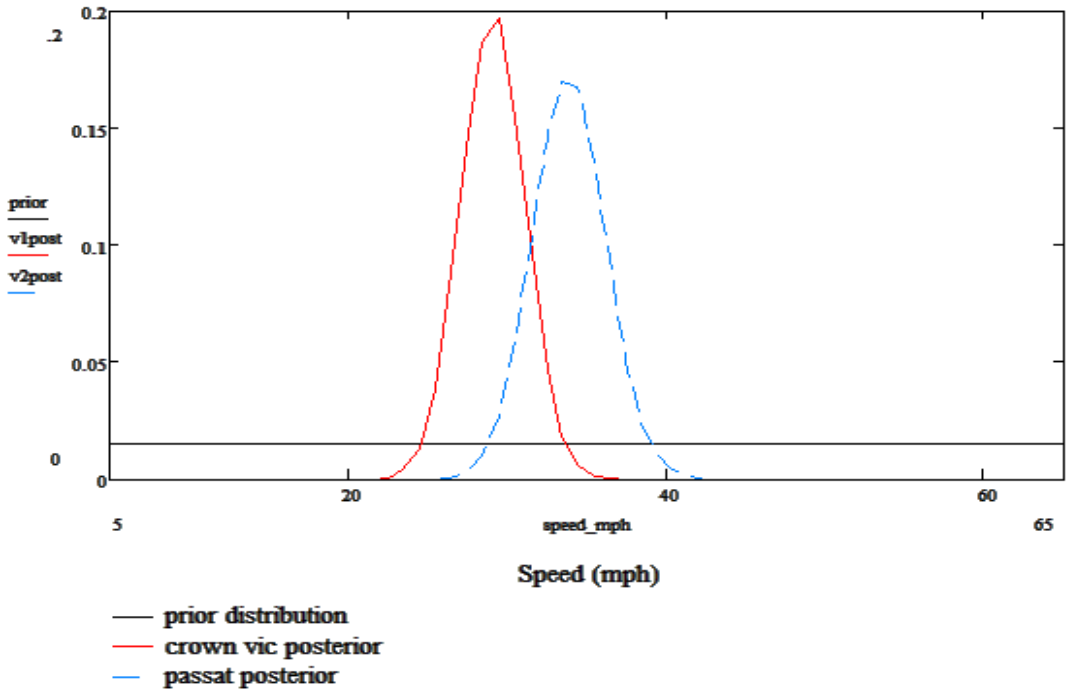

Figure 3.10 Prior and posterior probability distributions for impact speeds.

3.3 SUMMARY AND CONCLUSIONS

As noted earlier, nonlinear least squares (NLS) has been used to estimate impact speeds from different combinations of EDR, crush, and exit angle measurements from two-vehicle planar impact crashes, but an open question is how to quantify the resulting uncertainty. After illustrating the basic ideas with a simple computational example, Markov Chain Monte Carlo (MCMC) was applied to (1) several crashes from the literature which have been previously reconstructed using NLS, (2) six staged collisions, and (3) a staged collision from the 2016 ARC-CSI conference. As would be expected, in each case the MCMC point estimates were similar to those produced by NLS, but defensible confidence intervals for the estimates were also produced. For the six staged crashes posterior 95% confidence intervals for the impact speeds tended to catch the observed values but the uncertainty associated with the estimated impact speeds varied substantially. For the ARC-CSI crash test, vehicle exit angles plus longitudinal delta-V from one vehicle were sufficient to substantially reduce prior uncertainty regarding impact speeds.

Further work should focus on identifying defensible measurement error models for the measured inputs. For example, we used the same measurement error for EDR-based lateral and longitudinal delta-V estimates although Niehoff et al. (2005) reported data only for longitudinal estimates. As EDRs which record both longitudinal and lateral crush pulses become more common it should be possible to determine not only that whether or not lateral and longitudinal delta-V measurements have different uncertainties but also to assess their correlation. Although our code allows for correlated measurement errors, in our computational examples we treated lateral and longitudinal EDR data as uncorrelated, mainly because of a lack of information regarding reasonable values for the correlations.

In summary, for cases where a reconstruction model can be expressed as a set of algebraic equations, MCMC offers a very flexible method for computing estimates from measurements that vary in type and quality. A challenge for future research is to identify reasonable measurement error models for the data that can be included in a reconstruction.

CHAPTER 4: BAYESIAN ESTIMATION OF DRIVERS' ACTIONS IN LEFT-TURNING CRASHES

4.1 INTRODUCTION

Although road crash reconstruction is most often undertaken to support legal proceedings, it has also been used in road safety research. Examples include the Tri-Level Study (Treat et al., 1979), work done at the Center for Automotive Safety Research regarding speed in fatal and serious crashes (Kloeden et al., 1997), and research into the impact conditions of road-departures crashes (Mak et al. 2010). There is also increasing interest in using reconstructed crashes to assess the potential of vehicle automation to reduce the frequency and severity of crashes (Rosen et al., 2010; Kusano and Gabler, 2011; Scanlon et al., 2016; Sander 2017); Davis (2014) proposed warrants (i.e. sufficient conditions) for using reconstructed crashes to estimate a crash modification factor associated with a safety-related intervention. Key features of this treatment were a structural equation and a set of input variables, called elements, so that evaluating the structural equation at a given assignment of values to the crash elements determined whether or not a crash occurred. For example, in a gap selection event the crash elements could be the time needed by a gap selector, such as a pedestrian or a driver making a left-turn, to clear the conflict point, the position and speed of an opposing vehicle when the selector initiates movement, and the reaction time and deceleration of the opposing driver. The structural equation could be a simple kinematic model that describes whether or not the selector and the opposing vehicle arrive at the conflict point at the same time.

For an actual crash, a structural model and estimates for the crash elements provide an explanation of why the crash occurred, while a sample of estimated elements from crashes of a given type could be used to cluster the crashes into common scenarios. Crash elements tend to include pre-crash positions and actions, and obtaining reliable estimates of elements has been challenging. However, with the increasing prevalence of event data recorders (EDR) providing pre-crash data, this situation might be changing. Gabler and Hinch (2009) conducted an exploratory investigation of drivers' behavior prior to rear-ending crashes, producing aggregate measures of brake application and throttle release times. Kusano and Gabler (2011) used pre-crash speed and brake application data to estimate time to collision at the start of braking in rear-ending crashes, and Scanlon et al. (2016) used pre-crash speed data to reconstruct vehicle trajectories in angle crashes.

This chapter describes a similar approach in that pre-crash speed data from EDRs are used to reconstruct the pre-crash movements for a left-turning vehicle and for an opposing vehicle initially traveling straight (LTOP). The reconstructed movements are then used to estimate five crash elements:

t_1 - the time between when the turning driver begins the turn and when he or she reaches the conflict point,

v_2 – the speed of the opposing vehicle when the turn begins,

x_2 – the opposing vehicle's distance from the conflict point when the turn begins,

r_2– the opposing driver's braking reaction time,

a_2 – the opposing driver's braking deceleration.

The method will be illustrated using data from a staged crash test and from six cases from the National Highway Traffic Safety Administration's (NHTSA) NASS/CDS database.

4.2 BAYESIAN CRASH RECONSTRUCTION

The basic tenets of the Bayesian approach to crash reconstruction are:

1) the results of a crash reconstruction are more or less uncertain,
2) probability theory is an appropriate logic for reasoning about this uncertainty,
3) uncertainty in expert opinion can be quantified using probability distributions.

A probability distribution which express a reconstructionist's prior opinion about important crash features is updated, using Bayes theorem from probability theory, to produce a posterior distribution which accommodates the available evidence (Davis, 2003; 2011; 2015). To illustrate the Bayesian approach, Figure C. 1 in the Appendix shows part of an after-crash scene diagram, prepared by NASS/CDS investigators for Case 2012-12-044, in which a 2011 Chevrolet Malibu (Vehicle 1) attempted to turn left across the path of a 2000 Chevrolet Blazer (Vehicle 2). As part of the investigation, EDR reports for both vehicles were downloaded and imaged using the Bosch CDR tool. For the Blazer this crash was a non-deployment event and so no crash pulse was recorded, but the Malibu's EDR gave longitudinal and lateral delta-V's of -8.8 mph and -7.45 mph, respectively. The NASS/CDS case file also included estimates of delta-V for both vehicles derived from their crush profiles and estimates of the principal directions of force (PDOF) for both vehicles.

Chapter 3 described a Bayesian adaptation of the planar impact model (Brach and Brach, 2011) for estimating the impact speeds of vehicles involved in two-vehicle crashes, along with tests of this method using data from several instrumented crash tests. For NASS/CDS Case 2012-12-044, scale drawings of the two vehicles were prepared showing their crush surfaces and the collision impact center was then estimated by overlaying these drawings. Vehicle dimensions and inertial parameters were taken from Expert Autostats (4NXPRT Systems, 2014). For this case the EDR pre-crash data indicated that the Malibu stopped prior to impact so the problem was to estimate the Blazer's impact speed using the delta-V's from the Malibu's EDR, the NHTSA estimates for delta-V and PDOF from the crush analyses, and the vehicles' exit angles estimated from the scene diagram. The prior distribution for the Blazer's impact speed was taken to be uniform between 2 and 66 mph and, since for this problem analytic application of Bayes theorem was intractable, the posterior distribution was simulated using the Markov Chain Monte Carlo (MCMC) software WinBUGS (Lunn et al., 2013). Figure 4.1 shows the assumed prior distribution and simulated posterior distribution for the Blazer's speed at impact.

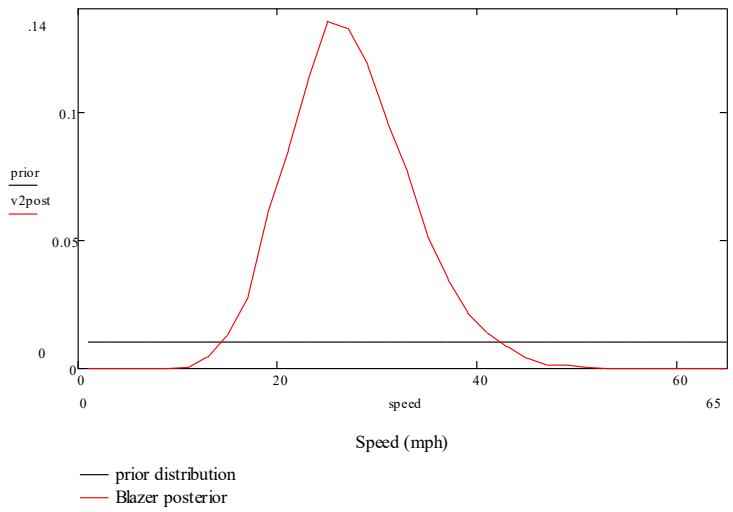

Figure 4.1 Prior and posterior probability distributions for Blazer's speed at impact, NASS/CDS Case 2012-12-044.

4.2.1 Bayes Estimation of Crash Elements

4.2.1.1 Data Acquisition

Since it is necessary to relate the actions of an opposing driver to the actions of the turning driver, estimating the five crash elements (t_1, v_2, x_2, r_2, a_2) requires pre-crash data from both vehicles involved in a LTOP crash. The NASS/CDS EDR reports for 2012 and 2013 were downloaded and scanned to identify cases where EDR reports were available for two vehicles. Each of these cases was then viewed using the NASS/CDS case viewer to identify LTOP crashes, and the EDR reports were reviewed to identify those LTOP cases where both vehicles had at least five seconds of pre-crash data. This left three cases from 2012 and five from 2013. Three of the cases involved two General Motors (GM) vehicles while the other five involved combinations of GM, Ford, Chrysler, and Toyota vehicles. The six cases involving non-Toyota vehicles will be presented here.

4.2.1.2 Illustration Using NASS/CDS Case 2012-12-044

As noted above, Figure C. 1 shows the post-crash diagram prepared for NASS/CDS Case 2012-12-044. NHTSA investigators downloaded and imaged the pre-crash data from both vehicles' EDRs and, a subset of these are shown in Table 4.1.

Table 4.1 EDR pre-crash data for NASS/CDS Case 2012-12-044

Vehicle 1 (Malibu)				
Time (seconds)	Speed (mph)	Engine RPM	Percent Throttle	Brake Switch
-5	6	1216	15	ON
-4	3	1152	16	ON
-3	6	2304	36	OFF
-2	12	2432	40	ON
-1	0	1088	21	ON
Vehicle 2 (Blazer)				
Time (seconds)	Speed (mph)	Engine RPM	Percent Throttle	Brake Switch
-5	42	2240	59	OFF
-4	44	2368	54	OFF
-3	45	1856	0	OFF
-2	41	1088	0	ON
-1	31	768	4	ON

To start, assume for illustrative purposes that the two EDRs were synchronized and that Time=0 represented the time of the crash for both vehicles; these assumptions will be relaxed later. Under these assumptions Table 4.1 suggests that the Malibu was initially entering the intersection at a low speed but that between 3 and 4 seconds prior to the crash the Malibu's driver began accelerating to make the turn. However, shortly after starting to turn, the Malibu's driver applied the brake and came to a stop in the intersection. The Blazer was approaching the intersection at 40-45 mph when the Malibu began to turn across its path and between 2 and 3 seconds before the crash the driver of the Blazer applied the brake, slowing the vehicle but not avoiding the crash. Using the pre-crash speeds one can estimate an acceleration (a) between recorded time points as

$$a = \frac{v_e - v_i}{\Delta} \qquad (4.1)$$

where v_i denotes the speed at the beginning of an interval, v_e is the speed at the end of the interval, and Δ denotes the interval's duration. The distance (*d*) traveled during an interval is then

$$d = v_i\Delta + \frac{a\Delta^2}{2} \qquad (4.2)$$

Wilkinson et al. (2006) reported that pre-crash data from GM Sensing and Diagnostic Modules (SDM) can be shifted significantly in time relative to the SDM's reported times, so to synchronize the two sets of pre-crash data it is necessary to estimate, for each vehicle, the time elapsing between Time=-1 and the crash. The impact speed for the Blazer was estimated using the Bayesian version of the planar impact model described above. The EDR data showed that the Malibu had stopped when the crash occurred, and the Bayesian planar impact reconstruction gave 40.1 feet/second as the posterior mean for the Blazer's impact speed. Taking this as the Blazer's impact speed, and extrapolating the braking deceleration between times -2 and -1 (14.67 feet/second^2) to the period between Time=-1 and impact, it is possible to estimate the time between the last recorded pre-crash data point and the impact

$$\Delta_0 = \frac{40.1 - 45.5}{-14.67} = 0.37\,\text{sec} \qquad (4.3)$$

Applying this time shift to the Blazer's pre-crash data and using equations (4.1) and (2) then gives a pre-crash trajectory for the Blazer, displayed in Table 4.2.

Since the Malibu stopped prior to impact a similar estimate of its final Δ_0 is not available so for the purposes of illustration Δ_0=0.5 seconds will be used. (A method allowing for uncertainty in this value will be presented later.) Knowing the time shifts (Δ_0) for each vehicle allows approximate synchronization of the pre-crash data from both EDRs, and plotting a subset of these on a common time scale gives Figure 4.2. Figure 4.2 shows the estimated speed and position data for the Blazer, along with the Blazer's Brake Status, with 0 for OFF and 100 for ON. Figure 4.2 also shows the Percent Throttle for the Malibu, multiplied by 10. Note that the time shift for the Malibu, 0.5 seconds, is different from that for the Blazer, 0.37 seconds. The marked increase in the Malibu's throttle between 2.5 and 3.5 seconds prior to the crash indicates a start of the turning movement sometime during that interval. 3.5 seconds prior to the crash the Blazer was approximately 205 feet from the impact point while 2.5 seconds prior to impact the Blazer was approximately 140 feet from the impact point, giving a range of possible distances when the turning movement started. The Blazer's speed was approximately constant during this interval, at 65 feet/second. The driver of the Blazer then started braking between 1.37 and 2.37 seconds prior to the crash. Applying interval arithmetic to these values gives interval estimates for reaction time of the Blazer's driver and the apparent time gap (x_2/v_2) accepted by the Malibu's driver. These are summarized in Table 4.3.

Table 4.2 Estimated trajectory for opposing vehicle (Blazer) in NASS/CDS Case 2012-12-144.

Time Prior to Crash	Speed	Speed (mph)	Distance from	Brake Switch
-4.37	61.6	42	259.9	OFF
-3.37	64.5	44	196.8	OFF
-2.37	66	45	131.5	OFF
-1.37	60.1	41	68.5	ON
-0.37	45.5	31	15.7	ON
0	40.1	27.3	0	--

.

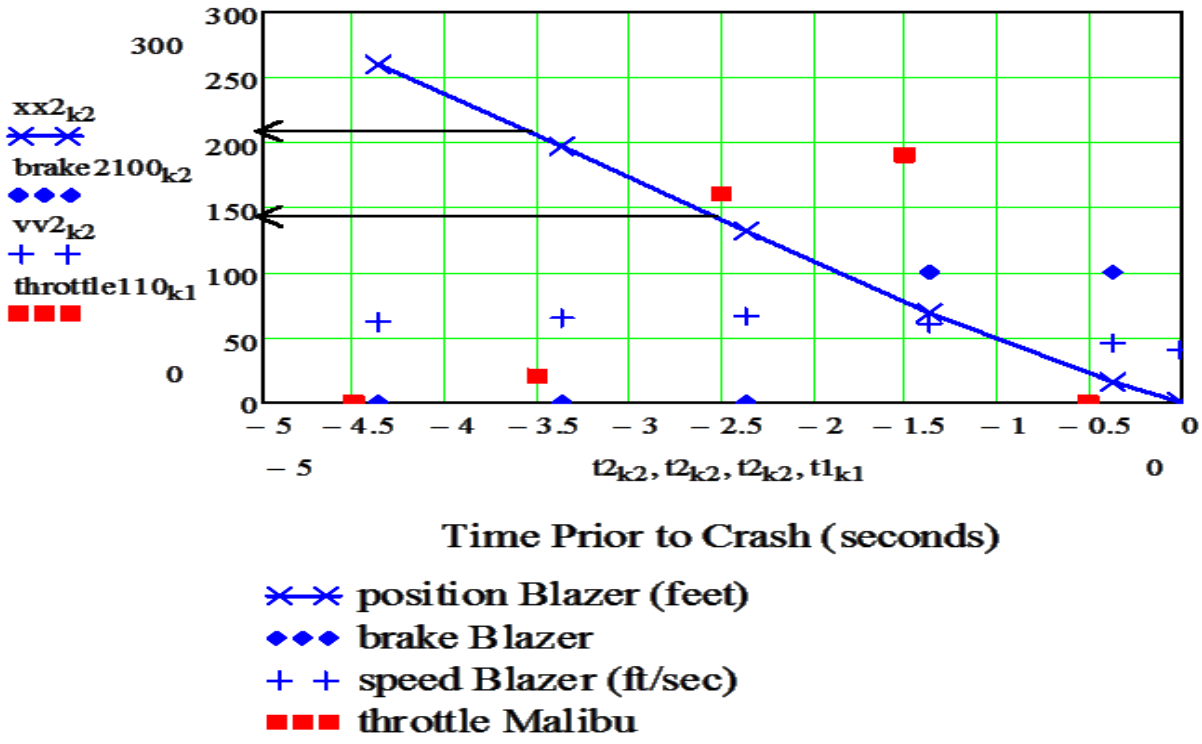

Figure 4.2 Illustrative graph showing the trajectory of the opposing vehicle (Blazer) and actions by both drivers in NASS/CDS Case 2012-12-044.

Table 4.3 Illustrative elements for NASS/CDS Case 2012-12-144. The Malibu (Vehicle 1) is the turning vehicle, the Blazer (Vehicle 2) is the opposing vehicle

Feature	Lower Bound	Upper Bound
Malibu Time to Collision (t_1)	2.5 sec	3.5 sec
Blazer Initial Speed (v_2)	64.1 feet/sec	65.8 feet/sec
Blazer Initial Distance (x_2)	140.3 feet	205.2 feet
Apparent Gap	2.1 sec	3.2 sec
Blazer Driver Reaction Time (r_2)	0.1 sec	2.1 sec
Blazer Driver Deceleration (a_2)	14.7 feet/sec^2	14.7 feet/sec^2

In practice the data used by this estimation method are more or less uncertain which leads to additional uncertainties in the elements' estimates. The pre-crash speed data obtained from EDRs are subject to measurement errors (Bortles et al., 2016), the estimates of pre-crash speeds obtained via planar impact reconstruction have uncertainties which can be quantified, and there is non-trivial prior uncertainty regarding Δ_0 for the Malibu (Wilkinson et al., 2006). If one could specify appropriate probability distributions describing these uncertainties, the distributions could be coupled with the computational procedure described above and Monte Carlo (MC) simulation used to simulate distributions for the crash elements. Initial applications of this approach, however, identified a serious weakness: the MC samples tended to contain sets of elements where the opposing driver could stop before reaching the collision point. That is, possible outcomes consistent with the uncertainties in the pre-crash data contained non-crash as well as crash events, and it was necessary to restrict the MC sampling so that only crash-producing estimates were generated. One way to do this is via Markov Chain Monte Carlo (MCMC) sampling, where a realization of a stochastic process called an ergodic Markov chain is generated in such a way that the chain's stationary distribution is the target distribution (Lunn et al., 2013). As with MC sampling, descriptive summaries can then be computed by simple averaging.

Using the MCMC software WinBUGS (Lunn et al., 2013) the model described above was coded and used to generate Bayesian posterior distributions for the elements describing NASS/CDS case 2012-12-044. Since the Malibu apparently stopped prior to the crash a constraint was added that required the stopping distance for the Blazer to be greater than its initial distance (x_2). The pre-crash speeds from the EDRs were treated as normal random outcomes with standard deviations equal to 1.5 feet/second, chosen so that ±2 standard deviation range roughly covered the ranges reported in Bortles et al., 2016. The impact speed

for the Blazer was treated as a normal random outcome with a standard deviation of 9.1 feet/second, consistent with the results of the planar impact reconstruction. Prior uncertainty for the final time lag (Δ_0) for the Malibu was treated as a uniform random variable bounded by 0 and 1 seconds. A summary of the resulting posterior distributions is shown in Table 4.4.

Comparing Table 4.4 with Table 4.3 shows that the Bayes estimates are generally consistent with the interval estimates shown in Table 3 although the uncertainty ranges in Table 4.4 tend to be wider than those in Table 4.3. This is to be expected since the Bayes estimates in Table 4.4 account for additional sources of uncertainty. The 2.5 percentile point for the reaction time of the Blazer's driver was -0.05 seconds, indicating that the Blazer's driver might have begun decelerating in anticipation of the Malibu's turn.

Table 4.4 Summary of the posterior distribution for elements characterizing NASS/CDS Case 2012-12-044.

Element	Posterior Summary			
	Mean	Standard Deviation	2.5 %-ile	97.5 %-ile
(t_1) Turning Vehicle Time to Collision (seconds)	3.0	0.4	2.2	3.8
(v_2) Opposing Vehicle Initial Speed (feet/second)	64.7	1.5	61.5	67.6
(x_2) Opposing Vehicle Initial Distance (feet)	170.6	27.8	118.2	224.1
(x_2/v_2) Apparent Gap (seconds)	2.6	0.45	1.8	3.6
(r_2) Opposing Driver Reaction Time (seconds)	1.1	0.6	-0.05	2.3
(a_2) Opposing Driver Deceleration (feet/second^2)	-14.5	2.0	-18.4	-10.5

4.2.2 Evaluation Using Crash Tests

As indicated in Figure 4.2, a key feature of this estimation method is reconstruction of the pre-crash distance and speed trajectories for the opposing vehicle. As a partial check on the method's accuracy it was applied to a staged collision between a 2008 Chevrolet Malibu and a 2005 Mazda 3, conducted at the 2015 ARC-CSI Conference (ARC-CSI 2015). The Mazda was stationary while the Malibu was driven by a test driver who began braking shortly before striking the Mazda broadside. Test instrumentation gave estimated impacts speeds for the Malibu between 23.7 mph and 26.6 mph. This instrumentation included a Vbox video GPS system which provided speed and time prior to and during the crash, at 30 frames/second. Using the Bosch CDR tool it was possible to download pre-crash data from the Malibu's EDR, shown in Table 4.5, as well as longitudinal and lateral crash pulses. The Malibu's longitudinal delta-V was -11.5 mph and its lateral delta-V was 0 mph.

Table 4.5 Pre-Crash data from Crash Test 4 at 2015 ARC-CSI conference

Time (seconds)	Vehicle 1 (Malibu)			
	Speed (mph)	Engine RPM	Percent Throttle	Brake Switch
-5	32	3072	53	OFF
-4	34	3136	43	OFF
-3	35	2176	35	OFF
-2	35	1920	24	OFF
-1	35	1792	17	ON

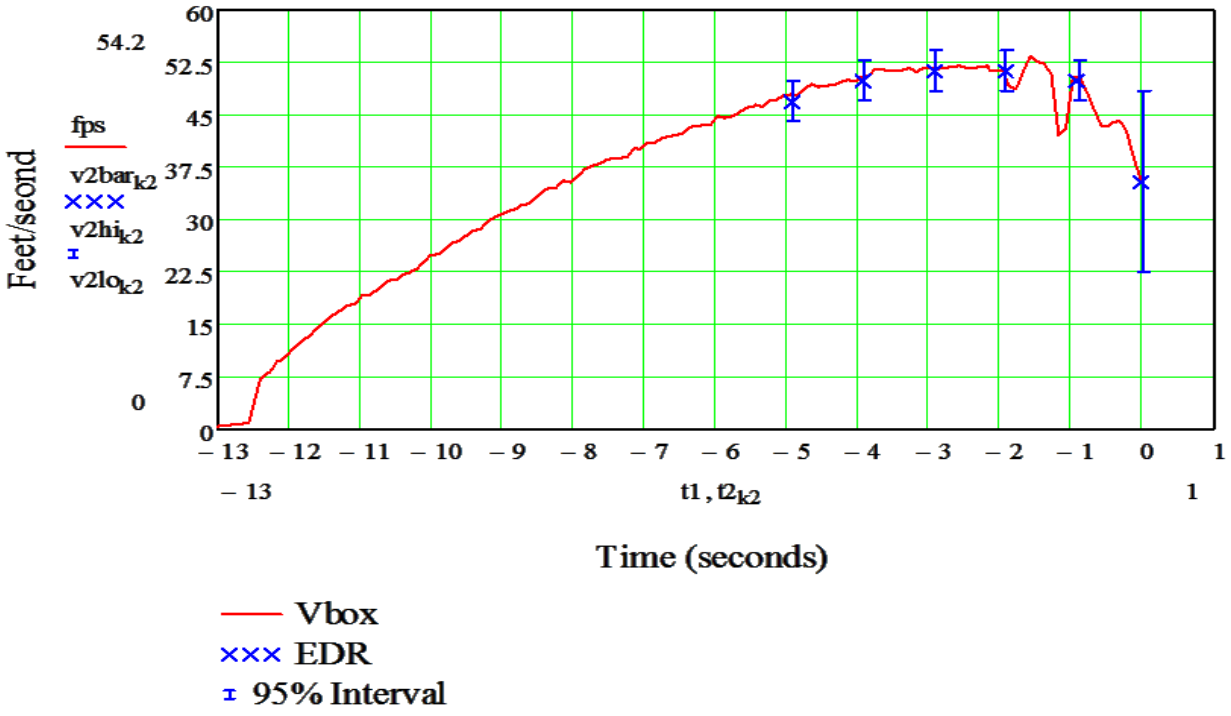

Figure 4.3 Speed versus Time for the Malibu in Crash Test 4 at the 2015 ARC-CSI conference.

A planar impact reconstruction using the delta-Vs from the EDR gave an estimated impact speed for the Malibu of 35 feet/sec (23.9 mph), with a posterior standard deviation of 6.5 feet/sec. This compared favorably with the impact speed from the Vbox, 36.1 feet/sec (24.6 mph). The Vbox speeds were then used to construct speed and distance trajectories for the Malibu, which were compared to trajectories reconstructed from the EDR pre-crash data using the methods described in the preceding section. For this case the Malibu's braking was too late to estimate its final deceleration using EDR pre-crash speeds and so this was taken to be uniformly distributed with bounds of 0.3g and 0.7g. Figure 4.3 shows the speed profile as generated from the Vbox data; the fluctuations occurring after Time=-2 seconds were caused by the Malibu being driven up and over a ramp prior to the collision. Also shown are the speeds as estimated from the EDR pre-crash data and the impact speed as estimated from the planar impact reconstruction, together with their 95 percent confidence intervals. The posterior mean time lag between the final EDR sample point and the impact was 0.79 seconds, with a standard deviation of 0.26 seconds, and the EDR estimates are plotted using this posterior mean. Figure 4.4 shows similar results for the Malibu's distance from the impact point.

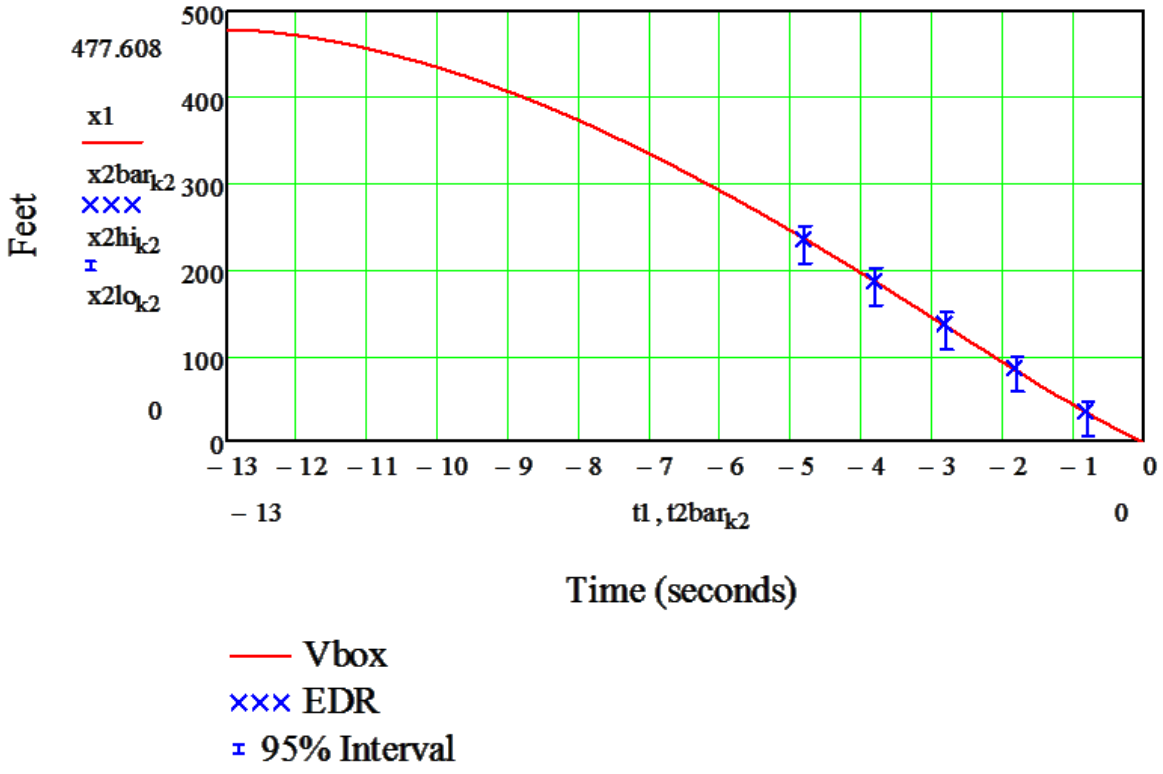

Figure 4.4 Distance versus Time for the Malibu in Crash Test 4 at the 2015 ARC-CSI conference

4.3 ADDITIONAL NASS/CDS CASES

4.3.1 Case 2013-75-034

Figure C. 2, in the Appendix, shows a post-crash scene diagram for NASS/CDS case 2013-74-034 in which a 2004 Chevrolet Lumina turned left in front of a 2002 Chevrolet Blazer. In what follows the Lumina will be called Vehicle 1 and the Blazer Vehicle 2. Table 4.6 shows the EDR pre-crash data for both vehicles. Interestingly, the pre-crash data for the Blazer indicate that at Time= -1 both the brake and the throttle were being applied.

Planar impact reconstruction yielded estimated impact speeds of 22.7 feet/second, or 15.5 mph, (standard deviation 3.2 feet/second) for the Lumina and 35.7 feet/second, or 24.3 mph, (standard deviation 7.6 feet/second) for the Blazer. These were then used as input for Bayesian trajectory reconstructions for both vehicles, with accelerations between Time = -1 and Time = 0 being extrapolations from the pre-crash data. For this case, since the turning vehicle did not stop, a constraint was imposed requiring that the arrival time of the opposing vehicle be within 0.25 seconds of the turning vehicle's arrival time. Bayes estimates of the crash elements are shown in Table 4.7

Table 4.6 EDR pre-crash data for NASS/CDS Case 2013-74-034

Vehicle 1 (Lumina)				
Time	Speed (mph)	Engine RPM	Percent Throttle	Brake Switch
-5	1	640	0	OFF
-4	4	1280	10	OFF
-3	7	1472	10	OFF
-2	11	1728	16	OFF
-1	15	2112	16	OFF
Vehicle 2 (Blazer)				
Time	Speed (mph)	Engine RPM	Percent Throttle	Brake Switch
-5	52	1920	31	OFF
-4	51	1600	31	OFF
-3	51	1536	31	OFF
-2	48	1408	0	ON
-1	29	1024	27	ON

Table 4.7 Summary of the posterior distribution for elements characterizing NASS/CDS Case 2013-74-034

Element	Posterior Summary			
	Mean	Standard Deviation	2.5 %-ile	97.5 %-ile
(t_1) Turning Vehicle Time to Collision (seconds)	2.8	0.5	2.1	3.8
(v_2) Opposing Vehicle Initial Speed (feet/second)	74.9	1.3	72.3	77.4
(x_2) Opposing Vehicle Initial Distance (feet)	181.3	36.1	123.1	259.5
(x_2/v_2) Apparent Gap (seconds)	2.4	0.47	1.7	3.4
(r_2) Opposing Driver Reaction Time (seconds)	1.4	0.5	0.5	2.4
(a_2) Opposing Driver Deceleration (feet/second^2)	-27.6	2.0	-31.6	-23.5

4.3.2 Case 2013-75-034

Figure C. 3, in Appendix C, shows a post-crash scene diagram for NASS/CDS case 2013-12-111 in which a 2013 Chevrolet Captiva turned left in front of a 2005 Chevrolet Impala. Table 4.8 shows EDR pre-crash data for both vehicles. while Table 4.9 shows Bayes estimates of the crash elements.

Table 4.8 Pre-Crash EDR data from NASS/CDS Case 2013-12-111

Vehicle 1 (Captiva)				
Time (seconds)	Speed (mph)	Engine RPM	Percent Throttle	Brake Switch
-5	16	1152	7	ON
-4.5	14	1024	8	ON
-4	12	960	9	ON
-3.5	11	960	8	ON
-3	10	896	9	ON
-2.5	9	1152	28	OFF
-2	9	1920	36	OFF
-1.5	11	1984	37	OFF
-1	12	2240	55	OFF
-.5	15	2688	70	OFF
Vehicle 2 (Impala)				
Time (seconds)	Speed (mph)	Engine RPM	Percent Throttle	Brake Switch
-5	32	1600	5	OFF
-4	32	1536	5	OFF
-3	33	1472	5	OFF
-2	34	1344	5	OFF
-1	33	1344	0	ON

Table 4.9 Summary of the posterior distribution for elements characterizing NASS/CDS Case 2013-12-111

Feature	Posterior Summary			
	Mean	Standard Deviation	2.5 %-ile	97.5 %-ile
(t_1) Turning Vehicle Time to Collision (seconds)	2.5	0.2	2.1	2.9
(v_2) Opposing Vehicle Initial Speed (feet/second)	49.1	1.2	46.7	51.5
(x_2) Opposing Vehicle Initial Distance (feet)	114.7	10.8	94.3	135.6
(x_2/v_2) Apparent Gap (seconds)	2.3	0.24	1.9	2.8
(r_2) Opposing Driver Reaction Time (seconds)	1.6	0.35	0.9	2.3
(a_2) Opposing Driver Deceleration (feet/second^2)	-21.9	3.7	-28.6	-16.3

4.3.3 Case 2013-49-059

Figure C. 4, in the Appendix, shows the after-crash scene diagram for NASS/CDS Case 2013-49-059 in which 2003 Chevrolet S-10 pickup turned left and collided with a 2010 Ford Taurus. Table 4.10 shows pre-crash data for both vehicles.

Table 4.10 Pre-Crash EDR data from NASS/CDS Case 2013-49-059

Vehicle 1 (S-10)				
Time (seconds)	Speed (mph)	Engine RPM	Percent Throttle	Brake Switch
-5	0	896	0	ON
-4	2	1856	100	OFF
-3	10	2624	100	OFF
-2	17	3136	100	OFF
-1	22	3968	100	ON
Vehicle 2 (Taurus)				
Time (seconds)	Speed (mph)	Engine RPM	Accelerator Pedal (%)	Brake Switch
-5.0	36.0	1200	13	OFF
-4.5	36.0	1200	13	OFF
-4.0	36.7	1200	13	OFF
-3.5	36.7	1200	12	OFF
-3.0	37.3	1300	12	OFF
-2.5	37.3	1300	12	OFF
-2.0	37.3	1500	21	OFF
-1.5	37.9	1400	20	OFF
-1.0	38.5	1300	14	OFF
-0.5	39.1	1300	13	OFF
0.0	37.9	1300	0	ON

Planar impact reconstruction yielded estimated impact speeds of 18.9 feet/second, 12.9 mph (standard deviation 5.3 feet/second) for the S-10 and 60.6 feet/second, 41.3 mph (standard deviation 16.2 feet/second) for the Taurus. These were used as input into Bayesian trajectory reconstructions for both vehicles, with the final deceleration for Taurus taken as uniformly distributed between 0.5g and 0.9g. The EDR pre-crash speed data from the Taurus was assumed to follow a bias and measurement error model derived from statistics reported by Ruth and Daily (2011). A constraint was imposed requiring that the arrival time of the opposing vehicle be within 0.25 seconds of the turning vehicle's arrival time. Bayes estimates of the crash elements are shown in Table 4.11.

Table 4.11 Summary of the posterior distribution for elements characterizing NASS/CDS Case 2013-49-059

Element	Posterior Summary			
	Mean	Standard Deviation	2.5 %-ile	97.5 %-ile
(t_1) Turning Vehicle Time to Collision (seconds)	4.0	0.4	3.2	4.7
(v_2) Opposing Vehicle Initial Speed (feet/second)	54.0	1.0	51.9	56.0
(x_2) Opposing Vehicle Initial Distance (feet)	218.6	21.7	177.2	260.0
(x_2/v_2) Apparent Gap (seconds)	4.0	0.43	3.2	4.9
(r_2) Opposing Driver Reaction Time (seconds)	3.5	0.45	2.6	4.4
(a_2) Opposing Driver Deceleration (feet/second^2)	-25.7	1.9	-28.8	-22.7

4.3.4 Case 2013-12-126

Figure C. 5, in the Appendix, show the after-crash scene diagram for NASS/CDS Case 2013-12-126 in which 2002 Impala turned left and collided with a 2012 Ford Fusion. Table 4.12 shows EDR pre-crash data for both vehicles.

Table 4.12 Pre-Crash EDR data from NASS/CDS Case 2013-12-126

Vehicle 1 (Impala)				
Time (seconds)	Speed (mph)	Engine RPM	Percent Throttle	Brake Switch
-5	28	960	1	ON
-4	24	960	1	ON
-3	22	960	1	ON
-2	19	2112	50	OFF
-1	17	2176	26	ON
Vehicle 2 (Fusion)				
Time (seconds)	Speed (mph)	Engine RPM	Accelerator Pedal (%)	Brake Switch
-5.0	46.6	1400	15	OFF
-4.5	46.6	1500	37	OFF
-4.0	47.2	2400	91	OFF
-3.5	47.8	4200	96	OFF
-3.0	49.7	4400	85	OFF
-2.5	52.2	4500	85	OFF
-2.0	52.8	4400	0	OFF
-1.5	49.7	4500	0	ON
-1.0	43.5	3400	0	ON
-0.5	37.9	2200	0	ON
0.0	26.7	1500	0	ON

Planar impact reconstruction yielded estimated impact speeds of 20.2 feet/second, 13.8 mph (standard deviation 8.1 feet/second) for the Impala and 44.9 feet/second, 30.6 mph (standard deviation 15.0 feet/second) for the Fusion. For this case the final deceleration for the Fusion was extrapolated from the preceding deceleration rates and the impact speed was then computed by extrapolating the last EDR speeds and deceleration rates, assuming the final time to collision was uniformly distributed between 0 on 0.5 seconds. As with the preceding case, bias and measurement error for the Fusion's pre-crash speed data was modeled using statistics reported by Ruth and Daily (2011). A constraint was imposed requiring that the arrival time of the opposing vehicle be within 0.25 seconds of the turning vehicle's arrival time, and Bayes estimates of the crash elements are shown in Table 4.13..

Table 4.13 Summary of the posterior distribution for elements characterizing NASS/CDS Case 2013-12-126

Element	Posterior Summary			
	Mean	Standard Deviation	2.5 %-ile	97.5 %-ile
(t_1) Turning Vehicle Time to Collision (seconds)	2.2	0.30	1.6	2.7
(v_2) Opposing Vehicle Initial Speed (feet/second)	77.8	1.0	75.2	79.1
(x_2) Opposing Vehicle Initial Distance (feet)	136.7	21.5	95.8	178.6
(x_2/v_2) Apparent Gap (seconds)	1.8	0.27	1.3	2.3
(r_2) Opposing Driver Reaction Time (seconds)	0.44	0.29	-0.10	1.00
(a_2) Opposing Driver Deceleration (feet/second^2)	-26.7	2.4	-31.0	-21.7

4.3.5 Case 2013-04-123

Figure C. 6, in the Appendix, show the after-crash scene diagram for NASS/CDS Case 2013-04-123 in which 2013 Dodge Charger turned left and collided with a 2005 Chevrolet Silverado. Table 4.14 shows pre-crash data for both vehicles. EDR pre-crash data for the Charger was provided for five seconds at 10 Hz, for a total of 50 data points, and only a subset of these are shown in Table 4.14.

Planar impact reconstruction yielded estimated impact speeds of 12.4 feet/second, 8.5 mph (standard deviation 6.0 feet/second) for the Charger and 20.6 feet/second, 14.0 mph (standard deviation 5.4 feet/second) for the Silverado. These were used as input into Bayesian trajectory reconstructions for both vehicles, with the final deceleration for Silverado taken as uniformly distributed between 0.5g and 0.9g. Measurement error and bias in the Charger's pre-crash speeds were modeled using statistics presented in Ruth and Reust (2009). A constraint was imposed requiring that the arrival time of the opposing vehicle be within 0.25 seconds of the turning vehicle's arrival time. Bayes estimates of the crash elements are shown in Table 4.15

Table 4.14 Pre-Crash EDR data from NASS/CDS Case 2013-04-123

Vehicle 1 (Charger)				
Time (seconds)	Speed (mph)	Engine RPM	Accelerator Pedal %	Brake Switch
-5.0	0	581	0	ON
-4.5	0	588	3	ON
-4.0	1	536	31	OFF
-3.5	2	1545	14	OFF
-3.0	5	1204	17	OFF
-2.5	7	1921	16	OFF
-2.0	11	1777	9	OFF
-1.5	12	1788	0	ON
-1.0	12	1679	0	ON
-0.5	11	1606	0	OFF
-0.1	4	754	0	OFF

Vehicle 2 (Silverado)				
Time (seconds)	Speed (mph)	Engine RPM	Throttle (%)	Brake Switch
-5	34	1728	17	OFF
-4	35	2048	23	OFF
-3	38	2496	43	OFF
-2	40	2624	52	OFF
-1	30	1088	0	ON

Table 4.15 Summary of the posterior distribution for elements characterizing NASS/CDS Case 2013-04-123

Element	Posterior Summary			
	Mean	Standard Deviation	2.5 %-ile	97.5 %-ile
(t_1) Turning Vehicle Time to Collision (seconds)	3.9	0.15	3.6	4.1
(v_2) Opposing Vehicle Initial Speed (feet/second)	52.4	1.2	50.2	54.7
(x_2) Opposing Vehicle Initial Distance (feet)	189.9	8.6	175.3	206.5
(x_2/v_2) Apparent Gap (seconds)	3.6	0.19	3.3	4.0
(r_2) Opposing Driver Reaction Time (seconds)	2.7	0.26	2.2	4.3
(a_2) Opposing Driver Deceleration (feet/second^2)	-21.4	3.6	-28.4	-16.3

4.4 CONCLUSION

What do drivers do when involved in crashes? Historically, quantitative answers to this question have been difficult to come by but for at least 15 years it has been hoped that pre-crash data from event data recorders might support development of an "objective driver behavior database" (Chidester et al., 1999). This chapter described a method for using EDR pre-crash data from two vehicles to estimate features of left-turn opposing path collisions. Efforts were made to quantify the uncertainties resulting from measurement errors, coarseness of sampling intervals, and uncertainty regarding the relation between the pre-crash data and the time of impact. Experience with the method in reconstructing six crashes from the NASS/CDS database suggested the following lessons:

1) Estimation is feasible but significant uncertainties remain. Precise characterization of individual events continues to be difficult but statistical analyses of suitably large samples should now be feasible.
2) Each crash showed unique features, and informed judgment was needed in applying the method to individual cases.
3) Comparing case 2013-12-111, where one vehicle had pre-crash data collected at a 0.5 second sampling rate, to the preceding two cases suggests that some uncertainty reduction should result from shorter sampling intervals. As vehicles compliant with 49CFR563 become more prevalent the results reported here should represent upper bounds on the uncertainty intervals associated with estimates rather than typical outcomes.

CHAPTER 5: LEFT-TURN CRASH SIMULATION MODEL

The design and operation of highway components is generally governed by twin objectives of efficiency and safety. In many situations, however, these objectives are in conflict. Rational balancing of efficiency and safety to produce a design or operational plan for a given location requires causal prediction of the effects of different alternatives. The *Highway Capacity Manual* (HCM), and more recently, micro-simulation programs, can be used to evaluate the operational efficiency of proposed alternatives; more recently, the *Highway Safety Manual* (HSM) offers engineers tools for predicting safety-related impacts. The HSM methodology essentially uses regression-type statistical models to predict crash frequency at a location under clearly defined base conditions and then uses empirically-developed crash modification factors (CMFs) to predict the effects of altering the base conditions. Although a substantial advance in the state of art, certain limitations of the HSM method have been identified, particularly that the CMFs describe at best average causal effects that ignore the possibility that the causal effect of safety-related treatment can vary across different locations as local conditions vary (Hauer, 2004; 2006).

If we possessed a complete theory of traffic crash causation, analytic or simulation models could be used to give the needed predictive power, much as simulation modeling is now used for operational decision support. In many areas of engineering, however, there may exist structural knowledge concerning some, but not all, relevant aspects of a phenomenon. In such cases, a mechanistic/empirical approach, which supplements the limited structural knowledge with empirically-developed relationships, can be used to produce useable design tools. The term “mechanistic/empirical” is borrowed from pavement design, where mechanical models are used to predict the stresses and strains in pavement layers caused by tire loadings, while empirical models are used to predict pavement damage from a history of stresses and strains

Protected-only left-turn phasing reduces left-turn crashes by eliminating conflicts between left-turning drivers and opposing drivers. Because it restricts left-turns to a limited portion of the signal cycle, when adequate gaps exist in the opposing traffic stream protected-only left-turn phasing can also increase the delay experienced by left-turning drivers (Hauer, 2004). This makes the safety versus efficiency trade-off especially salient, and unfortunately there does not appear to be a generally accepted estimate of the crash-reduction effect of shifting from permitted to protected phasing. FHWA’s Desktop Reference (Bahar et al., 2007) gives estimates of crash reductions ranging from 16% to 70%, while the HSM recommends 99%. This last estimate appears to be based on findings at a single intersection described in Davis and Aul (2007), where a change from permitted to protected phasing produced no left-turn crashes during a 3-year after period. At this intersection, the positioning of the left-turn lanes was such that views of opposing traffic were blocked when vehicles were waiting in the opposing left-turn lane (McCoy et al 2001), while highlights the site-specific nature of crash reduction effects.

Left-turn cross-path crashes occur when a driver attempts to turn left in front of a vehicle approaching from the opposite direction and is unable to complete the turn before colliding with the opposing vehicle.

For this project, a microscopic simulation model of left-turning conflicts and crashes, originally described in Davis and Aul (2007), was extended and enhanced based on the findings described in Chapter 2. The simulation model consists of three main components: (1) a traffic generation model employing Cowan's M3 distribution (Cowan, 1975), (2) gap-acceptance and turning-time models based on the empirical results described in Chapter 2, and (3) a simple kinematic braking model for the opposing vehicle, which uses statistics for reaction times and braking rates reported by Koppa et al. (1996). Development of the gap-acceptance model was described in Chapter 2, using video-based data collected at the intersection of Robert and Mendota. The model using log gap (Model 6) is currently implemented in the simulation model, and a statistical summary of its parameter estimates is presented in Table 5.1. To see how the parameter estimates in Table 5.1 are used, the fitted logit model states that the probability a typical driver at this intersection accepts a four-second gap would be estimated as

P [accept | gap=4 seconds] = exp(-8.3 + 4.8*log(4))/(1+exp(-8.3 + 4.8*log(4)) = 0.162

Table 5.1 Estimation summary of gap acceptance model parameters

Parameter	Estimate	Std. Error	Z-statistic	Significance
β_0	-8.3	0.6	-13.0	P < .0001
β_1	4.8	0.4	12.2	P < .0001

Figure 5.1 shows a plot of the probability of accepting a gap as a function of gap duration.

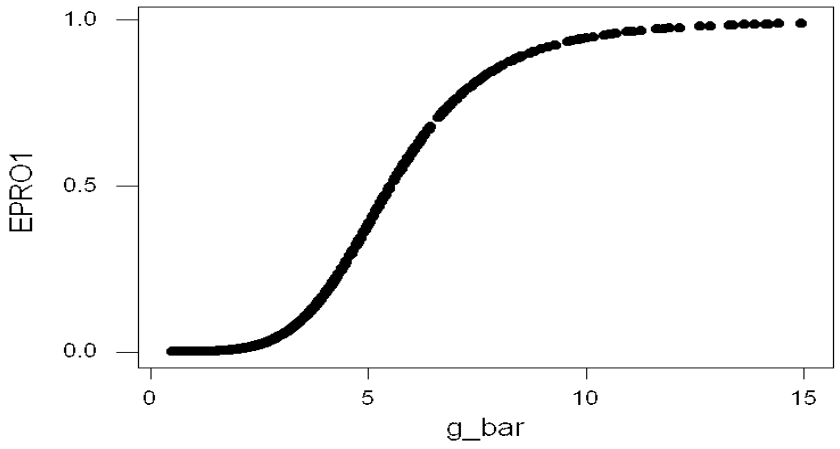

Figure 5.1 Acceptance probability as a function of gap.

Cowen's M3 distribution is a model of vehicle headways that assumes two types of traffic: platooned vehicles traveling with a constant headway Δ, and free-moving traffic with headways following a shifted exponential distribution. The cumulative distribution function for the headways is given by

$$F(t) = \begin{cases} 1 - \alpha \exp(-\lambda(t-\Delta)), & t \geq \Delta \\ 0, & t < \Delta \end{cases} \tag{5.1}$$

Where α is the proportion of freely moving vehicles in the traffic stream. The parameter λ is related to the traffic flow q via

$$\lambda = \frac{\alpha q}{1 - \Delta} \tag{5.2}$$

The field study described in Chapter 2 produced 749 observed headways, and Figure 5.2 is a histogram showing the frequencies of the observed headways.

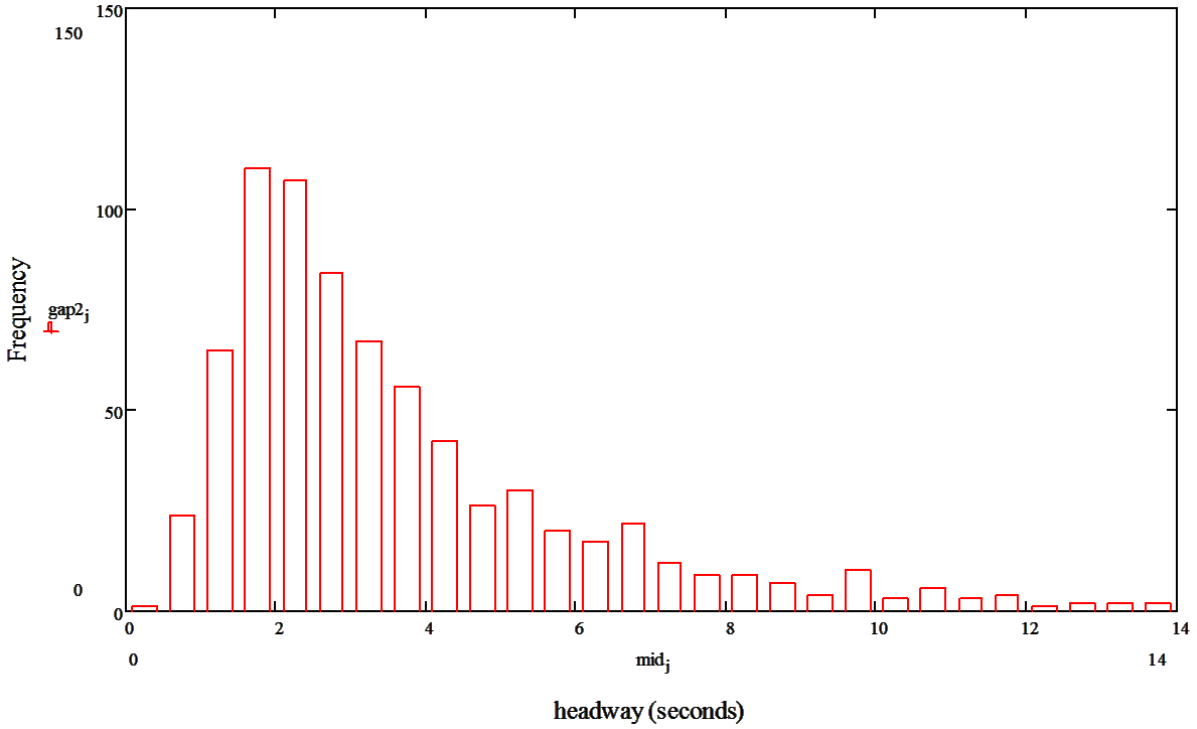

Figure 5.2 Headway (gap) distribution from field study.

Figure 5.2 suggests that the headway distribution is approximately exponential for headways greater than 2.0 seconds. Cowan's M3 distribution was then fit to these data using the method of moments and assuming a minimum free gap of 2.0 seconds (Sullivan and Troutbeck, 1994; Troutbeck, 1997). This gave an estimated proportion of "free" vehicles α=0.612 and an estimated decay parameter λ=0.359. Figure 5.3 compares the observed and fitted distributions for headways greater than 2.0 seconds.

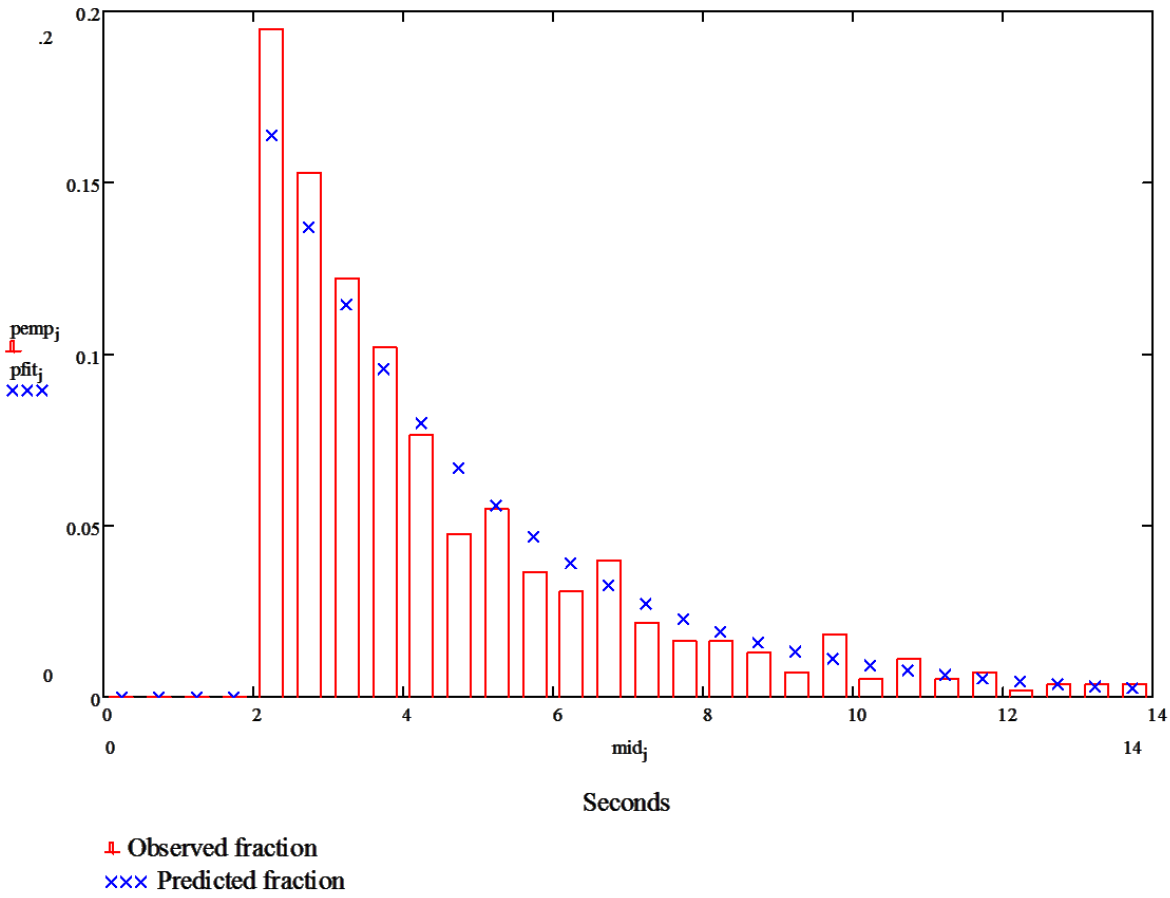

Figure 5.3 Gap distribution from field study compared to Cowan M3 model, for gaps>2.0 seconds.

The LT collision model is an adaptation of one described in Davis and Aul (2007). Basically, the model takes as input a mean and standard deviation for the distribution of opposing vehicle speeds, a value for the opposing traffic flow, and means and standard deviations describing distributions for the reaction times and braking rates for opposing drivers. In addition, the logit model parameters for the gap-acceptance model, and the linear regression model relating clearance times to accepted gaps are input. The model then proceeds as follows:

1) A random speed for the oncoming vehicle is drawn from a normal distribution.
2) A random gap for the oncoming vehicle is drawn from a Cowan M3 distribution.
3) The probability of acceptance is computed using the above logit model, and the corresponding distance is computed from the gap and speed.
4) A random gap acceptance decision is then drawn from a Bernoulli distribution with the above acceptance probability.
5) Random values are drawn for the oncoming driver's reaction time, braking deceleration, and the left-turn clearance time.
6) Crash/no crash is determined by comparing vehicle arrival times at the conflict point.

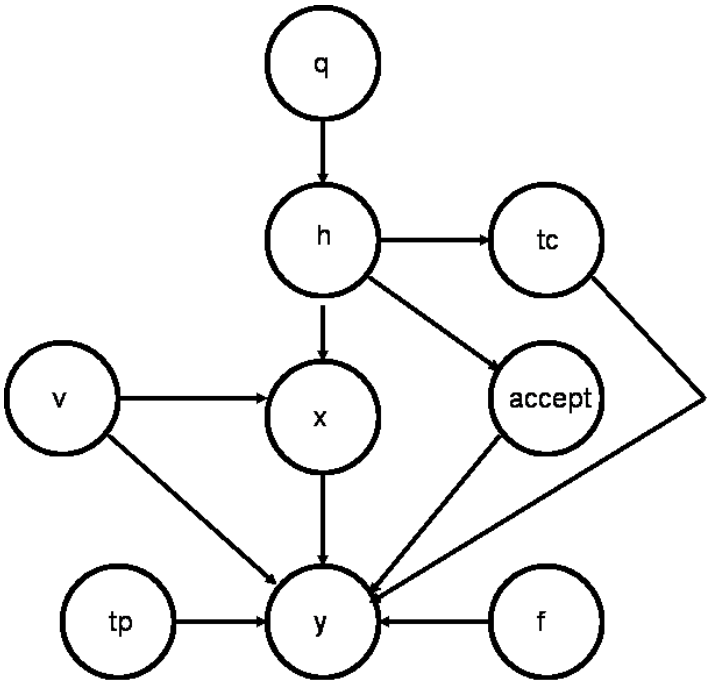

Figure 5.4 Left-turn crash simulation model as directed acyclic graph.

Figure 5.4 shows the dependency structure of the model as a directed acyclic graph (DAG), where

q = opposing traffic flow (vehicles/second)
h = traffic stream gap (seconds)
tc = left-turning vehicle's turning time (seconds)
v = opposing vehicle speed (feet/second)
x = opposing vehicle's distance at start of turn (feet)
accept = 0, gap rejected
1, gap accepted
tp = opposing driver's reaction time (seconds)
f = opposing driver's braking rate (g-units)
y = 0, no crash
1, crash.

The model was implemented using the simulation freeware WinBUGS (Lunn et al., 2013) and example model code is given in the Appendix.

5.1 SIMULATION EXPERIMENTS

The first version of the simulation model was designed to represent the Chapter 2 field study site at Robert and Mendota. The opposing vehicles' speeds were assumed to have a mean and standard deviation equal to those observed at the field site and gap acceptance and LT turning times were assumed to follow the models described in Chapter 2. Since the opposing approach had two through

lanes, the two-lane version of the Cowan headway model described by Sullivan and Troutbeck (1997) was used to generate the gaps in the opposing vehicle stream. Finally, the opposing drivers' reaction times and braking rates were generated from lognormal distributions with means and standard deviations taken from estimates reported by Koppa et al. (1996) for alerted drivers.

5.1.1 Simulating Gaps

The first test of the simulation model was to see if it could adequately reproduce traffic features observed in our field study. A Monte Carlo simulation was run for 100,000 iterations. Table 5.2 shows descriptive statistics from the field study, while Table 5.3 shows similar statistics as simulated by the model.

Table 5.2 Descriptive statistics for opposing vehicle characteristics from field study, all vehicles

	Mean	Std. Deviation	25%	50%	75%
Gap (second)	3.7	2.6	1.9	2.9	4.7
Speed (mph)	35.6	9.0	28.4	35.4	42.3
Distance (feet)	188.2	136.8	99.0	148.6	234.7
Clearance Time (second)	3.0	1.0	2.4	2.8	3.5

Table 5.3 Results from first simulation run: all gaps considered

Variable	Mean	Std. Deviation	2.5 %-ile	25 %-ile	75 %-ile	97.5 %-ile
Speed (mph)	35.6	9.0	17.9	29.5	41.7	53.3
Distance (ft)	193.7	146.2	61.0	104.5	233.7	603.1
Gap (second)	3.7	2.6	0.8	2.0	4.5	10.9

Comparing Table 5.3 with the corresponding rows of Table 5.2, we see that the simulated speeds and gaps match the observed data very well, as would be expected since the simulation was constructed so as to replicate these distributions. However, the derived variable, distance, also matches reasonably well and we concluded that the simulation model provides a reasonable representation of gap generation.

5.1.2 Simulating Crash Rates

Our second simulation exercise sought to look at the population of accepted gaps, in part to compare with data from the field study but mainly to see if our model generated reasonable collision rates. Since the denominator in an estimated conflict or collision rate is usually the number of left-turning vehicles, these rates need to be computed as fractions of accepted, rather than all, gaps. To implement this, we took advantage of WinBUGS ability to simulate conditional as well as unconditional distributions by setting the model's variable 'accept.sim' to the value 1; that is, a gap was accepted. Because we expected collisions to be relatively rare, this time the Monte Carlo simulator was run for 500,000 iterations. Table 5.5 summarizes the results from this run. Comparing Table 5.4 to the corresponding rows of Table 5.5 shows that the simulation model realistically replicated the accepted gaps.

Table 5.4 Descriptive statistics from field study for opposing vehicle characteristics in accepted gaps

	Mean	Std. Deviation	25 %-ile	50 %-ile	75 %-ile
Gap (second)	7.2	2.7	5.2	6.7	8.7
Speed (mph)	34.3	7.9	27.8	33.9	40.2
Distance (feet)	360.0	161.4	250.3	316.2	430.9

Table 5.5 Results of second simulation run: accepted gaps only

Variable	Mean	Std. Deviation	2.5 %-ile	25 %-ile	75 %-ile	97.5 %-ile
Speed (mph)	35.6	9.0	18.0	29.5	41.7	53.2
Distance (ft)	391.4	197.6	132.2	253.9	482.4	889.7
Gap (second)	7.5	3.2	3.2	5.3	9.0	15.5
Clearance Time (second)	3.0	1.0	1.6	2.4	3.6	5.3
Reaction Time (second)	0.6	0.3	0.2	0.4	0.7	1.4
Braking (g units)	0.75	0.1	0.57	0.68	0.81	0.96

The simulation model treats the LT and opposing vehicles as point masses, which can collide only if they arrive at the conflict point at exactly the same instant, but since vehicles occupy space, collisions can occur for a range of non-instantaneous arrivals. One of the model's parameters was the appropriate value for this range, and this was to be determined so that the simulation model tended to produce LT crash rates similar to those reported in the literature. Since turning movement volumes tend to be hard

to come by, most safety-related research uses average annual daily traffic on the major and minor approaches as predictors of intersection crash frequency, but a literature search turned up three studies that gave estimates of LT crash rates. Upchurch (1991) reported rates ranging from 0.55 to 4.54 crashes per million left-turning vehicles, while Maze et al. (1994) reported left-turn crash rates ranging from approximately 0 to 7 crashes per million left-turning vehicles. More recently, Shahdah et al. (2014) presented data on left-turn crashes from intersections in Toronto and the information in its Tables 6 and 7 can be used to compute a crash rate of approximately 2.3 left-turn crashes per million left-turning vehicles. After some experimentation, it was found that requiring gaps shorter than 2.5 seconds to be rejected and using a crash time window of 0.5 seconds appeared to give reasonable results. A simulation of 5 million accepted gaps was run, producing 38 simulated crashes. The estimated crash rate would then be 7.6 crashes/million LTs with an approximate 95% confidence interval of (5.1, 10.1). Since the simulation was run to replicate peak-period (3 PM – 6 PM) conditions the model appeared to give reasonable LT crash rates.

5.1.3 Simulating Variation in Crash Risk

The next check on the simulation model was to compare it to a relative risk regression model described in Davis et al., 2016. This regression model was developed to predict how risk of a LT crash varies as LT and opposing traffic volumes vary throughout a typical day. For intersections similar to the one used in the field study (Robert and Mendota in Inver Grove Heights), the fitted regression model took the form

$$RR = \exp\left((.38)\ln\left(\frac{LT_{t\arg et}}{LT_{base}}\right) + (.37)\ln\left(\frac{OP_{t\arg et}}{OP_{base}}\right)\right) \tag{5.3}$$

Here LT_{target} and OP_{target} denote hourly left-turn and opposing flows during target conditions, while LT_{base} and OP_{base} denote corresponding flows during a base condition. RR then gives the proportional change in LT crash risk during the target condition compared to the base condition. For example, a base condition of LT_{base}=50 vehicles/hour, OP_{base}=1000 vehicles/hour and a target demand of LT_{target}=150 vehicles/hour and Op_{target}=1500 vehicles/hour gives a risk ratio of

$$RR = \exp\left((.38)\ln\left(\frac{150}{50}\right) + (.37)\left(\frac{1500}{1000}\right)\right) = 1.76$$

That is, a left-turn crash is 76% more likely during the target condition than during the base condition.

The second term in equation (5.3), which can be re-written as

$$\left(\frac{OP_{t\arg et}}{OP_{base}}\right)^{0.37} \tag{5.4}$$

which describes how LT crash risk changes as opposing traffic flow changes. That is, since $2^{.37}$=1.29, a doubling of opposing traffic flow is associated with a 29% increase in LT crash risk. Using the simulation model 10,000,000 accepted LT gaps were simulated for opposing flows 200, 400, 600, 800, and 1000 vehicles/hour, and the numbers of simulated left crashes were recorded. Figure 5.5 compares simulated risk ratios to those computed using the empirical relationship (5.4), when there is no change in LT flow and the base opposing flow is 200 vehicles/hour. Also shown in Figure 5.5 are approximate ±1 standard error intervals to the simulation-based estimates.

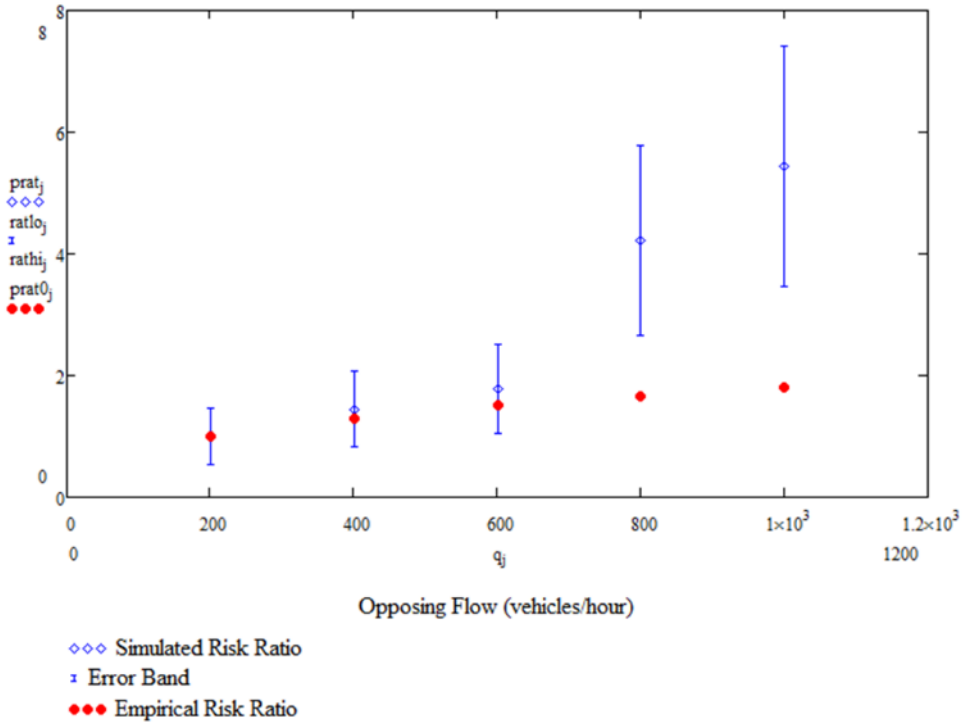

Figure 5.5 Comparison of Empirical and Simulated Estimates of Left-Turn Crash Risk Ratio.

Figure 5.5 shows that, for low opposing demand flows, the empirical and simulation risk ratios are comparable but that these diverge for higher demand flows. In the simulation model, the fraction of short gaps increases as opposing flow increases, and thus other things being equal, the likelihood of LT crash is a convex function of opposing flow. For the empirical model, however, the estimated coefficient of 0.37 means that the relationship between crash risk and opposing flow is concave. That is, according to the empirical model, doubling the opposing flow produces only a 29% increase in crash risk. Concave relationships between traffic volume and crash experience are very common in empirical safety models, and to date, there is no satisfactory explanation for this effect. (One possibility of course is that drivers tend to be more alert in higher traffic situations and so less likely to make errors.) In any case, an inability to replicate this effect is a weakness of the simulation model and absent a convincing theoretical explanation for this effect, only *ad hoc* adjustments are possible.

5.1.4 Simulating Crash Modification Factors

Crash modification factors (CMF) are used in the *Highway Safety Manual* to describe how expected crash frequencies change as roadway conditions change. They are most commonly estimated using before-after and cross-sectional data from numerous road locations, but Davis (2014) has recently described how, in certain situations, CMFs might also be estimated from detailed information about individual crashes. Of interest here is the nonparametric estimator given in equation (16) (Davis, 2014, p. 298). From Figure 5.4 it can be seen that the node h intercepts all paths connecting q to y. This means that the crash outcome y is conditionally independent of traffic flow (q), given the traffic stream gap (h) (Pearl, 2010). Applying a continuous version of equation (16) in Davis (2014), the CMF associated with a change in traffic flow from q_0 to q_1 can be computed via

$$CMF = \frac{P(y=1 \mid q_1)}{P(y=1 \mid q_0)} = \int \frac{f(h \mid y=1, q_0) f(h \mid q_1)}{f(h \mid q_0)} dh \qquad (5.5)$$

To apply equation (5.5) we need to know the distribution of gaps (h) under both flow conditions and the distribution of gaps in crashes that occur during flow condition q_0. In principle, these can be simulated with sample sizes much smaller than those needed to estimate raw crash rates. As an initial investigation of this possibility, we selected a scenario consisting of a one-lane opposing approach, where traffic gaps follow a Cowan M3 distribution with a minimum gap of Δ=2.0 seconds, and where the proportion of free vehicles is related to traffic flow via Tanner's (1962) linear relation

$$\alpha = 1 - \Delta q \qquad (5.6)$$

This gives a relationship such that when traffic flow is 1800 vehicles/hour/lane (q=0.5 vehicles/second) all vehicles are platooned, with no freely moving vehicles. All other features of this simulation were the same as used earlier.

Table 5.6 Mean elements of simulated crashes at two levels of opposing traffic flow

Opposing Flow	Speed (feet/second)	Distance (feet)	Turn time (second)	Reaction time (second)	Deceleration (g)	Gap (second)
200	64.8 (13.0)	183.8 (43.1)	3.61 (0.49)	2.03 (0.68)	0.70 (0.10)	2.84 (0.36)
400	64.4 (13.0)	181.6 (41.4)	3.58 (0.46)	2.03 (0.66)	0.71 (0.10)	2.83 (0.33)
600	64.6 (12.8)	180.2 (39.4)	3.55 (0.43)	1.99 (0.62)	0.70 (0.10)	2.79 (0.28)

800	64.9 (12.9)	180.6 (39.2)	3.55 (0.42)	1.96 (0.64)	0.70 (0.10)	2.79 (0.28)
1000	64.2 (12.7)	179.6 (39.9)	3.57 (0.44)	1.99 (0.62)	0.70 (0.10)	2.80 (0.29)

Table 5.7 Left-turn crash element estimated from six actual left-turn crashes

NASS/CDS Case	Speed (feet/second)	Distance (feet)	Turn time (second)	Reaction time (second)	Deceleration (g)	Gap (second)
2012-12-044	56.7 (1.5)	170.6 (27.8)	3.0 (0.4)	1.1 (0.6)	0.45 (0.06)	2.6 (0.45)
2013-74-034	74.9 (1.3)	181.3 (36.1)	2.8 (0.5)	1.4 (0.5)	0.86 (0.06)	2.4 (.0.47)
2012-12-111	49.1 (1.2)	114.7 (10.8)	2.5 (0.2)	1.6 (0.35)	0.68 (0.11)	2.3 (0.24)
2013-49-059	54.0 (1.0)	218.6 (21.7)	4.0 (0.4)	3.5 (0.45)	0.80 (0.06)	4.0 (0.43)
2013-12-126	77.8 (1.0)	136.7 (21.5)	2.2 (0.3)	0.44 (0.29)	0.83 (0.08)	1.8 (0.27)
2013-04-123	52.4 (1.2)	189.9 (8.6)	3.9 (0.15)	2.9 (0.26)	0.66 (0.11)	3.6 (0.19)
Average	60.8	168.6	3.1	1.82	0.71	2.8

Table 5. 7 summarizes the posterior means and standard deviation for the elements estimated from the six NASS/CDS crashes described in Chapter 4. The bottom row of Table 5. 7 presents averages the individual posterior means and comparing the bottom row of Table 5. 7 to the simulated means in Table 5. 6 indicates that the simulated crashes are not dissimilar from the actual crashes investigated so far.

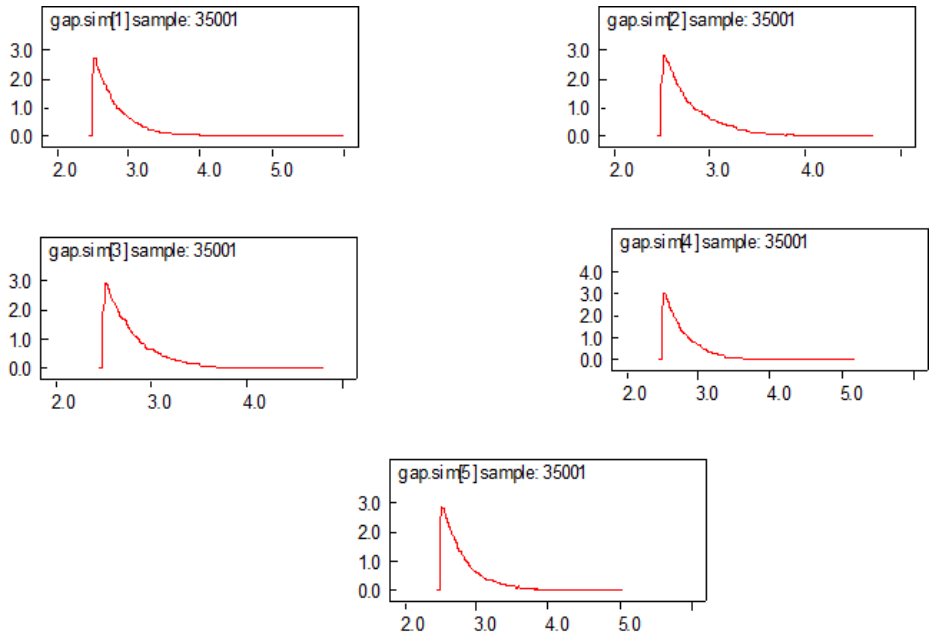

Figure 5.6 Probability density functions for gaps in simulated crashes.

Figure 5.6 shows the kernel density estimates of the probability density functions (PDF) for simulated crash-involved gaps, with opposing traffic flows of 200, 400, 600, 800, and 1000 vehicles/hour. Each of the PDFs shown in Figure 5.6. is consistent with that of a shifted exponential distribution with a minimum value of 2.5 seconds, and the similarities among the means and standard deviations for these simulated gaps indicate that the same shifted exponential describes crash-involved gaps in each flow condition. If the population of crash-involved gaps follows a shifted exponential distribution while the original gap distributions follow Cowan M3 distributions with the fraction of free vehicles given by equation (5.6), then the integral in (5.5) can be evaluated in closed form to give

$$CMF = \left(\frac{1-\Delta q_1}{1-\Delta q_0}\right)\left(\frac{q_1}{q_0}\right)\left(\frac{\lambda_c}{\lambda_c + q_1 - q_0}\right)\exp\left(-(q_1 - q_0)(\Delta_c - \Delta)\right) \quad (5.7)$$

Here λc and Δ_c denote, respectively, the rate and minimum value parameters for the shifted exponential describing the crash-involved gaps in the initial (q_0) condition.

Table 5.8 compares CMFs computed using equation (5.7), with crash-involved gaps assumed to follow and shifted exponential distribution with minimum values of 2.6 seconds and a mean of 2.8 seconds, with risk ratio estimates computed using the empirical relationship given in equation (5.4). As before, the base condition was taken to be an opposing flow of 200 vehicles/hour. Overall, the simulation-based CMFs computed using equation (5.7) are roughly similar to the empirical CMFs computed using equation (5.4).

Table 5.8 Comparison of risk ratio estimates computed using equations (5.4) and (5.7)

Flow (vehicles/hour)	Equation (5.4)	Equation (5.7)
200	1.0	1.0
400	1.29	1.67
600	1.50	2.06
800	1.67	2.19
1000	1.81	2.09

5.2 CONCLUSION

This chapter described a microscopic simulation model of left-turn crash occurrence where left-turns are permitted but not protected. The simulation model produced traffic flow and gap-acceptance behavior similar to that observed in Chapter 2's field study and, after some calibration, left-turn crash rates similar to those reported in the literature. When comparing how left-turn crash risk varies with opposing traffic flow, there was a noticeable discrepancy between the simulated risk and the risk as predicted by an empirical model developed by Davis et al. (2016). On the other hand, the characteristics of simulated crashes were consistent with characteristics estimated for the six actual crashes described in Chapter 4, and application of a method for computing risk variation described in (Davis, 2014) produced better comparability with the empirical model.

Overall, the simulation model appears promising but is not yet ready for application. The discrepancy between the simulated and empirical risk shown in Figure 5.4 needs to be explained, and it would be helpful to have a larger sample of reconstructed crashes for comparison. Especially interesting is the possibility of using variants of equation (5.5) to simulate crash-modification effects without having to generate the many millions of events needed to simulate raw crash rates.

REFERENCES

ARC-CSI, 2015 Conference Data Flash Drive (2015). *Collision*, 10(2).

Archer, J. (2005). *Indicators of Traffic Safety Assessment and Prediction and their Application in Micro-Simulation Modelling: A Study of Urban and Suburban Intersections*. Doctoral Dissertation, Dept. of Infrastructure, Royal Institute of Technology, Stockholm, Sweden.

Bahar, G. B., Masliah, M., Wolff, R., and Park, P. (2007). *Desktop reference for crash reduction factors* (No. FHWA-SA-07-015), FHWA, Washington, D.C.

Ball, J. K., Danaher, D. A., and Ziernicki, R. M. (2007). *Considerations for applying and interpreting monte carlo simulation analyses in accident reconstruction* (No. 2007-01-0741). SAE Technical Paper, SAE International, United States.

Bleyl, R. (1976). Using photographs to map traffic accident scenes: A mathematical technique. *Journal of Safety Research*, 8, 59-64.

Bortles, W., Biever, W., Carter, N., and Smith, C. (2016). *A Compendium of Passenger Vehicle Event Data Recorder Literature and Analysis of Validation Studies* (No. 2016-01-1497). SAE Technical Paper, SAE International, United States.

Brach, R. M. (1991). *Mechanical impact dynamics: rigid body collisions*. New York: J. Wiley.

Brach, R. M., and Brach, R. M. (2011). *Vehicle accident analysis and reconstruction methods Methods (2nd edition)*. SAE International.

Brach, R. M., Brach, R. M., and Mink, R. A. (2015). Nonlinear optimization in vehicular crash reconstruction. *SAE International Journal of Transportation Safety*, *3*(1), 17-27.

Caird, J.and P. Hancock. (1994). The perception of arrival time for different oncoming vehicles arriving at an intersection. *Ecological Psychology*, 6, 83-109

Carlin, B. and T. Louis. (2000). *Bayes and Empirical Bayes Methods for Data Analysis*, 2nd Edition. Boca Raton: Chapman & Hall/CRC, 2000.

Chidester, A., Hinch, J., Mercer, T. C., and Schultz, K. S. (1999). *Recording automotive crash event data*. Presented at the International Symposium on Transportation Recorders, Arlington, VA, May 3-5.

Cowan, R. J. (1975). Useful headway models. *Transportation Research*, 9(6), 371-375.

Daganzo, C. (1981). Estimation of gap-acceptance parameters within and across the population from direct roadside observation. *Transportation Research*, *15B,* 1-15.

Davis, G. (2003). Bayesian reconstruction of traffic accidents. *Law, Probability and Risk*, *2(2)*, 69-89.

Davis, G. (2011). A Bayesian approach to cross-validation in pedestrian accident reconstruction. *SAE International Journal of Passenger Cars-Mechanical Systems, 4(1), 293-303.*

Davis, G. (2014). Crash reconstruction and crash modification factors. *Accident Analysis and Prevention*, *62*, 294-302.

Davis, G. (2015). *A Comparison of Bayesian Speed Estimates from Rollover and Critical Speed Methods* (No. 2015-01-1434). SAE Technical Paper, SAE International, United States.

Davis, G. A., Hourdos, J., and Moshtagh, V. (2015). *Development of Guidelines for Permitted Left-Turn Phasing Using Flashing Yellow Arrows*. Minnesota Department of Transportation Report, St. Paul, MN.

Davis, G. and N. Aul. (2007). *Safety Effects of Left-Turn Phasing Schemes at High-Speed Intersections*. Report No. MN/RC-2007-03, Minnesota Department of Transportation, St. Paul, MN.

Davis, G. and Mudgal, A. (2013). *Field Study of Driver Behavior at Permitted Left-Turn Indications*, Final Report. Intelligent Transportation Systems Institute, University of Minnesota.

Davis, G. and Swenson, T. (2004). Field study of gap-acceptance by left-turning drivers. *Transportation Research Record*, *1899,* 71-75.

Expert Autostats, 4NXPRT Systems (2014).

Gabler, H. C., and Hinch, J. (2009). *Feasibility of using event data recorders to characterize the pre-crash behavior of drivers in rear-end collisions*. In Proceedings of the 21st International Conference on the Enhanced Safety of Vehicles, Stuttgart, Germany.

Gattis, J. and Low, S. (1999). Gap-acceptance at atypical stop-controlled intersections. *ASCE J. of Transportation Engineering, 125*, 201-207.

Geman, S., and Geman, D. (1984). Stochastic relaxation, Gibbs distributions, and the Bayesian restoration of images. *IEEE Transactions on Pattern Analysis and Machine Intelligence, (6)*, 721-741.

Google Maps. (2012). Robert Street and Mendota Road Intersection. Retrieved from: https://www.google.com/maps/.

Hampton, C. E., and Gabler, H. C. (2010). Evaluation of the accuracy of NASS/CDS Delta-V estimates from the enhanced WinSmash algorithm. *Annals of Advances in Automotive Medicine/Annual Scientific Conference, 54,* 241-252.

Hanley, J. A., and McNeil, B. J. (1982). The meaning and use of the area under a receiver operating characteristic (ROC) curve. *Radiology, 143(1),* 29-36.

Hauer, E. (2004). *Left-Turn Protection, Safety, Delay and Guidelines: A Literature Review*. October 2004. Retrieved from: http://www.roadsafetyresearch.com.

Hosmer, D., and Lemeshow, S. (2000). *Applied Logistic Regression (2nd edition)*. New York: J. Wiley.

Hutton, J. M., Bauer, K. M., Fees, C. A., and Smiley, A. (2015). *Analysis of Naturalistic Driving Study Data: Offset Left-Turn Lanes* (No. SHRP 2 Report S2-S08B-RW-1). Washington, DC: The National Academies Press.

Kita, H (1993). Effects of merging lane length on the merging behavior at expressway on-ramps. Proceedings of the 12th International Symposium on Transportation and Traffic Theory, Berkeley, USA.

Jones, I., and Baum, A. (1978). Research Input for Computer Simulation of Automobile *Collisions, volume IV*, Report DOT-HS-805-040. National Highway Traffic Safety Administration, Washington, DC.

Kloeden, C. N., McLean, A. J., Moore, V. M., and Ponte, G. (1997). *Traveling Speed and the Risk of Crash Involvement*. NHMRC Road Accident Research Unit, The University of Adelaide, Australia.

Koppa, R., Fambro, D., & Zimmer, R. (1996). Measuring driver performance in braking maneuvers. *Transportation Research Record*, (1550), 8-15.

Kusano, K. D., and Gabler, H. (2011). Method for estimating time to collision at braking in real-world, lead vehicle stopped rear-end crashes for use in pre-crash system design. *SAE International Journal of Passenger Cars-Mechanical Systems, 4(1),* 435-443.

Kusano, K. D., and Gabler, H. C. (2013). Automated crash notification: Evaluation of in-vehicle principal direction of force estimations. *Transportation research part C: Emerging technologies*, *32*, 116-128.

Lindley, D. V. (1991). Subjective probability, decision analysis and their legal consequences. *Journal of the Royal Statistical Society. Series A (Statistics in Society)*, *154(1),* 83-92.

Lunn, D., Jackson, C., Best, N., Thomas, A., and Spiegelhater, D. (2013) *The BUGS Book: A Practical Introduction to Bayesian Analysis*. Boca Raton, FL: CRC Press.

Madanat, S., Cassidy, M., & Wang, M. (1994). Probabilistic Delay Model at Stop-Controlled Intersection. Journal of Transportation Engineering, 120(1), 21-36.

Mahmassani, and Sheffi. (1981). Using gap sequences to estimate gap acceptance functions. *Transportation Research Part B, 15*(3), 143-148..

Mak, K. K. (2010). *Identification of vehicular impact conditions associated with serious ran-off-road crashes*. National Cooperative Highway Research Program Report 665, Transportation Research Board, Washington, DC.

Maze, T., Henderson, J., and Sankar, R. (1994). *Impacts on Safety of Left-Turn Treatment at High-Speed Signalized Intersection*. Iowa Transportation Center, Iowa State University, IA.

McCoy, P. T., Pesti, G. S., Byrd, P. A., & Singh, V. (2001). Guidelines for opposing left-turn lane-line widths. *Transportation Research Record, 1751,* 26-34.

Metropolis, N., Rosenbluth, A. W., Rosenbluth, M. N., Teller, A. H., and Teller, E. (1953). Equation of state calculations by fast computing machines. *The journal of chemical physics, 21(6),* 1087-1092.

Minitab Inc (2010). *Minitab 17 Statistical Software*. State College, PA: Minitab, Inc.

Minnesota Department of Public Safety (2012). *Minnesota Motor Vehicle Crash Facts 2012.* Retrieved from https://dps.mn.gov/divisions/ots/educational-materials/Documents/CRASH-FACTS-2012.pdf. Accessed Jan, 2015.

MnDOT (2007). *Minnesota Strategic Highway Safety Plan*. Minnesota Department of Transportation, St. Paul, MN.

Moser, A., Steffan, H., Spek, A., and Makkinga, W. (2003). *Application of the monte carlo methods for stability analysis within the accident reconstruction software pc-crash* (No. 2003-01-0488). SAE Technical Paper, SAE International, United States.

National Research Council, Transportation Research Board. (2010). *HCM 2010: Highway Capacity Manual*. Transportation Research Board, Washington, D.C.

Niehoff, P., Gabler, H. C., Brophy, J., Chidester, C., Hinch, J., and Ragland, C. (2005). *Evaluation of event data recorders in full systems crash tests* (Paper No. 05-0271). In Proceedings of the Nineteenth International Conference on Enhanced Safety of Vehicles, Washington, D.C., USA.

Osius, G., and Rojek, D. (1992). Normal goodness-of-fit tests for multinomial models with large degrees of freedom. *Journal of the American Statistical Associatio*n*, 87(420),* 1145-1152.

Pearl, J. (2009). *Causality (2nd edition)*. New York: Cambridge University Press.

R Core Team (2015). R: A language and environment for statistical computing. *R Foundation for Statistical Computing*, Vienna, Austria. Retrieved from: https://www.R-project.org/.

Ragland, D.R., Arroyo, S., Shladover, S.E., Misener, J.A., Chan, C.Y. (2006). Gap acceptance for vehicles turning left across on-coming traffic: Implications for intersection decision support design. *TRB 85th Annual Meeting Compendium of Papers CD-ROM*.

Rose, N. A., Fenton, S. J., and Hughes, C. M. (2001). *Integrating Monte Carlo simulation, momentum-based impact modeling, and restitution data to analyze crash severity* (No. 2001-01-3347). SAE Technical Paper, SAE International, United States.

Rosén, E., Källhammer, J. E., Eriksson, D., Nentwich, M., Fredriksson, R., and Smith, K. (2010). Pedestrian injury mitigation by autonomous braking. *Accident Analysis and Prevention, 42(6),* 1949-1957.

Ruth, R., and Daily, J. (2011). Accuracy of Event Data Recorder in 2010 Ford Flex During Steady State and Braking Conditions. *SAE International Journal of Passenger Cars-Mechanical Systems, 4(1),* 677-699.

Ruth, R. R., and Reust, T. J. (2009). Accuracy of Selected 2008 Chrysler Airbag Control Module Event Data Recorders. *SAE International Journal of Passenger Cars-Mechanical Systems, 2(1),* 983-990.

Sander, U., (2017) Opportunities and Limitations for Intersection Collision Intervention-A Study of Real World 'Left Turn Across Path' Accidents. *Accident Analysis and Prevention*, 99, 342-355.

Scanlon, J. M., Page, K., Sherony, R., and Gabler, H. C. (2016). *Using event data recorders from real-world crashes to investigate the earliest detection opportunity for an intersection advanced driver assistance system* (No. 2016-01-1457). SAE Technical Paper, SAE International, United States.

Shaddah, U., Saccomanno, F., and Persaud, B. (2014). Integrated traffic conflict model for estimating crash modification factors. *Accident Analysis and Prevention, 71,* 228-235.

Shahdah, U., Saccomanno, F., & Persaud, B. (2015). Application of traffic microsimulation for evaluating safety performance of urban signalized intersections. *Transportation Research Part C: Emerging Technologies*, 60, 96-104.

Srinivasan, R., Smith, S., Sundstrom, C., Lyon, C., Persaud, B., Baek, J., & Gross, F. (2012). Crash modification factors for changes to left-turn phasing. *Transportation Research Record, 2279,* 108-117.

Staplin, L. (1995). Simulator and field measures of driver age differences in left-turn gap judgments. *Transportation Research Record, 1485,* 49-55.

StataCorp (1999). *Stata data analysis and statistical Software: Release 6.0.* College Station, TX.

Stukel, T. A. (1988). Generalized logistic models. *Journal of the American Statistical Association, 83(402),* 426-431.

Sturtz, S., Ligges, U., and Gelman, A. (2005). R2WinBUGS: A Package for Running WinBUGS from R. *Journal of Statistical Software, 12(3),* 1-16.

Sullivan, D., & Troutbeck, R. (1994). The use of Cowan's M3 headway distribution for modelling urban traffic flow. *Traffic Engineering and Control, 35(7-8)*, 445-450.

Sullivan, D. P., & Troutbeck, R. J. (1997). An exponential relationship for the proportion of free vehicles on arterial roads. *Transportation Research Part A: Policy and Practice*, *31*(1), 21-33.

Tanner, J. (1962) A Theoretical Analysis of Delays at an Uncontrolled Intersection, *Biometrica*, 49, 163-170.

Treat, J., Tumbas, N., McDonald, S., Shinar, D., Hume, R., Mayer, R., Stansifer, R., and Castellan, N. (1979). *Tri-Level Study of the Causes of Traffic Accidents*, Report HS-034-3-535. National Highway Traffic Safety Administration, Washington, DC.

Troutbeck, R. (1997). A review on the process to estimate the Cowan M3 headway distribution parameters. *Traffic Engineering and Control, 38,* 600-603.

Upchurch, J., (1991). Comparison of left-turn accident rates for different types of left-turn phasing. *Transportation Research Record, 1324,* 33-40.

Wang, X. and M. Abdel-Aty. (2008). Analysis of Left-turn Crash Injury Severity by Conflicting Pattern Using Partial Proportional Odds Models. *Accident Analysis and Prevention, 40,* 1674–1682.

Weesie, J. (1999). Windmeijer's goodness-of-fit test for logistic regression. *Stata Technical Bulletin*, *8(44).*

Wilkinson, C. C., Lawrence, J. M., Heinrichs, B. E., and King, D. J. (2006). *The Timing of Pre-Crash Data Recorded in General Motors Sensing and Diagnostic Modules* (No. 2006-01-1397). SAE Technical Paper, SAE International, United States.

Windmeijer, F. A. G. (1990). The asymptotic distribution of the sum of weighted squared residuals in binary choice models. *Statistica Neerlandica, 44(2),* 69-78.

Wood, D. P., and O'Riordain, S. (1994). *Monte Carlo simulation methods applied to accident reconstruction and avoidance analysis* (No. 940720). SAE Technical Paper, SAE International, United States.

Young, W., Sobhani, A., Lenné, M. G., & Sarvi, M. (2014). Simulation of safety: A review of the state of the art in road safety simulation modelling. *Accident Analysis & Prevention, 66,* 89-103

APPENDIX A: WINBUGS CODE IMPLEMENTING BAYESIAN RECONSTRUCTION USING PLANAR IMPACT MECHANICS

```
model planar recon
# reconstruction via Brach and Brach (2011) planar impact model
# English units
# ARC-CSI 2106 Test #1
# actual data
{

# constants

g <- 32.2
pi <- 3.141592
d2r <- pi/180
mph2fps <- 88/60

# initial conditions

# vehicle 1
# theta1.lo <- (theta1.deg-anglebound)*d2r
# theta1.hi <- (theta1.deg+anglebound)*d2r
# theta1 ~ dunif(theta1.lo, theta1.hi)
theta1 <- theta1.deg*d2r
phi1 <- phi1.deg*d2r
omega1 <- omega1.deg*d2r
# phi1.lo <- (phi1.deg-anglebound)*d2r
# phi1.hi <- (phi1.deg+anglebound)*d2r
# phi1 ~ dunif(phi1.lo,phi1.hi)
# d1.lo <- max(0,d1.in-dbound)
# d1.hi <- d1.in+dbound
# d1 ~ dunif(d1.lo,d1.hi)
d1 <- d1.in

# vehicle 2
# theta2.lo <- (theta2.deg-anglebound)*d2r
# theta2.hi <- (theta2.deg+anglebound)*d2r
# theta2 ~ dunif(theta2.lo, theta2.hi)
theta2 <- theta2.deg*d2r
omega2 <- omega2.deg*d2r
phi2 <- phi2.deg*d2r
# phi2.lo <- (phi2.deg-anglebound)*d2r
# phi2.hi <- (phi2.deg+anglebound)*d2r
# phi2 ~ dunif(phi2.lo,phi2.hi)
# d2.lo <- max(0,d2.in-dbound)
```

```
# d2.hi <- d2.in+dbound
# d2 ~ dunif(d2.lo,d2.hi)
d2 <- d2.in

# collision

# Gamma.lo <-(Gamma.deg-anglebound)*d2r
# Gamma.hi <- (Gamma.deg+anglebound)*d2r
# Gamma ~ dunif(Gamma.lo,Gamma.hi)
Gamma <- Gamma.deg*d2r
e <- 0.1
# e ~ dunif(.2,.6)
mupercent <- 100


# core computations

# v1 ~ dunif(41.5,42.5)
# v2 ~ dunif(50,51)
v1 ~ dunif(5,100)
v2 ~ dunif(5,100)

v1x <- v1*cos(theta1+pi)
v1y <- v1*sin(theta1+pi)
v2x <- v2*cos(theta2)
v2y <- v2*sin(theta2)

v1n <- v1x*cos(Gamma)+v1y*sin(Gamma)
v1t <- -v1x*sin(Gamma)+v1y*cos(Gamma)
v2n <- v2x*cos(Gamma)+v2y*sin(Gamma)
v2t <- -v2x*sin(Gamma)+v2y*cos(Gamma)

mbar <- (m1*m2)/(m1+m2)
k21 <- I1/m1
k22 <- I2/m2

da <- d2*sin(theta2+phi2-Gamma)
db <- d2*cos(theta2+phi2-Gamma)
dc <- d1*sin(theta1+phi1-Gamma)
dd <- d1*cos(theta1+phi1-Gamma)

vrn <- (v2n-da*omega2)-(v1n+dc*omega1)
```

```
r <-( (v2t-db*omega2)-(v1t+dd*omega1))/((v2n-da*omega2)-(v1n+dc*omega1))

A <- 1 +((mbar*dc*dc)/(m1*k21))+((mbar*da*da)/(m2*k22))
B <- ((mbar*dc*dd)/(m1*k21))+((mbar*da*db)/(m2*k22))
C <- ((mbar*dd*dd)/(m1*k21))+((mbar*db*db)/(m2*k22))

mu0 <- (r*A+(1+e)*B)/((1+e)*(1+C)+r*B)
mu <- mu0*mupercent/100
# mu ~ dunif(0,mu0)

q1 <- (mbar*da*da)/(m2*k22)
q2 <- (mbar*dc*dc)/(m1*k21)
q3 <- (mbar*dc*dd)/(m1*k21)
q4 <- (mbar*da*db)/(m2*k22)
q <- 1/(1+q1+q2-mu*(q3+q4))

V1n <- v1n+mbar*(1+e)*vrn*(q/m1)
V1t <- v1t + mu*mbar*(1+e)*vrn*(q/m1)
V2n <- v2n-mbar*(1+e)*vrn*(q/m2)
V2t <- v2t -mu*mbar*(1+e)*vrn*(q/m2)

Pn <- m1*(V1n-v1n)
Pt <- m1*(V1t-v1t)

Omega1 <- omega1 +mbar*(1+e)*vrn*(dc-mu*dd)*(q/(m1*k21))
Omega2 <- omega2 + mbar*(1+e)*vrn*(da-mu*db)*(q/(m2*k22))

V1x <- V1n*cos(Gamma)-V1t*sin(Gamma)
V1y <- V1n*sin(Gamma)+V1t*cos(Gamma)
V2x <- V2n*cos(Gamma)-V2t*sin(Gamma)
V2y <- V2n*sin(Gamma)+V2t*cos(Gamma)

V1 <- sqrt(V1x*V1x+V1y*V1y)
V2 <- sqrt(V2x*V2x+V2y*V2y)

de <- dc-mu*dd
df <- da-mu*db

TL <- (.5)*mbar*q*(vrn*vrn)*(1+e)*(2+2*mu*r-
(1+e)*q*(1+(mu*mu)+(mbar*de*de)/(m1*k21)+(mbar*df*df)/(m2*k22)))

#predicted delta v's
```

```
deltav1.x <- V1x-v1x
deltav1.y <- V1y-v1y
deltav2.x <- V2x-v2x
deltav2.y <- V2y-v2y

deltav1.fr <- deltav1.x*cos(pi+theta1)+deltav1.y*sin(pi+theta1)
deltav1.ss <- deltav1.x*sin(pi+theta1)-deltav1.y*cos(pi+theta1)
deltav2.fr <- deltav2.x*cos(theta2)+deltav2.y*sin(theta2)
deltav2.ss <- deltav2.x*sin(theta2)-deltav2.y*cos(theta2)

tau1 <- 1/(sig1*sig1)

# S[1,1] <- sig1*sig1
# S[2,2] <- sig1*sig1
# S[1,2] <- rho*sig1*sig1
# S[2,1] <- rho*sig1*sig1
# T[1:2,1:2] <- inverse(S[,])
deltav1.fr.dat ~ dnorm(deltav1.fr, tau1)
deltav1.ss.dat ~ dnorm(deltav1.ss, tau1)
# deltav1.dat[1] <- deltav1.fr.dat
# deltav1.dat[2] <- deltav1.ss.dat
# mu1[1] <- deltav1.fr
# mu1[2] <- deltav1.ss
# deltav1.dat[1:2] ~ dmnorm(mu1[],T[,])

deltav2.fr.dat ~ dnorm(deltav2.fr,tau1)
deltav2.ss.dat ~ dnorm(deltav2.ss,tau1)
# deltav2.dat[1] <- deltav2.fr.dat
# deltav2.dat[2] <- deltav2.ss.dat
# mu2[1] <- deltav2.fr
# mu2[2] <- deltav2.ss
# deltav2.dat[1:2] ~ dmnorm(mu2[],T[,])

# compute predicted doi

doi <- atan2.function(Pn,Pt)

pdof1.deg <- (theta1-Gamma-doi)/d2r
pdof2.deg  <- (theta2-Gamma-doi)/d2r

tau2 <- 1/(sig2*sig2)
```

```
pdof1.dat ~ dnorm(pdof1.deg,tau2)
pdof2.dat ~ dnorm(pdof2.deg,tau2)


# compute predicted exit angles
# atan2 function

Theta1 <- atan2.function(V1x,V1y)
Theta2 <- atan2.function(V2x,V2y)

Theta1.deg <- Theta1/d2r
Theta2.deg <- Theta2/d2r

tau3 <- 1/(sig3*sig3)
Theta1.deg.dat ~ dnorm(Theta1.deg,tau3)
Theta2.deg.dat ~ dnorm(Theta2.deg,tau3)

# delta v's from crush
deltav1 <- sqrt(deltav1.x*deltav1.x+deltav1.y*deltav1.y)
deltav2 <- sqrt(deltav2.x*deltav2.x+deltav2.y*deltav2.y)

deltav1.crush <-.8684*deltav1
deltav2.crush <- .8684*deltav2

tau4 <- 1/(sig4*sig4)
deltav1.crush.dat ~ dnorm(deltav1.crush,tau4)
deltav2.crush.dat ~ dnorm(deltav2.crush,tau4)

v1.mph <- v1*(60/88)
v2.mph <- v2*(60/88)

 }
```

Data list(m1=129.8,I1=2973, d1.in=5.8,phi1.deg=18,theta1.deg=0,omega1.deg=0,
m2=106.8,I2=2155,d2.in=5.2,phi2.deg=6,theta2.deg=0,omega2.deg=0,Gamma.deg=20,sig1=3.2,sig2=10,
sig3=10,sig4=9)
list(anglebound=10, dbound=2)
list(deltav1.fr.dat=-44)
list(deltav1.ss.dat=5.7, deltav2.fr.dat=-53,3, deltav2.ss.dat=6.9)
list(pdof1.dat=-10,pdof2.dat=350)
list(Theta1.deg.dat=73, Theta2.deg.dat=-126)

list(deltav1.crush.dat=36.8,deltav2.crush.dat=44.7)

Inits list(v1=42,v2=50.5)

APPENDIX B: DATA USED IN RECONSTRUCTING RICSAC COLLISIONS

RICSAC Crash	Vehicle	m	I	d	ϕ	θ	Γ	v	e	μ%	Δv long	Δv lat	Δv crush	B	PDOF
1	1	143.5	3728	7.59	-19.8	0	-30	-29.0	0	100	-16.0	6.6	15	153	-22
	2	95.8	1961	3.44	-38.7	60		29.0			-17.3	-13.0	19	108	37
6	1	133.6	3469	8.41	-17.9	0	-30	-31.5	0	100	-13.0	3.5	12	169	-15
	2	81.5	1669	2.00	-90.0	60		31.5			-15.5	-14.8	19	103	44
7	1	115.0	2985	8.41	-17.9	0	-30	-42.7	0	100	-17.2	3.5	15.2	172	-12
	2	81.1	1082	2.00	-90.0	60		42.7			-17.6	-22.9	25.1	103	52
8	1	139.1	3614	7.90	0.0	0	0	-30.5	0.79	100	-20.4	10.4	20	134	-27
	2	146.3	3800	2.77	-68.8	90		30.5			-10.4	-11.7	14	120	48
9	1	70.1	976	4.80	6.0	0	0	-31.1	.355	100	-26.3	11.4	25	113	-27
	2	152.2	3953	5.60	-29.7	90		31.1			-7.3	-10.1	11	113	63
10	1	71.6	998	3.47	0.0	0	0	-48.8	.419	100	-37.5	19.1	37	121	-27
	2	146.6	3008	5.29	-29.2	90		48.8			-12.8	-14.4	17	112	48

m – vehicle mass (lb-s^2/ft)

I – yaw moment of inertial (ft-lb-s^2)

d – distance from center of mass to contact center (feet)

ϕ – angle to contact center (degrees)

θ – initial heading angle (degrees)

Γ – crush angle (degrees)

v – initial speed (feet/second)

e – restitution coefficient (dimensionless)

μ% - impulse ratio (percent)

Δv long – delta-V in longitudinal (front-rear) direction (feet/second)

Δv long – delta-V in lateral (side-side) direction (feet/second)

Δv crush – idealized delta-V estimated from crush measurements (feet/second)

B – idealized exit angle measurements (degrees)

PDOF – idealized measurements of principal direction of force (degrees)]

APPENDIX C: POST-CRASH SCENE DIAGRAMS FOR NASS/CDS CASES, PREPARED BY NASS/CDS INVESTIGATORS

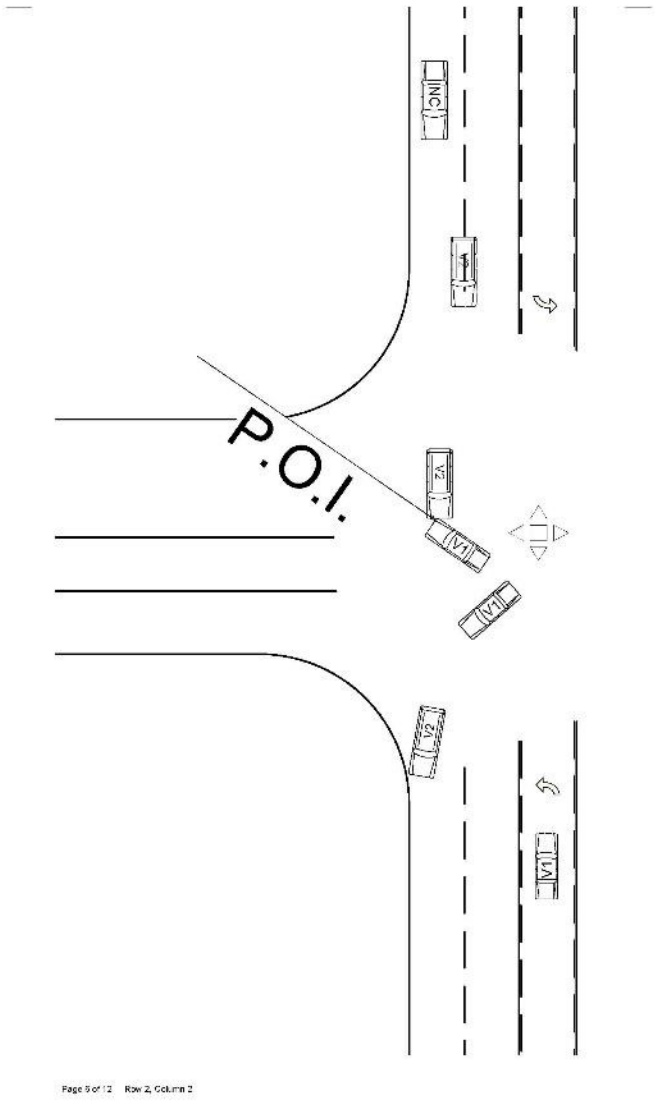

Figure C. 1 Post-crash scene diagram for NASS/CDS Case 2012-12-044. Vehicle 1 (Malibu) is turning left. Vehicle 2 (Blazer) is going straight.

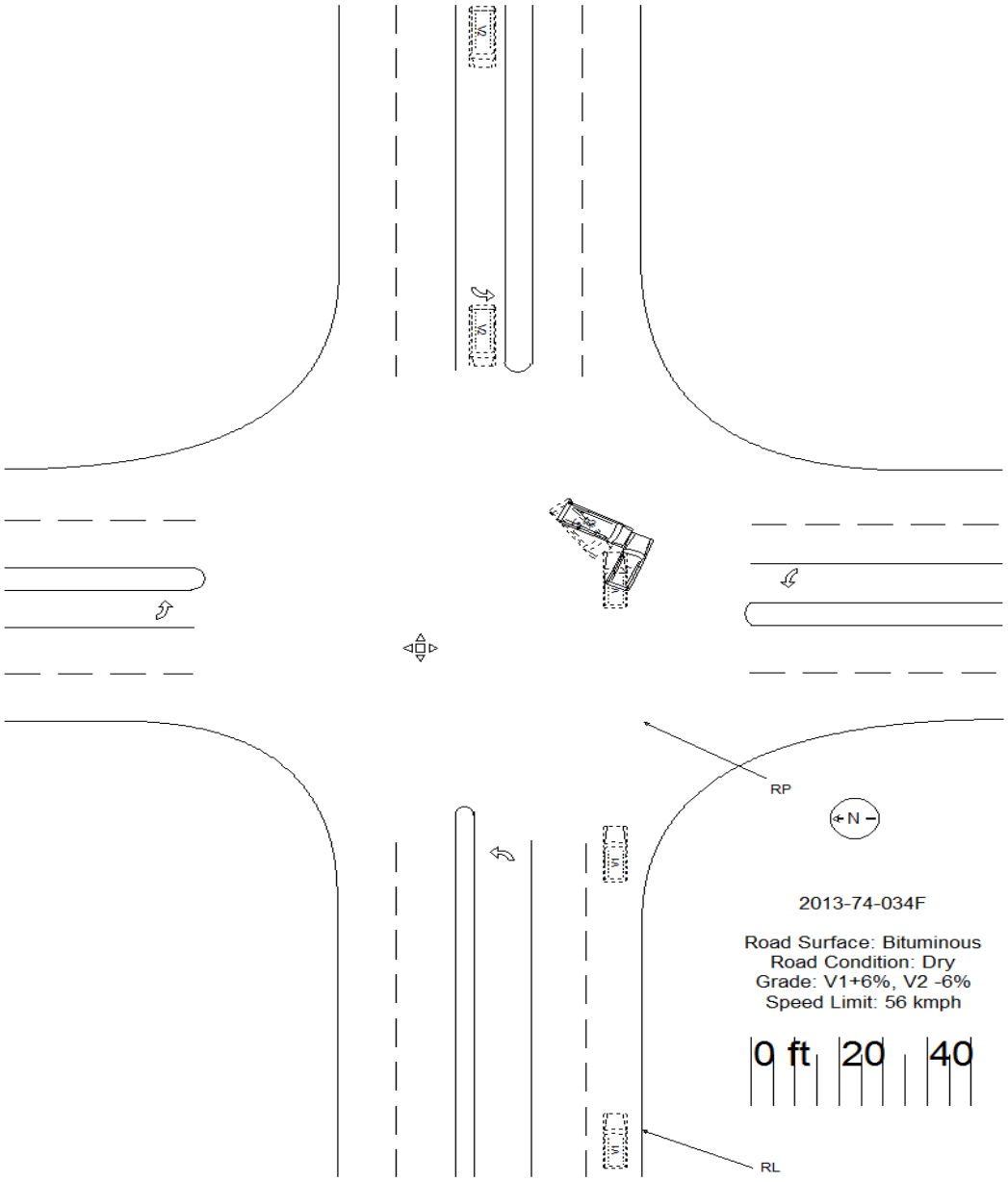

Figure C. 2 Post-crash scene diagram for NASS/CDS Case 2013-74-034.

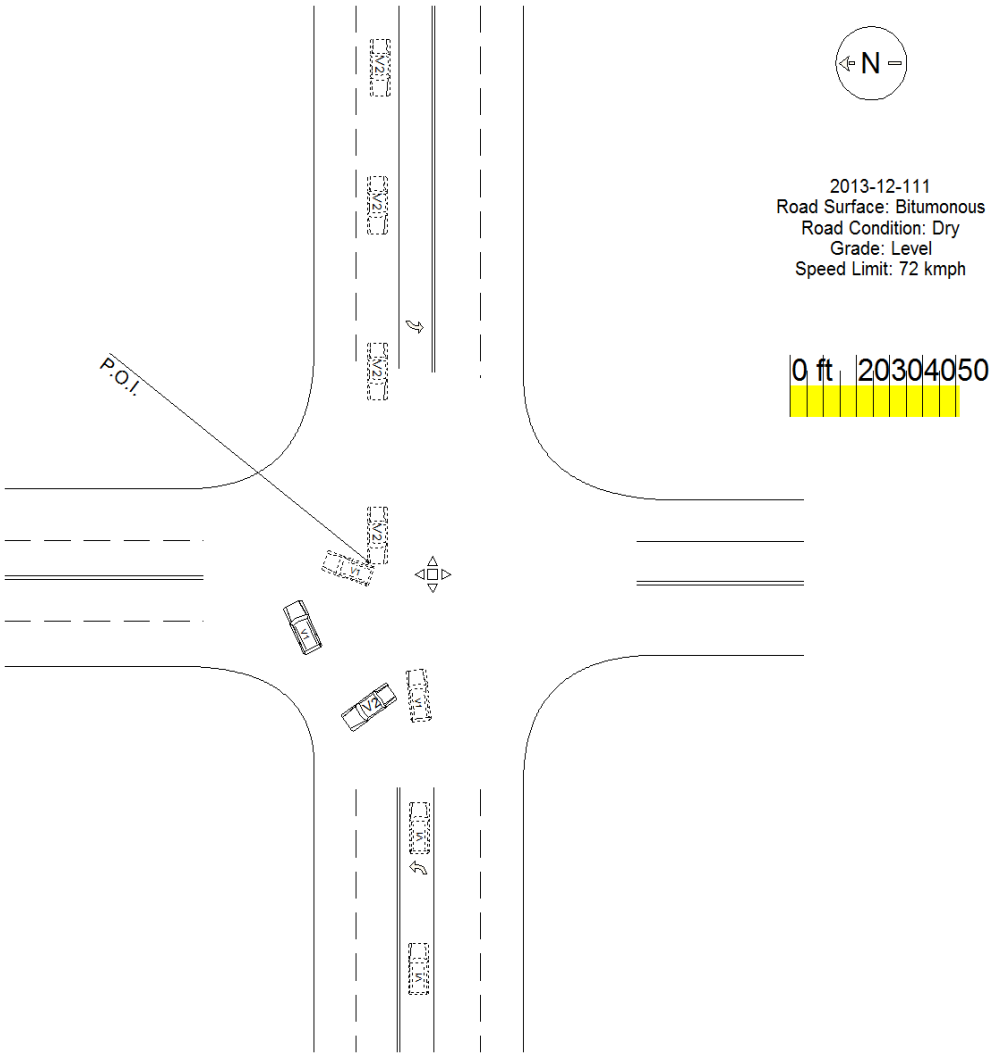

Figure C. 3 Post-crash scene diagram for NASS/CDS Case 2013-12-111.

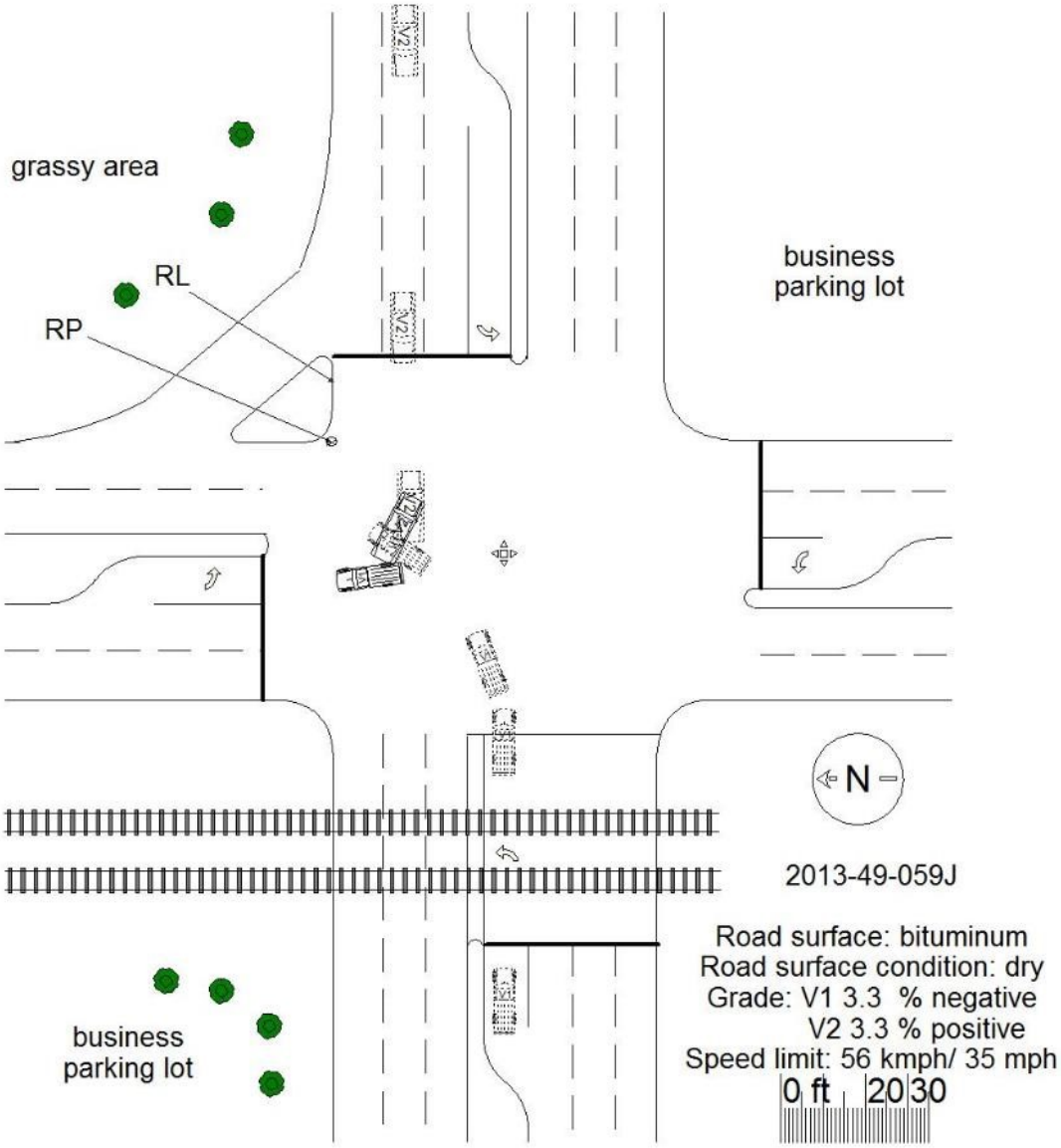

Figure C. 4 Post-crash scene diagram for NASS/CDS Case 2013-49-059.

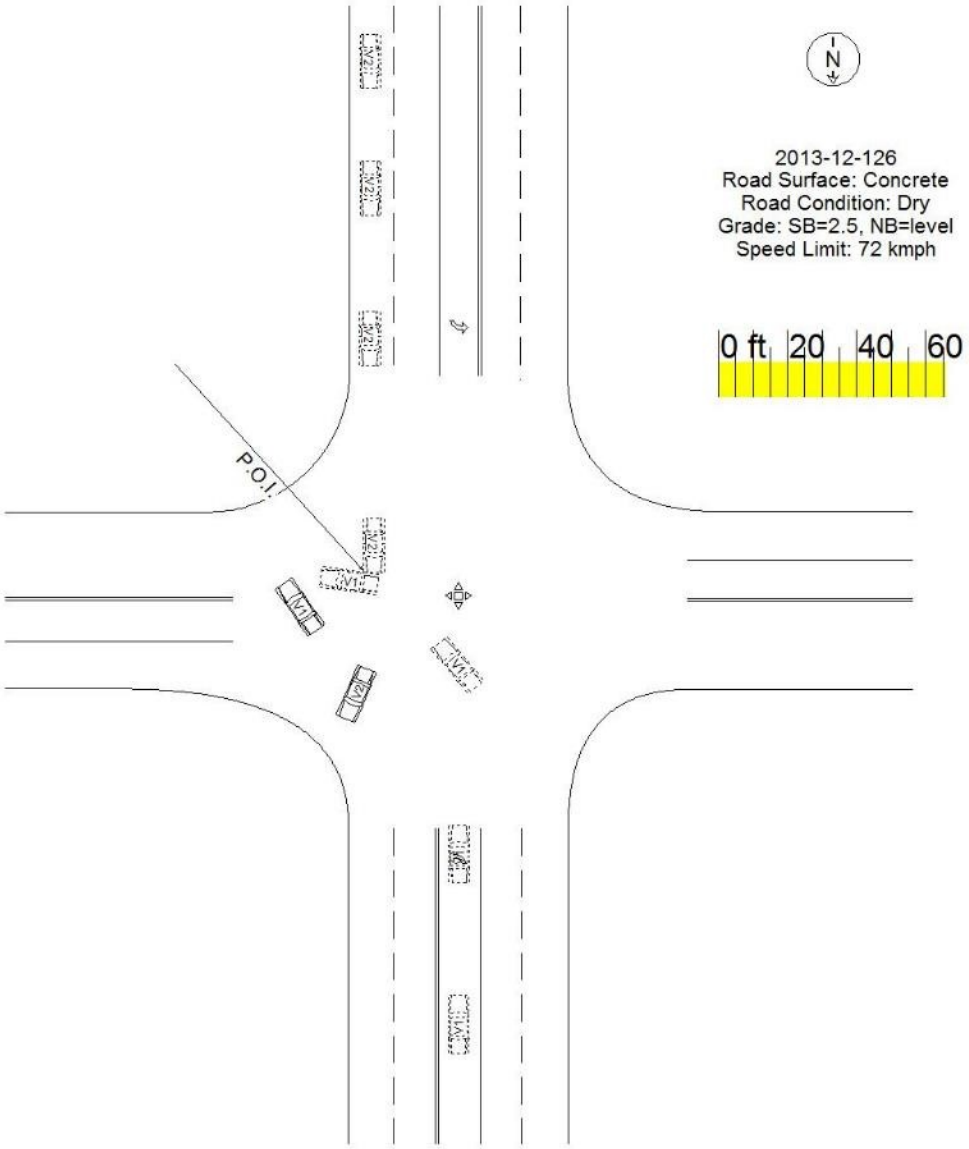

Figure C. 5 Post-crash scene diagram for NASS/CDS Case 2013-12-126.

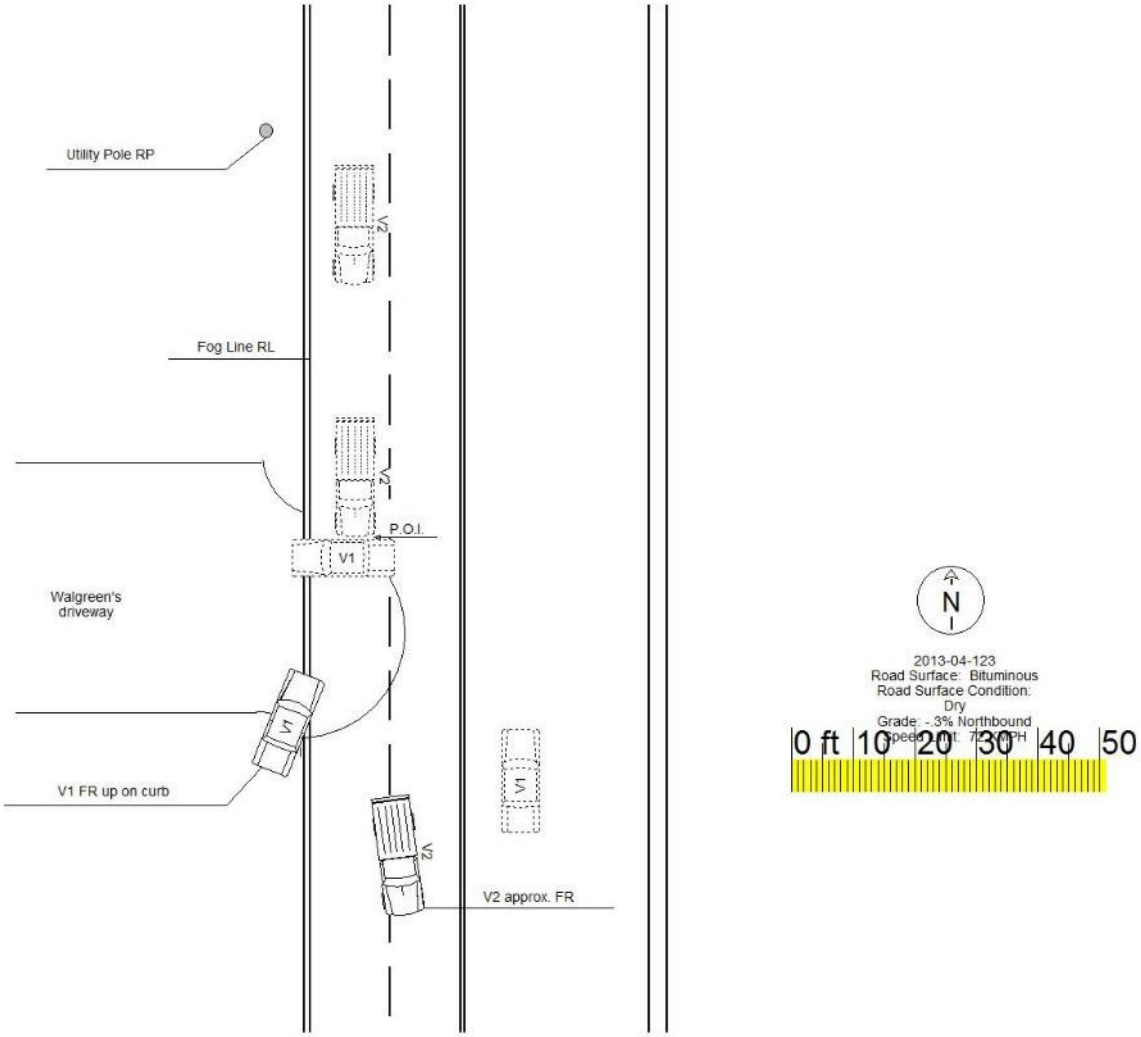

Figure C. 6 Post-crash scene diagram for NASS/CDS Case 2013-04-123

APPENDIX D: EXAMPLE WINBUGS MODEL FOR RECONSTRUCTING TRAJECTORIES FROM EDR PRE-CRASH DATA

```
model
# EDR simulation NHTSA case 2013-49-059
# Allows for different EDR timings
# Allows for uncertain reconstructed impact speeds
# Allows for EDR speed measurement error
# final adjustments:
# external prior for vehicle 2 final decel because brakes applied only during final second
# Ruth and Daily 2011 EDR error model for Ford
# Vehicle 2 final speed computed from last EDR speed and decelertion
{

tau0 <- 1/(sig0*sig0)
vv1.mph[1] ~ dunif(0,100)
vv1[1] <- 0
for (i in 2 : n1) {
vv1.mph[i] ~ dunif(0,100)
v1mph.dat[i] ~ dnorm(vv1.mph[i],tau0)
vv1[i] <- vv1.mph[i]*(88/60) }

# vehicle 1 impact speed from reconstruction
# vv1[n1+1]<- v1.recon*(88/60)
tau1 <- 1/(sig1*sig1)
vv1.last ~ dunif(0,100)
v1.recon.dat ~ dnorm(vv1.last,tau1)
vv1[n1+1] <- vv1.last

# vehicle 1 impact speed set equal to most recent precrash speed
# vv1[n1+1] <- vv1[n1]

for (i in 1:n2) {
brake2[i] <- step(t02[i]-brakestart2) }
brake2[n2+1] <- brake2[n2]

# Ruth and Daily 2010 EDR error model
for (i in 1 : n2) {
vv2.mph[i] ~ dunif(0,100)
vv2.bar[i] <- (1-brake2[i])*(-.075+.987*vv2.mph[i]) + brake2[i]*(-1.22 + .987*vv2.mph[i])
vv2.tau[i] <- (1-brake2[i])*12.1 + brake2[i]*1.28
v2mph.dat[i] ~ dnorm(vv2.bar[i],vv2.tau[i])
vv2[i] <- vv2.mph[i]*(88/60) }

# for (i in 1:n2) {
```

```
# vv2.mph[i] ~ dunif(0,100)
# v2mph.dat[i] ~ dnorm(vv2.mph[i],tau0)
# vv2[i] <- vv2.mph[i]*(88/60) }

# vehicle 2 impact speed from reconstruction
# vv2[n2+1] <- v2.recon*(88/60)
tau2 <- 1/(sig2*sig2)
# vv2.last~ dunif(0,100)
# v2.recon.dat ~ dnorm(vv2.last,tau2)
# vv2[n2+1] <- vv2.last

# vehicle 2 impact speed set equal to most recent precrash speed
# vv2[n2+1] <- vv2[n2]

for (j in 1:n1-1) {
delta1[j] <- delta01
a1[j] <- (vv1[j+1]-vv1[j])/delta1[j]}

for (j in 1:n2-1) {
delta2[j] <- delta02
a2[j] <- (vv2[j+1]-vv2[j])/delta2[j] }

# uncertainty in collision times

delta1.t ~ dunif(delta1lo,delta1hi)
delta2.t ~ dunif(delta2lo,delta2hi)

a1[n1] <- max(-g,(vv1[n1+1]-vv1[n1])/delta1[n1])
# a2[n2] <- max(-g,(vv2[n2+1]-vv2[n2])/delta2.t)

# informative prior for vehicle 2 final decel
f2_final ~ dunif(.7,.9)
a2[n2] <- -g*f2_final
# vehicle 2 final acceleration from extrapolation
# a2[n2] <- a2[n2-1]
vv2[n2+1] <- vv2[n2]+ a2[n2]*delta2[n2]

# case-specific final delta t's

delta1[n1] <- delta1.t
delta2[n2] <- delta2.t
```

```
for (i in 1:n1) {
d1[i] <- vv1[i]*delta1[i] + (a1[i]*delta1[i]*delta1[i])/2
t1[i] <- t01[i]+(delta01-delta1[n1]) }

# vehicle 2 time shift for Ford RCMs
for (i in 1:n2){
d2[i] <- vv2[i]*delta2[i] + (a2[i]*delta2[i]*delta2[i])/2
t2[i] <- t02[i]-delta2[n2] }

t1[n1+1] <- 0
t2[n2 +1] <- 0

for (i in 1:n1) { xx1[i] <- sum(d1[i:n1])}

for (i in 1:n2){ xx2[i] <- sum(d2[i:n2]) }

# vehicle 1 for GCM SDM
tstart1lo <- start1inlo + (delta01-delta1[n1])
tstart1hi <- start1inhi +(delta01-delta1[n1])
# vehicle 2 for Ford RCM
tstart2lo <- start2inlo -delta2[n2]
tstart2hi <- start2inhi-delta2[n2]

# tstart1 = time turning vehicle accepts gap
# tstart2 = time opposing vehicle begins braking

tstart1 ~ dunif(tstart1lo,tstart1hi)
tstart2 ~ dunif(tstart2lo,tstart2hi)

tc <- abs(tstart1)

tp <- tstart2-tstart1

# interpolation to estimmate opposing vehicle position at time of gap acceptance

for (i in 1:n2-1) {
tlov[i] <- (i+1)*step(tstart1-t2[i])*step(t2[i+1]+h-tstart1)}

tlo <- min(n2,sum(tlov[]))
thi <- tlo-1

x2 <- xx2[thi] +( (xx2[thi]-xx2[tlo])/(t2[thi]-t2[tlo]))*(tstart1-t2[thi])
```

```
v2 <-  vv2[thi]+((vv2[thi]-vv2[tlo])/(t2[thi]-t2[tlo]))*(tstart1-t2[thi])
gap <- x2/v2

      a2.end<- -a2[n2]
      xbrake <- pow(v2,2)/(2*a2.end)
      xprt <- v2*tp
      xstop <- xbrake + xprt
       stop <- step(x2-xstop)
       fullhit <- step(xprt-x2)
       tc1 <- x2/v2
             vbrake2 <- max(v2*v2-2*a2.end*(x2-xprt),0)
              vbrake <- sqrt(vbrake2)
       tc2 <-tp+(v2-vbrake)/a2.end
       tc0 <- stop*1000+(1-stop)*fullhit*tc1+(1-stop)*(1-fullhit)*tc2
# crash condition tc-crash.buffter < tc0 < tc
    v1.last <- vv1[n1+1]
     crash.buffer <- L1/(2*v1.last)
           close1 <- step((tc+crash.buffer)-tc0)*step(tc0-tc)
           phit <- .99999*close1
           hit ~ dbern(phit)
           v.impact <- hit*((fullhit*v2)+(1-fullhit)*vbrake)
}
```

Data list(start1inlo=-5,start1inhi=-4,start2inlo=-.5,start2inhi=0, delta1lo = 0, delta1hi=1, delta2lo=0, delta2hi=.5,n1=5,n2=11,delta01=1,delta02=.5,h=0.00001,t01=c(-5,-4, -3,-2,-1,0),t02=c(-5,-4.5,-4,-3.5,-3,-2.5,-2,-1.5,-1,-.5,0),v1.recon.dat=18.9,sig0=1,sig1 =5.3,sig2=8,g=32.2,L1=15,hit=1,brakestart2=0)

```
v1mph.dat[]
0
2
10
17
22
END
v2mph.dat[]
36
36
36.7
36.7
37.3
37.3
37.3
```

37.9
38.5
39.2
37.9
END

Inits list(vv1.last=15,vv1.mph=c(1,2,10,17,22),
vv2.mph=c(35,35,35,35,35,35,35,35,35,35,35),delta1.t=0.5,delta2.t=0.25,vv1.last=15,tstart1=-4,tstart2=-.5)]

APPENDIX E: LEFT-TURN CRASH SIMULATION MODEL

```
model
# simulation of conflicts and crashes using random acceptance
# Robert and Mendota opposing volumes for SB LTs
# clearance times from regression model 1/22/15
# IVs=log gap, ML estimates from Minitab; corrected as of 1/16/2015
# Koppa et al stats of braking and reaction times
# field statistics for distances, speeds, clearance times
#  Cowen M3 gaps
# revised crash criterion
# simulated accepted gaps

{

# conflict simulation
v.sim.mu <- v.bar*(88/60)
v.sim.tau <- 1/(v.sig*v.sig*(88/60)*(88/60))
tc.tau <- 1/(tc.sigma*tc.sigma)
v.sim ~ dnorm(v.sim.mu,v.sim.tau)I(1,)
v.sim.mph <- v.sim*(60/88)
# q.sim <- q.in/3600
# lambda.sim <- 1/q.sim
# lambda.sim <- 1/gap.bar
# gap.sim ~ dexp(lambda.sim)
u ~ dunif(0,1)
gap0.sim <- tm-log((1-u)/alpha)/lambda
littleu <- step((1-alpha)-u)
gap.sim <-(1- littleu)*gap0.sim + (littleu)*tm
x.sim <- gap.sim*v.sim
tc.mu <- tc.beta0+tc.beta1*log(gap.sim)
tc.sim ~ dlnorm(tc.mu,tc.tau)
linmod.sim <- beta0 + beta1*log(gap.sim)
logit(p.sim) <- linmod.sim
px.sim <- p.sim*step(gap.sim-gap.min)
# accept.sim <- step(p.sim-u.sim)*step(gap.sim-gap.min)
accept.sim ~ dbern(px.sim)

# arrival.sim <- (x.sim+x2hit)/(v.sim)
# conflict1.sim <- accept.sim*step(con.buffer-abs(tc.sim-arrival.sim))
ttc.sim <- gap.sim-tc.sim
conflict2.sim <- step(con.buffer-ttc.sim)
```

```
# collision simulation
        g <- 32.2
        # tp.sim ~dunif(0.5,1.5)
        # f.sim ~ dunif(.5,.9)

   tp.sigma2 <- log((pow(tp.sd,2)/pow(tp.bar,2))+1)
   tp.mu <- log(tp.bar)-0.5*tp.sigma2
   tp.tau <-1/tp.sigma2
   f.sigma2 <- log((pow(f.sd,2)/pow(f.bar,2))+1)
   f.mu <- log(f.bar)-0.5*f.sigma2
   f.tau <- 1/f.sigma2

   tp.sim ~dlnorm(tp.mu,tp.tau)
   f.sim ~dlnorm(f.mu,f.tau)
        a.sim <- f.sim*g
        v.sim.fps <- v.sim
     x0.sim <- x.sim+x2hit
     xbrake.sim <- pow(v.sim.fps,2)/(2*a.sim)
     xprt.sim <- v.sim.fps*tp.sim
     xstop.sim <- xbrake.sim + xprt.sim
      stop.sim <- step(x0.sim-xstop.sim)
      fullhit.sim <- step(xprt.sim-x0.sim)
      tc1.sim <- x0.sim/v.sim.fps
           vbrake2.sim <- max(v.sim.fps*v.sim.fps-2*a.sim*(x0.sim-xprt.sim),0)
      tc2.sim <-tp.sim+(v.sim.fps-sqrt(vbrake2.sim))/a.sim

      tc0.sim <- stop.sim*1000+(1-stop.sim)*fullhit.sim*tc1.sim+(1-stop.sim)*(1-fullhit.sim)*tc2.sim
# crash condition tc-crash.buffter < tc0 < tc
        close1.sim <- step(tc0.sim-(tc.sim-crash.buffer))*step(tc.sim-tc0.sim)
        hit.sim <- accept.sim*close1.sim
        # phit.sim <- .99999*close1.sim
        # hit.sim ~ dbern(phit.sim)
        v.impact <- hit.sim*((fullhit.sim*v.sim)+(1-fullhit.sim)*(sqrt(vbrake2.sim)))

}
```

Data list(tc.beta0=.4569, tc.beta1=.31524,tc.sigma=.2799,
con.buffer=1.5,crash.buffer=.5,gap.min=2.5,x2hit=10)
list(alpha=.612, lambda=.359,tm=2.0)
list(beta0=-8.2736,beta1=4.8475)
list(tp.bar=0.6,tp.sd=0.3,f.bar=0.75,f.sd=0.1)

list(v.bar=35.6,v.sig=9.0)
list(accept.sim=1)
list(hit.sim=1)

Inits list(u =.5,v.sim=50)